UNIVERSITÀ
DEGLI STUDI
FIRENZE

DOTTORATO DI RICERCA
INTERNATIONAL DOCTORATE IN STRUCTURAL BIOLOGY

CICLO XXXI

COORDINATOR Prof. Claudio Luchinat

MOLECULAR ASPECTS OF IRON–SULFUR PROTEIN BIOGENESIS

Settore Scientifico Disciplinare CHIM/03

PhD student
Dott. Spyridon Gourdoupis

Tutor
Prof. Lucia Banci

Coordinator
Prof. Claudio Luchinat

November 2015 – 2018

This thesis has been approved by the University of Florence, the University of Frankfurt and the Utrecht University.

Universiteit Utrecht

CERM Firenze

FRANKFURT AM MAIN

«…ἵνα μὴ λυπῆσθε καθὼς καὶ οἱ λοιποὶ οἱ μὴ ἔχοντες ἐλπίδα.»
Προς Θεσσαλονικείς Α΄ 4:13

«… so that ye sorrow not, like the rest who have no hope.»
1 Thessalonians 4:13

«Γέλα μου, χαμογέλα μου, ό,τι και να γίνει σ 'αγαπώ.
Γέλα μου, χαμογέλα μου, ό,τι και να γίνει θά 'μαι δω.»

Dedicated to Vicky and Spyros;
to us.
I kept my word; my duty is done.

INDEX

CHAPTER 1

INTRODUCTION

1.1 Iron and sulfur in biology

Biology concerns the study of living organisms. A clear definition of what constitutes a living organism is yet to be determined accurately, since the distinction between the living and the inanimate is a rather complex topic and often falls under thorough discussions, agreements and disagreements among scientists across the globe.

By joint acceptance, the main difference comes down to the occurrence, or not, of processes that promote the self-sustainability of a system. If such processes do exist, then, the system is characterized as life containing i.e. alive. [1]

Thirty years ago, Günter Wächtershäuser, supported by the philosopher Karl R. Popper, expressed and demonstrated his ideas that some of these self-sustaining processes, the first biological processes which signalized the early life forms, initialized on catalytic transition metal centers (mainly iron and nickel) localized on a hydrothermal mineral background, under high pressure and temperature (volcanic conditions). These metals produced organic compounds from inorganic compounds giving rise to a sulfur-dependent version of the reductive citric acid cycle. The produced organic compounds promoted autocatalytic processes by accelerating the catalytic potency of those metal centers (functioning like ligands), which then produced more organic compounds as metabolic products which in turn accelerated even more the catalytic process, and so on, giving birth to more complex systems. [2][3][4][5][6]

From then, millions of years of evolution passed, and iron and sulfur have been favored, by natural selection, as ones of the most dominant amongst the different chemical elements, for participating in various and complex biological processes in organisms.

Indeed, it is not a matter of plain chance that the average human body contains about 4 grams of iron and 140 grams of sulfur. [7] Iron, bound to proteins, participates in transport, storage and use of oxygen as well as in electron transfer. [8] Sulfur is a characteristic component of the amino acids methionine and cysteine, and it is present in almost all kinds of proteins. The disulfide bonds play a crucial role for the structure and, hence, the activity of each protein, [9] while thiols (R-SH) act like reducing agents protecting and repairing the cell from oxidation. Both elements are essential for the formation of iron-sulfur (Fe-S) cluster containing proteins, a group of metalloproteins present throughout

all the kingdoms of life which carry out oxidation-reduction reactions in the cell (electron transfer, enzymatic catalysis, protein regulation). [10]

1.2 Fe-S cluster classification and properties

Ferric iron is hardly soluble near pH 7, that is why iron uptake and storage are promoted in complexes and are strictly regulated by proteins. [8][60]

Some proteins coordinate iron and sulfur in clusters, hence the name of Fe-S proteins. These clusters are diverse and come in different types, and every type has its own biological role, characteristics and biochemical properties. **(Fig. 1)** [11]

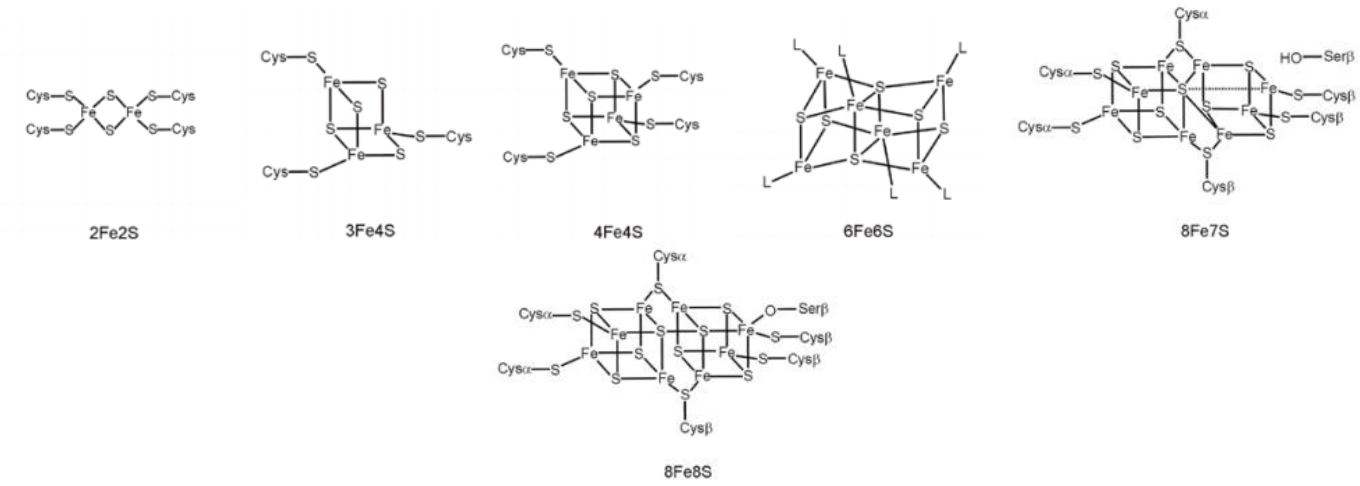

Figure 1. Different types of Fe-S clusters known in nature.

The most common Fe-S clusters in organisms are the [2Fe-2S], [3Fe-4S] and [4Fe-4S] clusters. [12][61] **(Fig. 1)** All of them contain iron on a Fe^{2+} and/or a Fe^{3+} oxidation state. Sulfur is on the S^{2-} sulfide state.

The [2Fe-2S] cluster **(Fig. 1)** is the simplest Fe-S cluster and it has a «diamond» structure with two irons bridged by two sulfides. Its redox potential range is from -155 to +300 mV. [13] Proteins containing [2Fe-2S] clusters are involved in electron transfer and in sensing of oxygen (O_2) and nitrogen oxide (NO).

The [4Fe-4S] cluster **(Fig. 1)** has a «cubane» structure with four irons bridged by four sulfides. Its redox potential range is very large from -645 to 450 mV. [13] Proteins containing [4Fe-4S] clusters are involved in electron transfer, catalysis of redox and non-redox reactions, stabilization of protein structure for DNA repair as well as sensing of O_2, NO and Fe.

The [3Fe-4S] cluster **(Fig. 1)** also belongs to the «cubane» structure type, like the [4Fe-4S] cluster, though one iron is missing. Its redox potential range is from -420 to -50 mV. [13] Proteins containing [3Fe-4S] clusters are involved in electron transfer and O_2 sensing.

The Fe-S clusters are essential for life and the main reasons reside on the combination of the chemical properties of the cluster cofactors with their redox properties which are affected also by the local protein environment. [62] Fe-S clusters have the ability to take or give one electron by changing their oxidation state when one Fe^{+2} changes to Fe^{3+} or vice versa. [63] On the other hand, sulfur provides ligation flexibility. [63] Including the effect of the ligands coordinating the cluster, which modulate the range of the redox potential of the cluster, we end up with a group of one of the most important and ancient electron carriers in nature. [14]

Their role as electron carriers has been extensively studied. The oxidation states of the iron ions define the final oxidation state of the cluster. The type of coupling between the individual electron spins determines the cluster total spin states, their separations and their order. Fe^{+2} has an individual spin of S = 2, while Fe^{+3} has an individual spin of S = 5/2. When a cluster contains an even number of iron ions of the same oxidation state, in presence of antiferromagnetic coupling between the iron ions, the total spin value of the ground state of the cluster is S = 0. Otherwise, the cluster has a total spin $S \neq 0$ i.e. also the ground state is paramagnetic. Furthermore, we need to consider that in the case of a combination of Fe^{2+} and Fe^{3+} ions, the extra electron, with respect to the oxidized state, can be either localized on an individual iron ion or can be fully delocalized between them, thus resulting in an oxidation state of 2.5+.

The oxidation states of the common Fe-S clusters and their ground state spins for the various oxidation states of the iron ions are summarized in **Table I.** [64]

Cluster – oxidation state	Iron ions	Ground state Spin
$[2Fe\text{-}2S]^{+}$	$1{\cdot}Fe^{2+}$, $1{\cdot}Fe^{3+}$	1/2
$[2Fe\text{-}2S]^{2+}$	$2{\cdot}Fe^{+3}$	0
$[3Fe\text{-}4S]^{0}$	$1{\cdot}Fe^{2+}$, $2{\cdot}Fe^{3+}$	2
$[3Fe\text{-}4S]^{+}$	$3{\cdot}Fe^{+3}$	1/2
$[4Fe\text{-}4S]^{0}$	$4{\cdot}Fe^{2+}$	0
$[4Fe\text{-}4S]^{+}$	$3{\cdot}Fe^{+2}$, $1{\cdot}Fe^{+3}$	1/2
$[4Fe\text{-}4S]^{2+}$	$2{\cdot}Fe^{+2}$, $2{\cdot}Fe^{+3}$	0
$[4Fe\text{-}4S]^{3+}$	$1{\cdot}Fe^{+2}$, $3{\cdot}Fe^{+3}$	1/2

Table I. oxidation states and ground state spin values for various Fe-S clusters [64]

1.3 Mitochondrial Fe-S cluster assembly machinery

The biogenesis of Fe-S proteins has been studied mainly in bacteria and yeast since the protein handling is easier and the involved proteins are ubiquitous and evolutionary well-conserved in humans. [15][16][17][18]

Three machineries have been identified to be responsible for the maturation of Fe-S cluster proteins in eukaryotes, (i) the mitochondrial Fe-S cluster assembly machinery, (ii) the mitochondrial intermembrane exporting machinery and (iii) the cytosolic Fe-S protein machinery. [35][36] **(Fig. 2)**

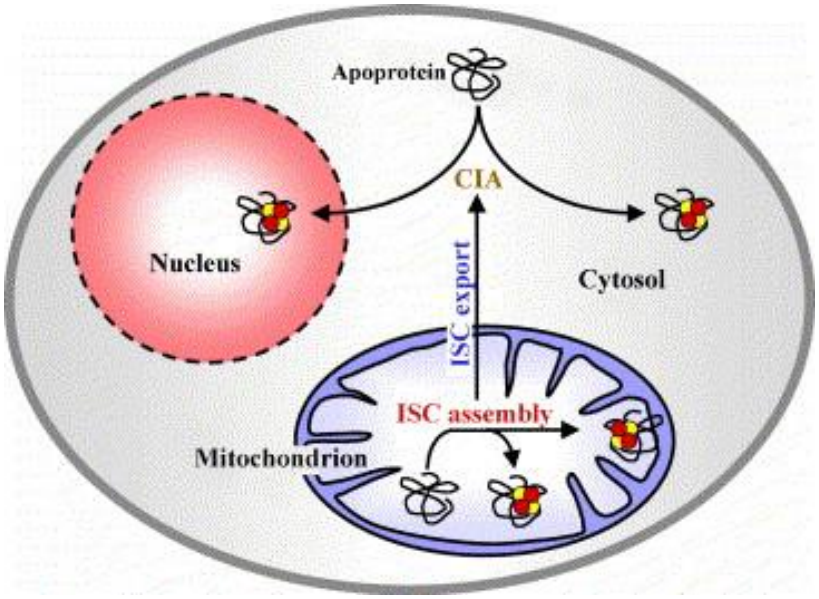

Figure 2. The three distinct machineries which participate in the maturation of Fe-S cluster proteins in eukaryotes. [35]

While all machineries are essential for maintaining the in-cell proper functionality, the mitochondrial Fe-S cluster assembly machinery is contributing to the maturation of all the Fe-S proteins in the cell [37] and hence, defects on the mitochondrial machinery are directly affecting functions both in the cytosol and the nucleus. [35] Such an observation, plus the existence of an exporting rather than an importing system from/into the mitochondria in the Fe-S cluster pathways, underlines an evolutionary connection between the three systems ultimately strengthening the endosymbiotic hypothesis about the origin of mitochondria. [33][34]

A map of the mitochondrial Fe-S cluster biosynthetic pathway for *homo sapiens* has been constructed by matching the bacterial and yeast proteins with their human homologues, by protein-protein interaction experiments and by mutational data from patients. However, this model still lacks direct experimental evidences so to be fulfilled and well understood. **(Fig. 3)**

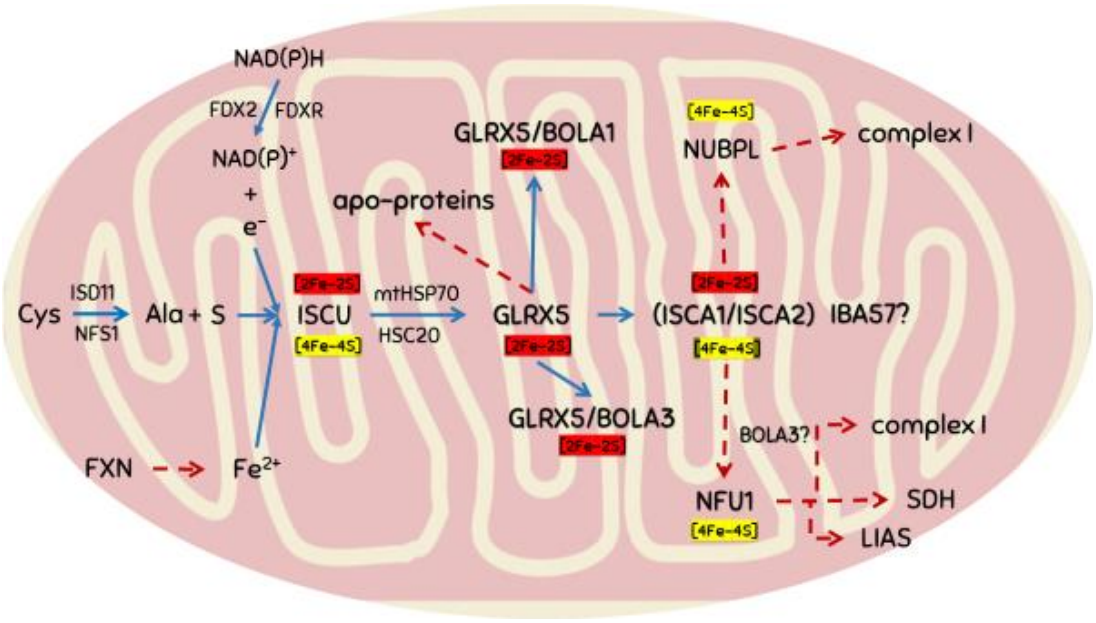

Figure 3. Mitochondrial Fe-S cluster assembly machinery pathway in *homo sapiens*. Blue arrows indicate well resolved steps of the pathway, while red-dashed arrows indicate hypothetical steps which have not yet been resolved.

In detail, cysteine desulfurase (NFS1) and iron-sulfur cluster biosynthesis protein ISD11 act as the sulfur donor by converting cysteine to alanine. [19][20] Frataxin (FXN) is considered to be the iron donor [21], while ferredoxin-2 (FDX2) along with ferredoxin reductase (FDXR) act as an electron transfer chain by oxidizing Nicotinamide Adenine Dinucleotide Phosphate (NAD(P)H to $NAD(P)^+$ and e^-). [22] As a result, a [2Fe-2S] cluster is initially assembled on the iron-sulfur cluster assembly protein (ISCU). [23] The chaperone mitochondrial Heat Shock Protein-70 (mtHSP70) and the co-chaperone Heat Shock protein Cognate-20 (HSC20) dissociate the cluster from ISCU and promote the transfer of the cluster to monothiol glutaredoxin-5 (GLRX5). [24] GLRX5 is known to constitute both an apo and a [2Fe-2S] heterodimer with BolA-like protein 1 (BOLA1) and BolA-like protein 3 (BOLA3) [25] and also mediating a [2Fe-2S] and/or a [4Fe-4S] cluster to iron-sulfur cluster assembly 1 and 2 homologs (ISCA1 and ISCA2) which can coordinate a cluster both together and separately. [26][27]

From this point onward, there is no clear experimental data to support any cluster transfer from the ISCA proteins to any other apo-protein, though, mutagenesis data from patients suggest that (i) the putative transferase CAF17 (IBA57) cooperates with the ISCA proteins [28], (ii) the iron-sulfur cluster scaffold homolog (NFU1) is involved in the maturation of the respiratory complex I (complex I), the succinate dehydrogenase (SDH) and the lipoyl synthase (LIAS), [29] and (iii) the Nucleotide-binding protein-like protein (NUBPL) is involved in the maturation of complex I. [30][31] Finally, NFU1 and NUBPL are implicated in functioning later in the pathway since the impact range of the silencing of their genes is narrower than that of ISCA proteins. [29][30][31]

1.3.1 Multiple Mitochondrial Dysfunction Syndrome (MMDS)

The mitochondrial Fe-S cluster assembly machinery has an impact farther than the cellular compartment of the mitochondrion since the maturation of all the Fe-S proteins in the cell depends on it. [32] In this respect, a single defect on this particular pathway could result in grave complications in the maintenance of life in cell.

Many diseases have been linked with the impairment of this machinery. The most common and well-studied is Friedreich's ataxia which is directly linked with mutations in the FXN gene. [38]

Recently, the correlation of mutations in genes with pathogenic symptoms and diseases, gave rise to the determination and taxonomy of a novel syndrome, the Multiple Mitochondrial Dysfunction Syndrome (MMDS), which is inextricably linked with protein partners of the mitochondrial Fe-S cluster assembly pathway. [39]

This syndrome is characterized by reduced function of multiple stages of energy production in the mitochondria, early life emergence and short life expectancy (usually not past infancy). The main symptoms are encephalopathy, hypotonia, psychomotor delay, failure to thrive, lactic acidosis, hyperglycinemia, hyperglycemia, pulmonary hypertension and cardiomyopathy. Six types have already been identified, each type linked with a specific, distinct protein deficiency.

MMDS type 1 is caused by mutation in the NFU1 gene (608100) and thirteen (13) cases have already been reported. [39][40] This type is characterized by muscle weakness, lethargy and failure to thrive.

MMDS type 2 is caused by mutation in the BOLA3 gene (613183) and four (4) cases have already been reported. [39][41] This type is characterized by lethargy, muscle spasticity, vomiting and abnormality of extrapyramidal motor function.

MMDS type 3 is caused by mutation in the IBA57 gene (615316) twenty-one (21) cases have already been reported. [42][43][44][45][46] This type is characterized by high palate, microcephaly and retrognathia.

MMDS type 4 is caused by mutation in the ISCA2 gene (615317) and nineteen (19) cases have already been reported. [47][48][49][50] This type is characterized by spasticity, optic atrophy and absent speech.

MMDS type 5 is caused by mutation in the ISCA1 gene (611006) and four (4) cases have already been reported. [51] This type is characterized by fibular aplasia or hypoplasia, femoral bowing, poly-, syn- and oligodactyly, and it is related with the Greig cephalopolysyndactyly syndrome (GCPS).

MMDS type 6 is caused by mutation in the Peptidase Mitochondrial Processing Beta Subunit (PMPCB) gene (617954) on chromosome 7q22 and five (5) cases have already been reported. [52] This type is characterized by microcephaly, optic atrophy, ataxia, dystonia, and spastic quadriplegia.

A potential cure for this severe disorder of systemic energy metabolism has yet to be discovered and the hope lays on the understanding of the function and role of the protein partners that are directly correlated with it and participate in the mitochondrial Fe-S cluster assembly machinery pathway.

1.4 Late mitochondrial Fe-S cluster assembly machinery

It is a rather interesting observation that almost all the protein partners implicated in MMDS are positioned after GLRX5, i.e. later in the mitochondrial Fe-S cluster assembly machinery pathway **(Fig. 4)**.

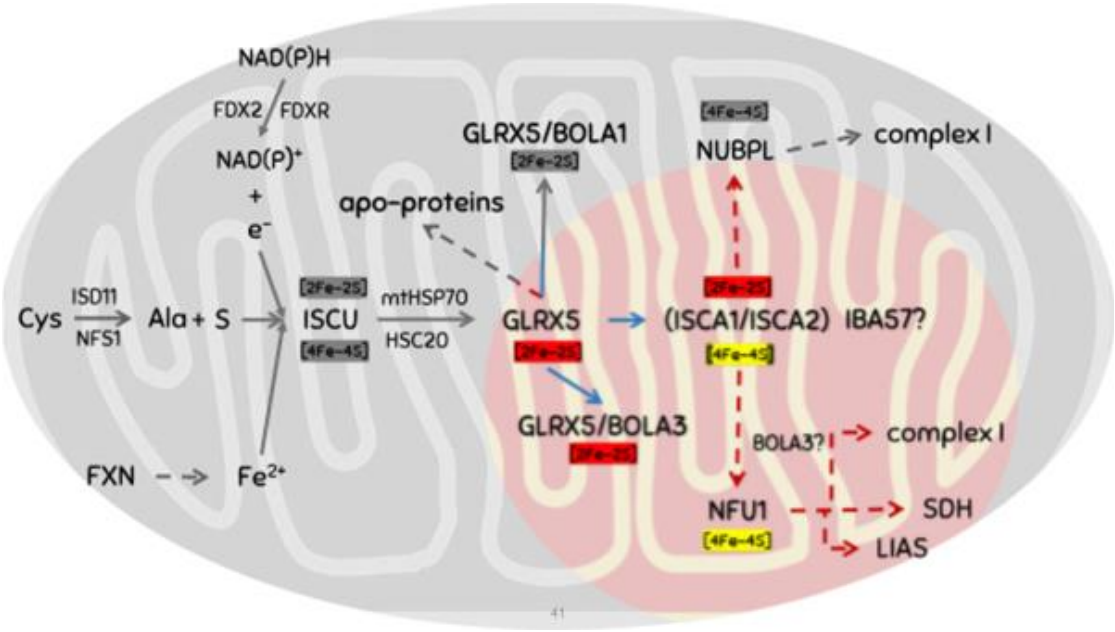

Figure 4. Mitochondrial Fe-S cluster assembly machinery pathway in *homo sapiens*. High-lighted pathway after GLRX5. Blue arrows indicate well resolved steps of the pathway while red-dashed arrows indicate hypothetical steps which have not yet been resolved.

GLRX5 is a small evolutionary conserved mitochondrial Fe-S protein which uses glutathione (GSH) as a cofactor. GLRX5 is involved in the Fe-S protein biogenesis and is essential for normal regulation of hemoglobin synthesis by Aconitase 1 (ACO1). Defects in the GLRX5 gene have been associated with non-ketotic hyperglycinemia [41] and sideroblastic pyridoxine-refractory autosomal recessive (PRARSA). [54] The holo-form in solution *in vitro* is dimeric and binds a [2Fe-2S] cluster whose coordination involves two GSH molecules and a conserved cysteine from each subunit of the dimer. NMR data has shown that GSH has two different conformations in the dimer. [27]

BOLA3 belongs to the BolA/IbaG family. BOLA3 is a novel protein with a non-classical mitochondrial targeting sequence. [55] BOLA3 cannot bind a cluster on its own but it coordinates a [2Fe-2S] cluster along with GLRX5 to form an hetero-dimeric holo-complex. This holo-hetero-complex is proposed to transfer a [2Fe-2S] cluster to recipient apo-proteins. [56] Defects in the BOLA3 gene have been associated with MMDS2. [39][41]

ISCA1 is a highly conserved mitochondrial Fe-S protein involved in the maturation of mitochondrial [4Fe-4S] cluster proteins functioning late in the Fe-S cluster assembly pathway. [28][57] ISCA1 can receive a cluster from GLRX5 to form a [2Fe-2S] homo-dimeric complex and, along with ISCA2, a [4Fe-4S] hetero-dimeric complex. ISCA1 forms, also, an hetero-dimeric apo-complex with ISCA2 [26][27] Defects in the ISCA1 gene have been associated with MMDS5. [51]

ISCA2 is involved in the maturation of mitochondrial [4Fe-4S] cluster proteins functioning late in the Fe-S cluster assembly pathway. [28] ISCA2 can receive a cluster from GLRX5 to form a [2Fe-2S] and/or a [4Fe-4S] cluster homo-dimeric complex and, along with ISCA1, a [4Fe-4S] hetero-dimeric complex. ISCA2 forms, also, an hetero-dimeric apo-complex with ISCA1. [26][27] Defects in the ISCA2 gene have been associated with MMDS4. [47][48][49][50]

IBA57 is involved in the maturation of mitochondrial [4Fe-4S] cluster proteins functioning late in the Fe-S cluster assembly pathway. [28] IBA57 is suspected to function along with the ISCA proteins for the maturation of [4Fe-4S] cluster proteins, though, its function in the mitochondrial Fe-S cluster assembly machinery is still elusive. [28] Defects in this gene have been associated with autosomal recessive spastic paraplegia-74 and MMDS3. [42][43][44][45][46]

NFU1 is an Fe-S protein which can bind a [4Fe-4S] cluster and potentially deliver it to specific apo-proteins. It has two domains (C-terminal and N-terminal domain) connected with a flexible linker. Defects in the NFU1 gene have been associated with MMDS1. [39][40]

1.5 Aim of the Research

My research activity, during my Ph.D. studies, was focused on the functional and structural characterization of the proteins involved in the late steps of the mitochondrial Fe-S cluster assembly machinery, with an ultimate goal to better characterize the pathway in which they are involved and potentially contribute to understanding their malfunction when mutated.

The human proteins that I have extensively characterized are NFU1, IBA57 and ISCA2, though, functional aspects of GLRX5, BOLA3 and ISCA1 were illuminated as well. All the proteins were recombinantly produced from *Escherichia coli* and purified by chromatographic techniques. The protocols for the production of GLRX5, BOLA3, ISCA1 and ISCA2 were already available in our lab, while developed protocols for NFU1 and IBA57have been developed *de novo* by me.

The techniques and methods that I handled were Polymerase Chain Reaction (PCR) (for DNA cloning and mutations), Transformation, recombinant protein Expression and Purification, Electrophoresis, High-performance liquid chromatography (HPLC), Ultraviolet–Visible spectroscopy (UV/Vis and UV/Vis CD), Multi-Angle Light Scattering (MALS), Size Exclusion Chromatography (SEC), Protein crystallization, Nuclear Magnetic Resonance (NMR) (1D ^{1}H NMR and 2D ^{1}H-^{15}N HSQC) and Sample preparation for the aforementioned. I also exploited techniques by preparing samples for Small-angle X-ray scattering (SAXS) performed at EMBL (Hamburg Syncrothon), X-ray crystallography performed at ESRF (Grenoble), Electron Paramagnetic Resonance (EPR) and Paramagnetic NMR (para-NMR) performed at CERM.

I contributed to the findings that NFU1 can bind a [4Fe-4S] cluster as a dimer after chemical reconstitution *in vitro*, while it can form a [4Fe-4S] cluster from [2Fe-2S] GLRX5-BOLA3 and not [2Fe-2S] GLRX5. The latter indicates a possible role of BOLA3 as a molecular «switch» for the NFU1-related pathway.

I managed to crystalize IBA57 and contributed to determine its structure by in-house protein X-ray crystal diffraction. I found that, *in vitro*, IBA57 cannot bind alone a cluster but cooperates with ISCA2 to bind a [2Fe-2S] cluster in an hetero-dimeric complex providing oxygen resistance with respect to the oxygen sensitive [2Fe-2S] ISCA2 system.

The ligands coordinating the cluster were also determined indirectly, following a mutagenesis scheme, while its functionality was validated by successfully increasing the activity of Aconitase. I also found that IBA57 does not interact with ISCA1 *in vitro*.

CHAPTER 2

RESULTS

2.1 Structure and potential role of IBA57

IBA57 is implicated, along with the ISCA proteins, in the late steps of the mitochondrial Fe-S protein biogenesis pathway for the maturation of [4Fe-4S] clusters. The phenotype of the impairment of the expression of this protein is similar to that of NFU1, BOLA3, ISCA1 and ISCA2 proteins (MMDS). [28][44] Little is known about the role and the actual functional partners of this protein since there are no structural or *in vitro/vivo* data to support any of the aforementioned.

2.1.1 Novel insights of the role of IBA57

I developed a protocol for the expression and purification of IBA57 from E. coli cells and I contributed to the determination of its structure by X-ray crystallography. By a combination of NMR, EPR, UV/Vis, UV/Vis CD, DLS, SAXS and SEC techniques, I discovered that, in vitro, (i) IBA57 cannot bind a cluster on its own but cooperates with ISCA2 to bind a [2Fe-2S] cluster in an hetero-dimeric complex which is stable upon oxygen exposure for ~15 hours, in contrast to the oxygen sensitive [2Fe-2S] ISCA2, (ii) the ligands coordinating the cluster at the [2Fe-2S] ISCA2-IBA57 are all cysteines and originate, one, from IBA57 and, three, from ISCA2, (iii) [2Fe-2S] ISCA2-IBA57 successfully increased the activity of Aconitase (~70% in 45 minutes) and (iv) IBA57 does not interact with ISCA1.

Based on these data, it is supported that IBA57 works as an oxygen protective agent during oxidative stress conditions and maybe could be partnering with ISCA2 to repair and/or mediate a [4Fe-4S] cluster to apo-proteins positioned later on the mitochondrial Fe-S cluster biogenesis pathway.

The whole study is described in the published scientific article which is apposed below.

……

JACS JOURNAL OF THE AMERICAN CHEMICAL SOCIETY
Article
Cite This: J. Am. Chem. Soc. XXXX, XXX, XXX−XXX
pubs.acs.org/JACS

IBA57 Recruits ISCA2 to Form a [2Fe-2S] Cluster-Mediated Complex

Spyridon Gourdoupis,[†,§] Veronica Nasta,[†,‡,§] Vito Calderone,[†,‡] Simone Ciofi-Baffoni,*[,†,‡] and Lucia Banci*[,†,‡]

[†]Magnetic Resonance Center CERM, University of Florence, Via Luigi Sacconi 6, 50019 Sesto Fiorentino, Florence, Italy
[‡]Department of Chemistry, University of Florence, Via della Lastruccia 3, 50019 Sesto Fiorentino, Florence, Italy

Supporting Information

ABSTRACT: The maturation of mitochondrial iron-sulfur proteins requires a complex protein machinery. Human IBA57 protein was proposed to act in a late phase of this machinery, along with GLRX5, ISCA1, and ISCA2. However, a molecular picture on how these proteins cooperate is not defined yet. We show here that IBA57 forms a heterodimeric complex with ISCA2 by bridging a [2Fe-2S] cluster, that [2Fe-2S] cluster binding is absolutely required to promote the complex formation, and that the cysteine of the conserved motif characterizing IBA57 protein family and the three conserved cysteines of the ISCA protein family act as cluster ligands. The [2Fe-2S] heterodimeric complex is the final product when IBA57 is either exposed to [2Fe-2S] ISCA2 or in the presence of [2Fe-2S] GLRX5 and apo ISCA2. We also find that the [2Fe-2S] ISCA2-IBA57 complex is resistant to highly oxidative environments and is capable of reactivating apo aconitase *in vitro*. Collectively, our data delinate a [2Fe-2S] cluster transfer pathway involving three partner proteins of the mitochondrial ISC machinery, that is, GLRX5, ISCA2 and IBA57, which leads to the formation of a [2Fe-2S] ISCA2-IBA57 complex.

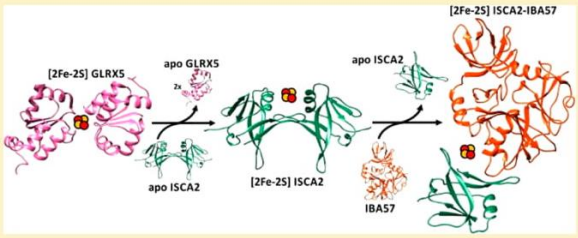

INTRODUCTION

The biogenesis of iron-sulfur (Fe-S) proteins in humans is a multistage process occurring in different cellular compartments.[1−4] In mitochondria, this process is accomplished by the so-called iron-sulfur cluster (ISC) assembly machinery.[5] Members of the mitochondrial ISC assembly machinery include the A-type ISC proteins and monothiol glutaredoxins.[6−10] The human genome encodes two A-type ISC proteins, termed ISCA1 and ISCA2, which are functionally related to the *Saccharomyces cerevisiae* Isa1 and Isa2.[11] The latter were shown to be specifically required for the maturation of mitochondrial [4Fe-4S] proteins.[12,13] In yeast, Isa1 and Isa2 interact with monothiol glutaredoxin-5, the protein receiving a *de novo* assembled [2Fe-2S] cluster from a scaffold protein of the mitochondrial ISC assembly machinery.[9,14] Isa1 and Isa2 form a heterocomplex, and both interact with Iba57, another mitochondrial protein of the ISC assembly machinery which contains a highly conserved motif, KGC(Y/F)XGQE, that characterizes a protein family (PTHR22602 and COG0354) of unknown biochemical function, widely represented across eubacterial and eukaryotic taxa, including humans.[12,15−17] Deletions of either yeast *ISA1*, *ISA2*, or *IBA57* genes elicit identical phenotypes, with yeast cells lacking a functional respiratory chain, functional mitochondrial aconitase proteins, and lipoic acid.[12,15] Based on all these data, it has been proposed that the three yeast proteins might act in the same biochemical process by forming a complex.[5] Specifically, it has been suggested that a hetero-oligomeric complex formed by Isa1, Isa2, and Iba57 is the functional unit in *S. cerevisiae* specifically devoted to convert two [2Fe-2S] clusters to a [4Fe-4S] cluster. This model has been proposed to hold also in humans[18] on the basis of the following experimental data: (i) the maturation of mitochondrial [4Fe-4S] proteins, including aconitase, respiratory complex I, succinate dehydrogenase, and lipoic acid synthase, was impaired upon depletion of each of the three human proteins, similarly to what it occurs in yeast;[11] (ii) the human IBA57 complements the yeast *iba57*Δ growth defects, demonstrating its conserved function throughout the eukaryotic kingdom.[15]

Recent data, however, outlined new possible views on how these three proteins can work in the mitochondrial ISC assembly machinery. Surprisingly, recent knockdown experiments in mouse skeletal muscle and in primary cultures of neurons indicated that ISCA1, and not ISCA2 and IBA57, is required for mitochondrial [4Fe-4S] proteins biogenesis.[19] Moreover, although ISCA1 and ISCA2 reciprocally interact both *in vivo* and *in vitro*,[19,20] only ISCA2 interacts with IBA57 at variance of what was observed in yeast.[19] These results suggested that human ISCA1, ISCA2, and IBA57 do not necessarily act as a ternary complex as proposed for the yeast homologues, but they might modulate their interactions network in a complex and dynamic manner, possibly depending on the physiological state of human cells, tissue, and termporal specificity.[19] Other data supporting the formation of a specific complex between ISCA2 and IBA57

Received: August 22, 2018
Published: October 1, 2018

DOI: 10.1021/jacs.8b09061
J. Am. Chem. Soc. XXXX, XXX, XXX−XXX

and not with ISCA1 originate from *in vivo* expression level studies. Specifically, patients with pathogenic *IBA57* mutations that markedly reduce the protein levels of IBA57 in fibroblasts mitochondria displayed expression levels of ISCA1 in normal range or slightly overexpressed, while the ISCA2 expression levels were found drastically decreased in all patients.[21] These results are in line with studies performed in HeLa cells where the silencing of IBA57 was associated with unchanged or increased expression of ISCA1.[11] It has also been shown by us through *in vitro* biochemical studies that a heterocomplex between ISCA1 and ISCA2 acts as a platform to assemble a [4Fe-4S] cluster from two [2Fe-2S] clusters donated by dimeric human glutaredoxin GLRX5, without any requirements of IBA57.[20,22,23] These data thus support the model that multiple pathways might be operative for ISCA1, ISCA2, and IBA57.[19] Collectively, the available functional and biochemical data do not allow yet to define a molecular picture on how the ISCA1, ISCA2, and IBA57 proteins cooperate in the mitochondrial ISC assembly machinery, but only suggest that cellular processes with different involvement of ISCA1, ISCA2, and IBA57 might exist. To get further insights on the function of these partner proteins, we have here characterized the interactions among GLRX5, ISCA1, ISCA2, and IBA57 via complementary biophysical techniques. Our results delinate a cluster transfer pathway involving GLRX5, ISCA2 and IBA57, which ends in the formation of a [2Fe-2S] cluster-mediated ISCA2-IBA57 complex, which is resistant to a highly oxidative environment and able to reactivate apo aconitase.

■ EXPERIMENTAL SECTION

Cloning and Mutagenesis. The gene of human IBA57 (lacking the mitochondrial targeting sequence of 30 amino acids) was made available and inserted in the *Eco*RI-SalI cloning site (MCS1) of a pETDuet-1 vector having a N-terminal His-tag at MCS1 site by Twin Helix Srl company. Cys 230 to Ala substitution in IBA57 was obtained by site-directed mutagenesis (QuickChange Site-directed Mutagenesis Kit, Agilent Technologies) applied on the pETDuet-1 vector containing the IBA57 gene.

Protein Expression and Purification. The pETDuet-1 plasmid containing N-terminal His-tag IBA57 was transformed in *Escherichia coli* BL21-Gold(DE3) (Agilent) competent cells. Cells were cultivated overnight (O/N) at 37 °C in Luria−Bertani (LB) media adding ampicillin (100 μg/mL) and 3% of ethanol per liter of sterile LB. The following day the cells were spun down (3000 rpm for 20 min) and resuspended in 1 L of fresh LB or minimal media [with 1 g $(^{15}NH_4)_2SO_4$ and 3 g glucose] containing ampicillin (100 μg/mL) and 3% of ethanol. The culture was left at 37 °C, 160 rpm for approximately 1 h, and then a heat shock procedure [10 min at 42 °C (160 rpm), 20 min at 37 °C (160 rpm), 30 min in ice and 20 min at 37 °C (160 rpm)] was performed on the culture to induce a high level of heat shock *E. coli* proteins, in order to allow effective enhancement of the solubility and thereby the yield of overexpressed protein in *E. coli*.[24] Protein expression was then induced by adding 0.1 mM of isopropyl β-D-1-thiogalactopyranoside (IPTG), shaking O/N at 18−20 °C (160 rpm).

The cell paste was dissolved in the binding buffer (50 mM phosphate buffer, 500 mM NaCl, 20 mM imidazole, pH 7.6), and after sonication, the N-terminal His-tag IBA57 protein was purified from *E. coli* using a HisTrap HP column (GE Healthcare). The His-tag was cleaved by tobacco etch virus protease (1 mg) O/N at room temperature in 50 mM phosphate buffer, 500 mM NaCl, 500 mM imidazole, pH 7.6. A second His-trap chromatography column on the latter mixture was performed to separate digested IBA57 from His-tag IBA57. Recovered IBA57 was pure enough to be used for spectroscopic and biochemical studies. To obtain a highly purified sample for crystallization trials, a size exclusion chromatography using a HiLoad 16/60 SuperdexTM 75 pg column, attached to an ÄKTA pure chromatography unit, was performed. The final yield was about 14 mg per liter of culture. 2.5 mM tris (2-carboxyethyl) phosphine (TCEP) was added in all the purification steps to avoid disulfide bond formation. The same procedure was followed to produce the Cys230Ala IBA57 mutant, wherein the yield was about 21 mg per liter of culture.

The expression and purification of wild-type apo- and holo- ISCA1, ISCA2, and GLRX5 proteins and of Cys79Ser, Cys144Ser, and Cys146Ser ISCA2 mutants were obtained as already reported.[20,22,23]

Apo ISCA1 and 1:1 (referring to monomeric protein concentrations) protein mixtures of apo ISCA1-IBA57, apo ISCA2-IBA57 (or Cys230Ala IBA57), and apo Cys79Ser or Cys144Ser or Cys146Ser ISCA2-IBA57 were chemically reconstituted in anaerobic conditions in 50 mM Tris-HCl, 100 mM NaCl, 5 mM DTT buffer at pH 8.0 with three-fold $FeCl_3$ and Na_2S for 16 h at room temperature. Chemical reconstitution was performed with protein concentration range from 30 to 50 μM. The [2Fe-2S] cluster-bound form of ISCA2 was obtained by anaerobic chemical reconstitution in the same conditions as above but with stoichiometric $FeCl_3$ and Na_2S for 16 h at room temperature. The latter procedure produced a mixture of apo and [2Fe-2S] cluster bound ISCA2 in ratios ranging from 30:70 to 40:60.

Cytosolic aconitase was expressed and purified by using pT7-his-hIRP1 plasmid, kindly provided by Prof. Matthias W. Hentze, European Molecular Biology Laboratory (EMBL), Heidelberg, Germany. The production and chemical reconstitution of aconitase was obtained following a previously reported protocol.[25]

Spectroscopic, Biophysical, and Activity Analysis. UV−vis and CD spectra were acquired at 20 °C, aerobically or anaerobically in degassed buffer (50 mM phosphate buffer, 150 mM NaCl, 5 mM DTT, pH 7.0) on a Cary 50 Eclipse spectrophotometer and JASCO J-810 spectropolarimeter, respectively.

SEC-MALS data were acquired by attaching a SuperdexTM 200 Increase 10/300 GL column to a DAWN HELEOS system with a continuous flow rate of 0.6 mL/min using a filtered buffer (50 mM phosphate buffer, 150 mM NaCl, pH 7.0). Analytical gel filtration was performed by attaching a SuperdexTM 200 Increase 10/300 GL column to an ÄKTA pure chromatography unit with a flow rate of 0.75 mL/min using a buffer consisting of 50 mM phosphate buffer, 150 mM NaCl, pH 7.0.

Aerobically purified cytosolic aconitase (5 μM) was incubated at 25 °C for 45 min with the five-fold excess of [2Fe-2S] ISCA2-IBA57 complex in 50 mM phosphate buffer, 150 mM NaCl, 5 mM DTT, pH 7.0. The reaction was then followed by measuring aconitase activity. The aconitase activity was assayed by the Aconitase Activity Assay kit (Sigma-Aldrich MAK051) as described in Maione et al.[25]

AMS-Based Alkylation Gel Shift Assay. A gel shift assay on samples previously modified with 4-acetamido-4-maleimidylstilbene-2,2-disulfonic acid (AMS) was performed.[26] For this purpose, IBA57, Cys230Ala IBA57, and the [2Fe-2S] ISCA2-IBA57 were incubated with 10 mM AMS in 50 mM phosphate buffer, pH 7.0, 150 mM NaCl for 30 min at 25 °C. Samples were then precipitated with 10% trichloroacetic acid. Pellets were washed with acetone and resuspended in 80 mM Tris-HCl, pH 6.8, 8 M urea. Samples were separated by nonreducing SDS-PAGE, and the gel was stained with Coomassie Blue. AMS reacts with available thiol groups, resulting in a mobility shift of the protein on SDS-PAGE due to its increase in size of 0.5 kDa per added molecule AMS.

X-ray Crystallography. Crystals of wild-type and Cys203Ala IBA57 were grown by the sitting-drop vapor diffusion method at 25 °C by mixing equal volumes (2 μL) of the protein solution and the reservoir solution. The protein concentration range was 0.2−0.4 mM, in 50 mM phosphate buffer, 150 mM NaCl, and 2.5 mM TCEP, pH 7.0. The reservoir solution used for both consisted of 20% (w/v) PEG 3350 and 200 mM NaCl. In the case of wild-type IBA57 crystals, a reservoir solution consisting of 20% (w/v) PEG 3350 and 200 mM NaCl and 100 mM MES pH 6.0 was also used. The structure determination has been carried out through anomalous dispersion.

DOI: 10.1021/jacs.8b09061
J. Am. Chem. Soc. XXXX, XXX, XXX−XXX

Journal of the American Chemical Society Article

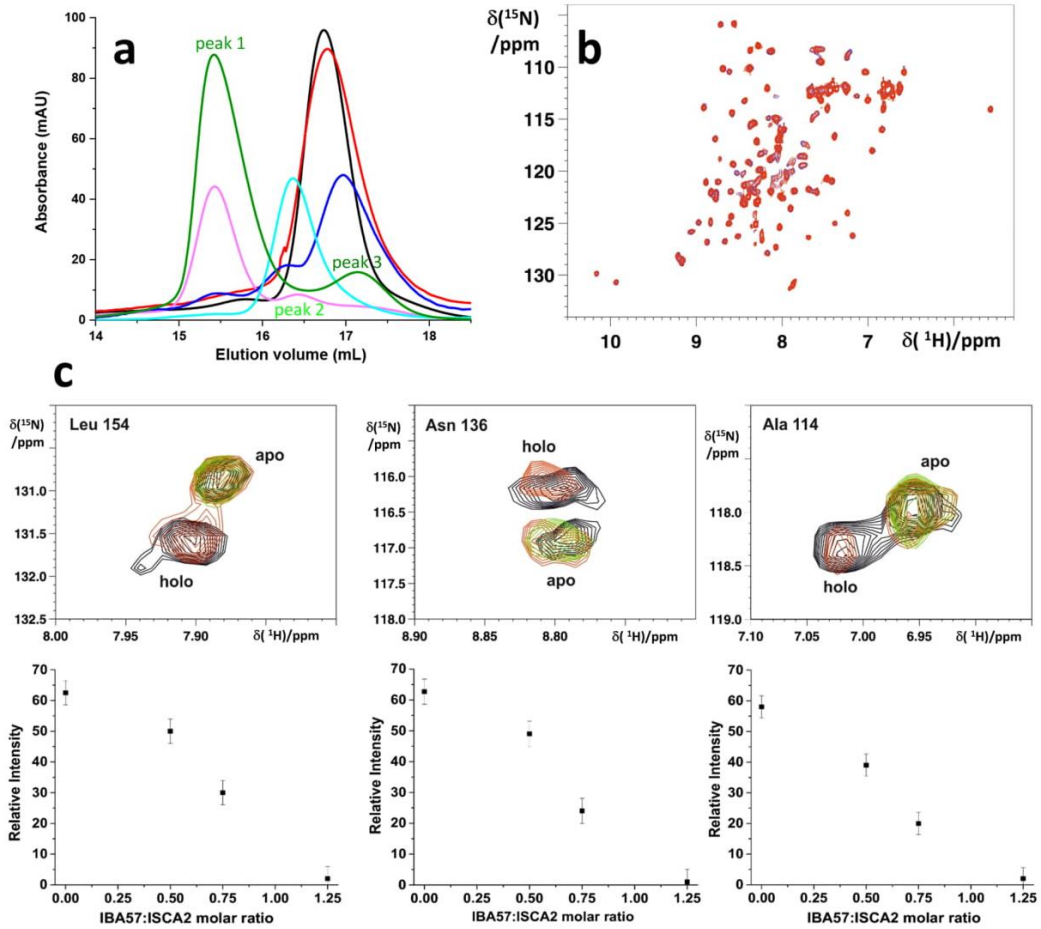

Figure 1. Complex formation between [2Fe-2S] ISCA2 and IBA57. (a) Elution profiles obtained for IBA57 (black), apo ISCA2 (blue), [2Fe-2S] ISCA2 (cyano), a 1:1 mixture of IBA57 and apo ISCA2 (red), a 1:0.5 and 1:1 (these two ISCA2:IBA57 ratios based on dimeric [2Fe-2S] ISCA2 concentration vs monomeric IBA57 concentration) mixture of IBA57 and [2Fe-2S]/apo ISCA2 (magenta and dark green, respectively) by gel filtration on analytical SuperdexTM 200 Increase 10/300 GL column. mAU: milli absorbance unit. (b) Overlay of $^{1}H-^{15}N$ HSQC spectra of ^{15}N-labeled apo ISCA2 (0.7 mM) in the absence (blue) and in the presence (red) of 1 equiv of IBA57. (c) In the upper panels, $^{1}H-^{15}N$ HSQC spectral regions for three residues of ^{15}N-labeled [2Fe-2S]/apo ISCA2 (0.6 mM: 0.35 mM [2Fe-2S] ISCA2 and 0.25 mM apo ISCA2) with the apo and the holo forms in slow exchange on the NMR time scale are shown in the absence (black) and in the presence of 0.5 equiv (red) and 1 equiv (green) of IBA57 relative to [2Fe-2S] ISCA2 concentration. In the lower panels, the relative intensity of the backbone amide signals of these three residues for the holo species is plotted against the IBA57:ISCA2 ratio. Data are represented as the mean of three measurements ± s.d.

EPR and NMR Spectroscopy. EPR spectra of the [2Fe-2S] ISCA2-IBA57 complex (400 μM) were recorded before and after anaerobic reduction of the cluster by addition of sodium dithionite and rapid freezing of the protein solution in liquid nitrogen. EPR spectra were recorded in degassed 50 mM phosphate buffer, 150 mM NaCl, 5 mM DTT, pH 7.0, and 10% (v/v) glycerol at 45 K or 5 K, using a Bruker Elexsys E500 spectrometer working at a microwave frequency of ca. 9.39 GHz, equipped with a SHQ cavity and a continuous cryostat He flow (ESR900, Oxford instruments) for temperature control. Acquisition parameters were as follows: microwave power 5 mW; modulation frequency 100 kHz; modulation amplitude 8.0 G; acquisition time constant 163.84 ms; number of points 1024.

NMR experiments were recorded on Bruker AVANCE 400, 700, 900, and 950 MHz spectrometers at 298 K on 0.3−1 mM protein samples, in 50 mM phosphate buffer, 5 mM DTT, and 150 mM NaCl, pH 7.0, and 10% (v/v) D_2O. Spectra were processed using TopSpin (Bruker BioSpin) and analyzed with CARA software. The interaction between [2Fe-2S]/apo ISCA2 and IBA57 was followed by $^{1}H-^{15}N$ HSQC NMR spectra titrating ^{15}N-labeled apo/[2Fe-2S] ISCA2 with unlabeled apo IBA57 up to a 1:1 protein ratio (ISCA2:IBA57 protein ratio based on dimeric [2Fe-2S] ISCA2 concentration vs monomeric IBA57 concentration). Cluster transfer from homodimeric [2Fe-2S] GLRX5 to apo ISCA2/IBA57 mixture was followed by $^{1}H-^{15}N$ HSQC NMR spectra titrating a 1:1 mixture of ^{15}N-labeled apo ISCA2 and unlabeled IBA57 up to a final 1:1:2 ratio referring to monomeric protein concentrations. NMR titrations were successfully repeated three times in all cases.

1D ^{1}H paramagnetic-tailored NMR experiments were performed at 400 MHz with a ^{1}H optimized 5 mm probe. Water signal was suppressed via fast repetition experiments and water selective irradiation. Experiments were typically performed using an acquisition time of 50 ms and an overall recycle delay of 90 ms. The heterocomplex concentration was 0.5 mM. Squared cosine and exponential multiplications were applied prior to Fourier transformation. Manual baseline correction was performed, using polynomial functions.

The interaction of IBA57 with tetrahydrofolic acid (THF) and the calcium salt of folinic acid (calcium folinate) was followed, respectively, by $^{1}H-^{15}N$ HSQC NMR titration experiments at 298

DOI: 10.1021/jacs.8b09061
J. Am. Chem. Soc. XXXX, XXX, XXX−XXX

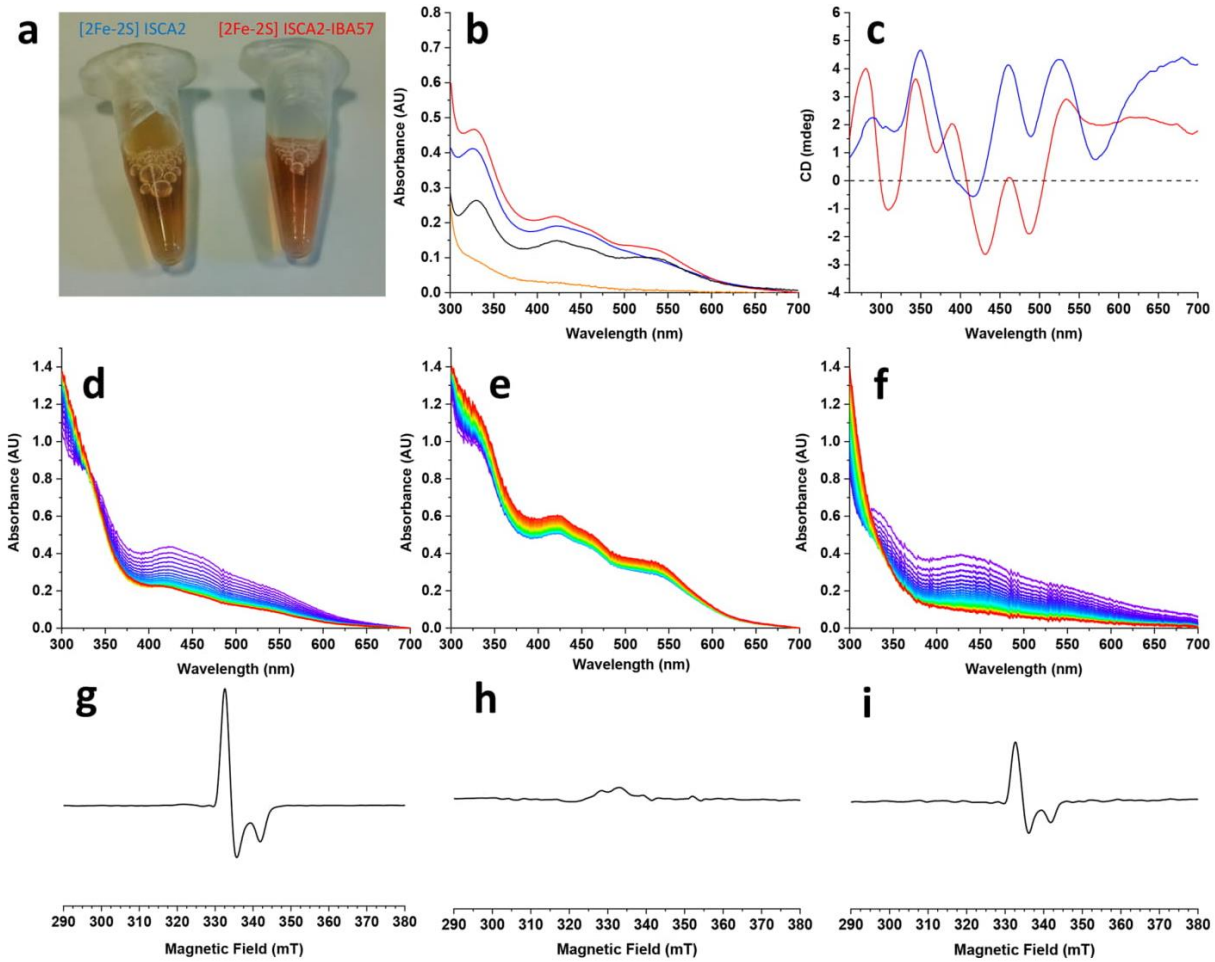

Figure 2. The ISCA2-IBA57 complex binds a [2Fe-2S] cluster as observed by UV−vis, CD, and EPR spectroscopies. (a) Pictures of [2Fe-2S]/apo ISCA2 before (on the left) and after (on the right) the addition of 1 equiv of IBA57 with respect to dimeric [2Fe-2S] ISCA2 concentration. (b) UV−vis spectra of [2Fe-2S]/apo ISCA2 (blue), of a 1:1 mixture of IBA57 and [2Fe-2S]/apo ISCA2 (red), of peak 1 fractions obtained by gel filtrating the 1:1 [2Fe-2S]/apo ISCA2-ISCA57 mixture (black), and of peak 3 fractions obtained by gel filtrating the 1:1 [2Fe-2S]/apo ISCA2-ISCA57 mixture (orange). AU: absorbance unit. (c) CD spectra of [2Fe-2S]/apo ISCA2 (blue), of a 1:1 mixture of IBA57 and [2Fe-2S]/apo ISCA2 (red). UV−vis spectra of (d) [2Fe-2S]/apo ISCA2, (e) of a 1:1 mixture of IBA57 and [2Fe-2S]/apo ISCA2, and (f) of the chemically reconstituted 1:1 ISCA2-Cys230Ala IBA57 mixture, collected upon air exposure every 30 min for 15 h. The colors of the traces follow visible spectrum trend from violet (starting point) to final point (red). X-band EPR spectra of the 1:1 mixture of IBA57 and [2Fe-2S]/apo ISCA2 at 45 K before (g) and after (h) being exposed overnight in air and (i) upon addition of two equivalents of dithionite. The experiments were conducted with protein concentration of dimeric ISCA2 ranging from 0.075 mM to 0.3 mM depending on the applied spectroscopic technique.

K and by ^{1}H 1D enhanced Protein Hydration Observed by Gradient Spectroscopy (ePHOGSY) NMR experiments at 298 K.[27] The sample for the ^{1}H−^{15}N HSQC NMR experiments was 0.35 mM in ^{15}N-labeled IBA57 final concentration and 0.7 mM in THF final concentration. Samples of ePHOGSY experiments were 10 μM in IBA57 concentration and 5 mM in calcium folinate concentration, in 50 mM phosphate buffer, 150 mM NaCl, 10% D_2O, and trimethylsilylpropanoic acid as an internal standard. NMR experiments to follow the interaction of tetrahydrofolate derivatives with IBA57 were repeated twice. ePHOGSY NMR experiments were also performed on the [2Fe-2S] ISCA2-IBA57 heterocomplex (10 μM) in the presence of 1 mM calcium folinate.

Data Availability. Coordinates and structure factors of IBA57 and Cys230Ala IBA57 have been deposited under accession codes 6ESR and 6GEU, respectively.

RESULTS

IBA57 Forms a Complex with ISCA2 upon [2Fe-2S] Cluster Binding. Analytical gel filtration equipped with multiangle light scattering (SEC-MALS) showed that IBA57 elutes as a single peak with a molar mass of 37.4 ± 0.5 kDa (Figure 1a and Figure S1), which is close to the molecular weight calculated from the cloned amino acid sequence (34925 Da). The protein is unable to bind a Fe-S cluster, either through various chemical reconstitution procedures or when produced by cells supplemented with excess of iron ions. Furthermore, IBA57 is unable to receive a [2Fe-2S] cluster from human monothiol glutaredoxin-5 (GLRX5), which typically donates [2Fe-2S] clusters to several possible acceptors.[23,28,29] These data indicate that the protein is monomeric and cannot bind a Fe-S cluster on its own.

DOI: 10.1021/jacs.8b09061
J. Am. Chem. Soc. XXXX, XXX, XXX−XXX

Since human ISCA2 has been found to specifically interact *in vivo* with IBA57,[19] the interaction of IBA57 with both apo and [2Fe-2S]-bound forms of ISCA2 was analyzed *in vitro* by SEC-MALS and NMR. ISCA2 is a dimer in both the apo and the holo forms and can bind a [2Fe-2S] or a [4Fe-4S] cluster at the same binding site, through Cys 79 from the two subunits of the dimer, Cys 144 from one subunit, and Cys 146 from the other subunit.[20,22] When IBA57 is mixed with apo ISCA2, no complex formation occurs between the two proteins. Indeed, SEC-MALS of the protein mixture at 1:1 protein ratio did not show the presence of any peak at elution volumes higher than those of monomeric IBA57 and dimeric apo ISCA2 in any tested condition (Figure 1a). $^{1}H-^{15}N$ HSQC NMR experiments, performed on ^{15}N-labeled apo ISCA2 stepwise titrated with unlabeled IBA57 up to a 1:1 protein ratio, did not show any chemical shift variation or line-broadening effect, indicating again that the two proteins do not interact with each other in the absence of a Fe-S cluster bound to ISCA2 (Figure 1b). On the contrary, when IBA57 is added, in anaerobic conditions, to the mixture of apo and $[2Fe\text{-}2S]^{2+}$ cluster-bound ISCA2, as it is obtained after ISCA2 chemical reconstitution ([2Fe-2S]/apo ISCA2, hereafter, see Experimental Section for details), SEC-MALS showed the formation of a new species eluting with a molar mass of 51.2 ± 0.5 kDa (peak 1 in Figure 1a and Figure S1), which is close to the sum of the molecular weights of a molecule of monomeric ISCA2 (12565 Da) and a molecule of monomeric IBA57 (34925 Da), as calculated from the cloned amino acid sequences. SDS-PAGE performed on the elution fractions of this new species showed that they contain both IBA57 and ISCA2 proteins, according to complex formation between the two proteins (Figure S2). In line with the formation of a heterodimeric ISCA2-IBA57 complex, a minor peak (peak 2 in Figure 1a) with an elution volume of [2Fe-2S] ISCA2 is present when IBA57 is substoichiometrically added to [2Fe-2S]/apo ISCA2, while a minor peak (peak 3 in Figure 1a) with the same elution volume of apo ISCA2 is observed when IBA57 is present at the stoichiometric ratio. $^{1}H-^{15}N$ HSQC NMR experiments were performed on a ^{15}N-labeled [2Fe-2S]/apo ISCA2 stepwise titrated with unlabeled IBA57. Line-broadening in the NMR spectra was observed exclusively on the backbone NH cross-peaks of the [2Fe-2S] ISCA2 species, while the line-width of the apo ISCA2 cross-peaks remain unchanged (Figure 1c). The line-broadening effects on the cross-peaks of the [2Fe-2S] ISCA2 species increase with the additions, until some signals disappeared once a final 1:1 protein ratio was reached (Figure 1c). Overall, SEC-MALS and NMR data showed that a subunit of homodimeric [2Fe-2S] ISCA2 is replaced by IBA57 to form a heterodimeric complex and that apo ISCA2, which does not interact with IBA57, is released in solution. These data also demonstrated that cluster binding is required to promote complex formation between ISCA2 and IBA57 proteins. We can therefore define such interaction as cluster mediated.

As a Fe-S cluster is required to induce complex formation, we could deem that IBA57 is involved in Fe-S cluster binding in the complex providing one or more cluster ligand(s). In order to investigate such a possibility, a combination of UV–vis absorption, UV–vis circular dichroism (CD), and EPR spectroscopies has been applied to analyze the nature and properties of the cluster bound to the complex. Upon mixing [2Fe-2S]/apo ISCA2 with IBA57, the UV–vis spectra showed an increase of the band at 540 nm, which is very weak in $[2Fe\text{-}2S]^{2+}$ ISCA2, with a simultaneous change of the color of the solution from yellowish-brown to pinkish-red (Figure 2a,b). The UV–vis spectrum of the mixture maintains all the absorption bands of biological oxidized $[2Fe\text{-}2S]^{2+}$ centers, which typically have bands centered at around 330, 420, 460, and 550 nm, all attributable to S–Fe(III) charge-transfer (CT) transitions (Figure 2b).[30] Also paramagnetic NMR spectroscopy indicates the presence of a bound $[2Fe\text{-}2S]^{2+}$ cluster. Indeed, the paramagnetic 1D ^{1}H spectrum showed the presence of broad signals at 37, 28, and 23 ppm and a sharper one at 13 ppm (Figure S3), all of them typical of H_{β} and H_{α} protons, respectively, of Cys residues bound to a $[2Fe\text{-}2S]^{2+}$ cluster with an $S = 0$ electronic ground state.[31,32]

The band at 540 nm in the UV–vis spectrum of the mixture has higher intensity and is better resolved than those typically observed in plant ferredoxins and adrenodoxin/putidaredoxin proteins,[33] whose UV–vis spectra resemble that of $[2Fe\text{-}2S]^{2+}$ ISCA2. An intense band at around 540 nm is present in the $[2Fe\text{-}2S]^{2+}$ centers of the so-called "red paramagnetic" ferredoxins, that is, from *Clostridium pasteurianum* and *Azotobacter vinelandii*, also having all-cysteinyl ligands as found in plant ferredoxins and adrenodoxin/putidaredoxins.[34,35] The observed spectral changes originate from the formation of the ISCA2-IBA57 complex, where the [2Fe-2S] cluster is exclusively bound to the complex. Indeed, when the [2Fe-2S] ISCA2-IBA57 1:1 protein mixture was passed through an analytical gel filtration column and the fractions of peaks 1 and 3 collected, the UV–vis spectrum of peak 1 fractions showed the same visible bands as those observed before gel filtrating the [2Fe-2S]/apo ISCA2-IBA57 mixture, while the visible bands in peak 3 fractions were absent (Figure 2b). These results strongly support that, upon mixing [2Fe-2S]/apo ISCA2 with IBA57, [2Fe-2S] ISCA2 quantitatively forms a complex with IBA57 via a shared binding of a [2Fe-2S] cluster. In agreement with this model, the CD spectrum of the $[2Fe\text{-}2S]^{2+}$ cluster in the [2Fe-2S]/apo ISCA2-IBA57 mixture is significantly different from that of the $[2Fe\text{-}2S]^{2+}$ cluster in [2Fe-2S] ISCA2 (Figure 2c), indicating differences in the cluster coordination and/or in the chirality of the cluster environment of the $[2Fe\text{-}2S]^{2+}$ clusters in ISCA2-IBA57 heterodimer with respect to ISCA2 homodimer.

The cluster stability of [2Fe-2S] ISCA2-IBA57 vs [2Fe-2S] ISCA2 upon oxygen exposure was then investigated by UV–vis spectroscopy, exposing the holo protein samples to air and collecting UV–vis spectra every 30 min for 15 h. It resulted that the Fe-S cluster in [2Fe-2S] ISCA2 is gradually degraded over a period of ~5 h, indicating that it is oxidatively labile. A rapid decrease of the adsorption bands between 300 and 700 nm characteristic of the $[2Fe\text{-}2S]^{2+}$ center was, indeed, observed (Figure 2d), resulting in the complete loss of the cluster, as assessed from the UV–vis spectrum acquired after gel-filtrating the final air-exposed protein. In contrast, in the heterodimer, the typical adsorption bands of the $[2Fe\text{-}2S]^{2+}$ cluster increased in intensity upon oxygen exposure and then remained stable in air for a few days (Figure 2e). This indicates that IBA57, by binding to [2Fe-2S] ISCA2, stabilizes the $[2Fe\text{-}2S]^{2+}$ cluster against oxidative degradation. The observed increase of the Fe-S cluster adsorption bands may be due to the presence of a fraction of the ISCA2-IBA57 complex having the cluster in a reduced $[2Fe\text{-}2S]^{+}$ state, which, then, slowly oxidizes to the $[2Fe\text{-}2S]^{2+}$ state upon oxygen exposure. The absorption bands of biological reduced $[2Fe\text{-}2S]^{+}$ clusters typically have lower intensities than those of oxidized $[2Fe\text{-}2S]^{+2}$ centers.[34] Therefore, upon cluster oxidation, the

DOI: 10.1021/jacs.8b09061
J. Am. Chem. Soc. XXXX, XXX, XXX–XXX

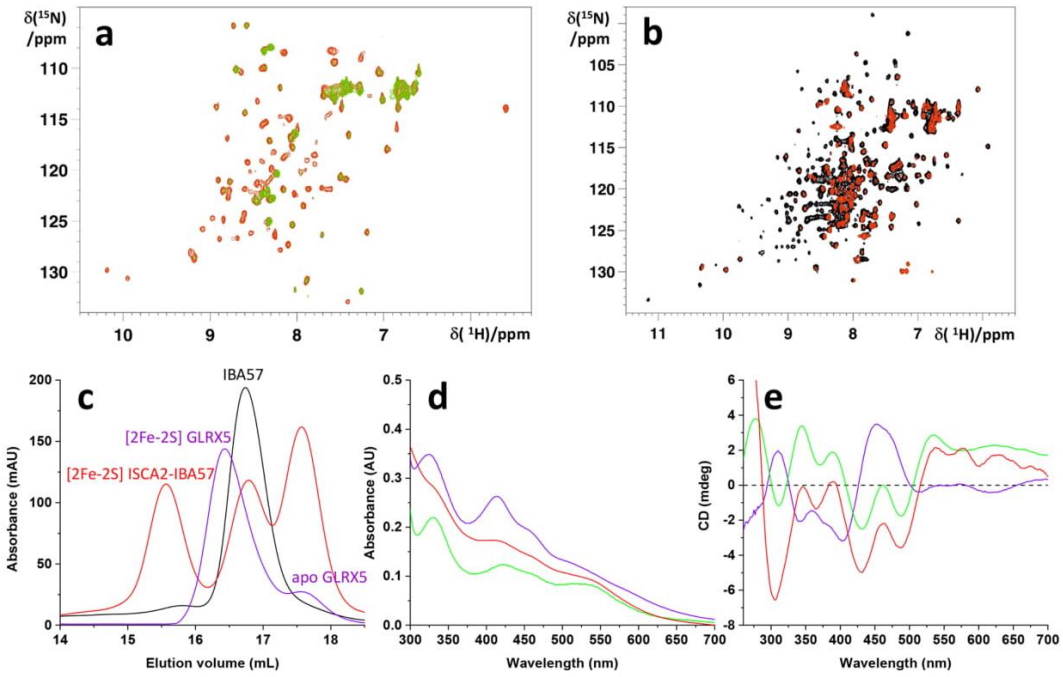

Figure 3. [2Fe-2S] ISCA2-IBA57 complex formation by mixing [2Fe-2S] GLRX5, apo ISCA2, and IBA57. Overlay of $^{1}H-^{15}N$ HSQC spectra: (a) ^{15}N-labeled apo ISCA2 (0.6 mM) (red) and a 1:1:2 mixture of ^{15}N-labeled apo ISCA2 (0.6 mM), unlabeled IBA57, unlabeled $[2Fe\text{-}2S]^{2+}$ GLRX5 (green), (b) ^{15}N-labeled IBA57 (0.5 mM) (black) and a 1:1:2 mixture of ^{15}N-labeled IBA57 (0.5 mM), unlabeled apo ISCA2, unlabeled $[2Fe\text{-}2S]^{2+}$ GLRX5 (red). (c) Elution profiles obtained for IBA57 (black), $[2Fe\text{-}2S]^{2+}$ GLRX5 (violet), a 1:1:1 mixture of apo ISCA2, IBA57 and $[2Fe\text{-}2S]^{2+}$ GLRX5 (red) by gel filtration on analytical SuperdexTM 200 Increase 10/300 GL column. mAU: milli absorbance unit. UV–vis (d) and CD (e) spectra of $[2Fe\text{-}2S]^{2+}$ GLRX5 (violet), of the 1:1 $[2Fe\text{-}2S]$/apo ISCA2-IBA57 mixture (green), and of the 1:1:2 apo ISCA2-IBA57-$[2Fe\text{-}2S]$ GLRX5 mixture (red). The experiments were conducted with monomeric protein concentration ranging from 0.15 mM to 0.6 mM depending on the applied spectroscopic technique.

intensities of the absorption bands of $[2Fe\text{-}2S]^{2+}$ cluster species are expected to increase, as experimentally observed in the UV–vis spectra acquired over time. In order to corroborate this hypothesis, we performed EPR measurements on [2Fe-2S] ISCA2-IBA57 before and after air exposure. The holo complex not exposed to air revealed an axial $S = 1/2$ resonance with $g_z < g_x = g_y$ ($g_\perp = 2.01$, $g_\parallel = 1.96$, $g_{av} \sim 1.99$ at 45 K, Figure 2g), with relaxation properties characteristic of a reduced $[2Fe\text{-}2S]^{+}$ cluster. The g_{av} value is comparable to those of $[2Fe\text{-}2S]^{+}$ centers with complete cysteinyl ligation (typically $g_{av} \sim 1.97$).[36,37] These EPR signals completely disappeared once the sample is exposed to air overnight (Figure 2h), and, upon dithionite reduction, the same signal reappeared (Figure 2i), indicating that the [2Fe-2S] center in the complex can undergo reversible redox cycling. Overall, the data demonstrate that the ISCA2-IBA57 complex can stabilize both reduced $[2Fe\text{-}2S]^{+}$ and oxidized $[2Fe\text{-}2S]^{2+}$ bound clusters.

The complex formation between [2Fe-2S] ISCA2 and IBA57 was also investigated by analyzing a protein mixture containing apo ISCA2, IBA57, and the physiological [2Fe-2S] cluster donor of ISCA proteins, that is, human GLRX5, which bridges an oxidized $[2Fe\text{-}2S]^{2+}$ cluster in a symmetric dimer, coordinating it by two glutathione molecules and two Cys ligands, one from each GLRX5 subunit.[23,38] $^{1}H-^{15}N$ HSQC NMR experiments were performed on a 1:1 apo ISCA2-IBA57 mixture, ^{15}N-labeled in ISCA2 or in IBA57, titrated with unlabeled human $[2Fe\text{-}2S]^{2+}$ GLRX5. Stepwise additions of $[2Fe\text{-}2S]^{2+}$ GLRX5 to the apo ISCA2-IBA57 1:1 mixture cause the NH cross-peaks broadening, until most of them disappear once 2 equiv of $[2Fe\text{-}2S]^{2+}$ GLRX5 were added (Figure 3a,b). Analytical gel filtration performed on the 1:1:1 apo ISCA2-IBA57-[2Fe-2S] GLRX5 mixture of the NMR titration showed the formation of the same peak as that observed by mixing [2Fe-2S]/apo ISCA2 with IBA57, which corresponds to the [2Fe-2S] ISCA2-IBA57 complex (Figure 3c). These data support the claim that the broadening effects observed for the backbone NHs in the $^{1}H-^{15}N$ HSQC experiments are determined by the formation of the large molecular mass protein complex of ISCA2 and IBA57. Analytical gel filtration data also showed the formation of apo GLRX5, whose peak increases in intensity in the 1:1:1 mixture, to the expense of dimeric [2Fe-2S] GLRX5, whose peak is not present in the 1:1:1 mixture (Figure 3c). UV–vis and CD spectra of the final mixture indicated the formation of the [2Fe-2S] ISCA2-IBA57 complex. They showed, indeed, the same bands as those described above (Figure 3d,e). The only difference with respect to the [2Fe-2S]/apo ISCA2-IBA57 mixture is observed in the EPR measurements. Indeed, no EPR signal was observed at 45 K in the final ISCA2-IBA57-GLRX5 mixture, indicating that only an oxidized $[2Fe\text{-}2S]^{2+}$ cluster is bound to the ISCA2-IBA57 complex. Overall, we can conclude that the oxidized $[2Fe\text{-}2S]^{2+}$ cluster is transferred from GLRX5 to ISCA2, which then forms the $[2Fe\text{-}2S]^{2+}$-bound complex with IBA57.

ISCA1 Does Not Form a Cluster-Mediated Complex with IBA57. The possible cluster-mediated interaction of

DOI: 10.1021/jacs.8b09061
J. Am. Chem. Soc. XXXX, XXX, XXX–XXX

IBA57 with ISCA1 was investigated by analytical gel filtration, UV−vis absorption, and CD spectroscopies. When IBA57 is mixed with apo ISCA1, analytical gel filtration of the protein mixture at 1:1 protein ratio did not show the presence of any peak at elution volumes higher than those of monomeric IBA57 and apo ISCA1 (Figure S4). Therefore, no complex formation occurs between the two proteins, as found in the case of apo ISCA2-IBA57 interaction. The 1:1 apo ISCA1-IBA57 mixture was then chemically reconstituted, and UV−vis and CD spectra recorded and compared with those of chemically reconstituted [2Fe-2S] ISCA2-IBA57 complex and [2Fe-2S] ISCA1. These data indicated that no cluster-mediated ISCA1-IBA57 heterocomplex is formed. Indeed, both UV−vis and CD spectra resemble those of [2Fe-2S] ISCA1. Specifically, the band at 540 nm, which is a marker of the formation of the [2Fe-2S] ISCA2-IBA57 heterocomplex, is not present in the UV−vis spectrum of the chemically reconstituted 1:1 ISCA1-IBA57 mixture (Figure S4). Consistent with no complex formation, the analytical gel filtration of the latter mixture did not show the presence of any peak at elution volumes higher than those of monomeric IBA57 and apo ISCA1 (Figure S4). Furthermore, a rapid decrease of the adsorption bands between 300 and 700 nm characteristic of the $[2Fe\text{-}2S]^{2+}$ center was observed upon oxygen exposure, as found in [2Fe-2S] ISCA2 and in contrast to what happened in the case of the [2Fe-2S] ISCA2-IBA57 complex.

Overall, these data indicate that ISCA2, and not ISCA1, specifically interacts with IBA57 to form a cluster-mediated interaction. They support the model proposed by Beilschmidt et al.,[19] which indicated that ISCA2, and not ISCA1, is complexed *in vivo* with IBA57. However, we cannot *a priori* exclude that, in some type of human cells or specific cellular conditions, even ISCA1 and IBA57 might cooperate in Fe-S protein maturation processes.

Structure of IBA57 and Cluster Coordination in ISCA2-IBA57. The crystal structure of IBA57 was determined at 1.75 Å resolution. IBA57 has a globular shape and consists of three tightly packed domains arranged in a rigid ring-like structure (Figure 4a). Only the regions on the protein surface have very poor electron density or high B-factors (Figure S5). Domain A includes residues 17−25 and 127−185 and is formed by a five-stranded antiparallel β-sheet and a short α-helix on one side of the sheet (yellow domain in Figure 4a). Domain B includes residues 26−126 and may be considered as an insertion in domain A. It is formed by a five-stranded antiparallel β-sheet and two α-helices on one side of the β-sheet (gray domain in Figure 4a). Domain C comprises 77 C-terminal residues; it has the topology of a six-strand antiparallel β-barrel with a Greek key connection pattern, and packs perpendicular to the β-sheets of domains A and B, closing the protein ring-like structure (red domain in Figure 4a). A 60-residue segment (residues 186 to 246) is sandwiched among the three domains and, with the exception of two long α-helices and one short 3_{10}-helix, lacks secondary structure elements (dark green domain in Figure 4a).

The 60-residue segment comprises the sequence motif KGC(Y/F)XGQE conserved in the COG0354 protein family, which is located in the region connecting the short 3_{10}-helix with the subsequent long α-helix of this segment (Figure 4a). The conserved sequence motif is well-packed to domain B via hydrophobic interactions (Figure 4b). As a result, the fully conserved Cys 230 of the KGC(Y/F)XGQE sequence motif resides highly exposed to the solvent and in a well-structured

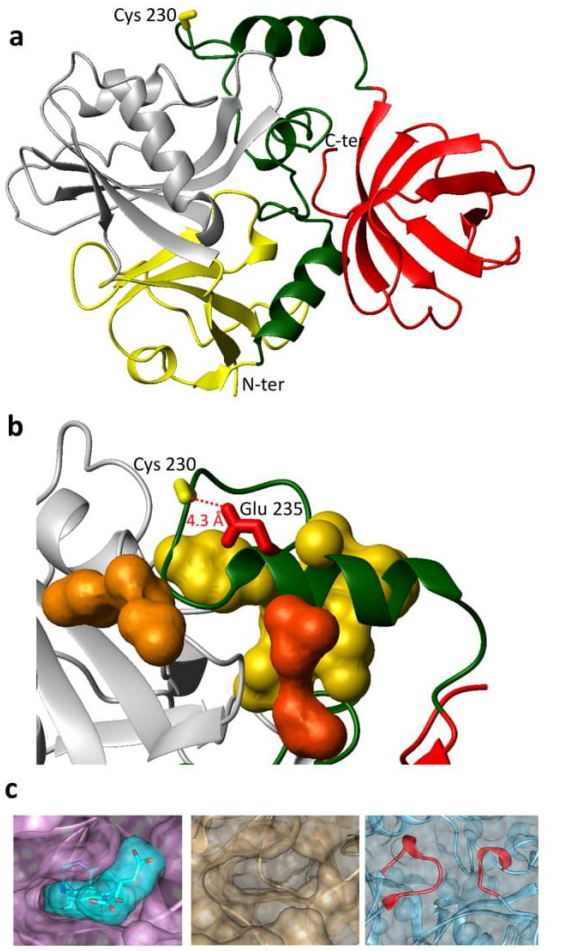

Figure 4. Crystal structure of IBA57. (a) Ribbon diagram of IBA57 with domains A, B, and C colored in yellow, gray, and red, respectively. The 60-residue segment sandwiched among the three domains is in dark green. (b) The region containing the conserved sequence motif KGC(Y/F)XGQE, is well-packed to domain B via hydrophobic interactions defined by three patches: Val 73, Ile 232, and Leu 44 (vdW side-chains in orange); Leu 214, Leu 218, Ala 219, Tyr 231, Val 224, Phe 226, His 241, and Ala 238 (vdW side-chains in yellow); Leu 212 and Leu 236 (vdW side-chains in red). (c) Transparent molecular surfaces of the tetrahydrofolate binding site/cavity in aminomethyl-transferase (on the left, the folinic acid-bound structure (PDB ID 1WOP) and, in the center, the apo structure (PDB ID 1WOS)), and, on the right, of the corresponding region in IBA57 structure. A loop of domain A and the 3_{10}-helix of the 60-residue segment of IBA57 are shown in red.

and rigid region (Figure 4b). The IBA57 structure supports a possible role of Cys 230 as a ligand of the [2Fe-2S] cluster, bridging the two proteins.

In order to corroborate such hypothesis, Cys 230 was substituted with Ala, the crystal structure of Cys230Ala IBA57 was determined, and the holo complex formation was investigated by SEC-MALS, and UV−vis, and CD spectroscopies. The structure of Cys230Ala IBA57 showed that the Cys to Ala substitution does not perturb neither protein fold nor the backbone and side chain conformations of the residues of the KGC(Y/F)XGQE motif containing Cys 230 (Figure

DOI: 10.1021/jacs.8b09061
J. Am. Chem. Soc. XXXX, XXX, XXX−XXX

S5). A 1:1 mixture of Cys230Ala IBA57 mutant and apo ISCA2 was chemically reconstituted with the same conditions as those used for the wild-type protein. SEC-MALS of this mixture showed that no complex is formed, while the peak of IBA57 was still largely present in the mixture, at variance with what was observed for the wild-type complex (Figure 5a). A very broad and weak peak (peak 4) with a molar mass of 43.1 ± 3.5 kDa elutes in between the peaks of [2Fe-2S] ISCA2 and [2Fe-2S] ISCA2-IBA57 (Figure 5a and Figure S1), suggesting that the Cys-to-Ala substitution affects the complex formation in terms of geometrical dimensions and yield, the latter being drastically reduced. The UV−vis spectrum of the chemically reconstituted ISCA2-Cys230Ala IBA57 mixture has the typical bands of [2Fe-2S] ISCA2 and lacks the band at 540 nm typical of the [2Fe-2S] ISCA2-IBA57 complex (Figure 5b). In addition, the CD spectrum of the chemically reconstituted ISCA2-Cys230Ala IBA57 mixture essentially showed the same bands as those observed in [2Fe-2S] ISCA2 and not those of the [2Fe-2S] ISCA2-IBA57 complex (Figure 5c). Finally, the cluster stability upon air exposure of the chemically reconstituted ISCA2-Cys230Ala IBA57 is the same as that observed for [2Fe-2S] ISCA2, that is, the Fe-S cluster is oxidatively labile and gradually degraded over a period of ∼5 h (Figure 2f). In conclusion, the substitution of Cys 230 largely abolished the formation of the [2Fe-2S] heterocomplex and consequently the oxygen resistance of the cluster. These data strongly support the participation of Cys 230 in cluster coordination. To further confirm this, we have performed a AMS-based alkylation gel shift assay, which showed that one of the four cysteines of IBA57 (i.e., Cys 230) is not available to be alkylated in the [2Fe-2S] ISCA2-IBA57 complex with respect to the uncomplexed IBA57 (Figure S6). This result suggested that Cys 230 cannot be alkylated by AMS once it is involved in cluster binding. From both site-directed mutagenesis and AMS results, we conclude that Cys 230 of IBA57 is involved in the cluster binding in the [2Fe-2S] complex.

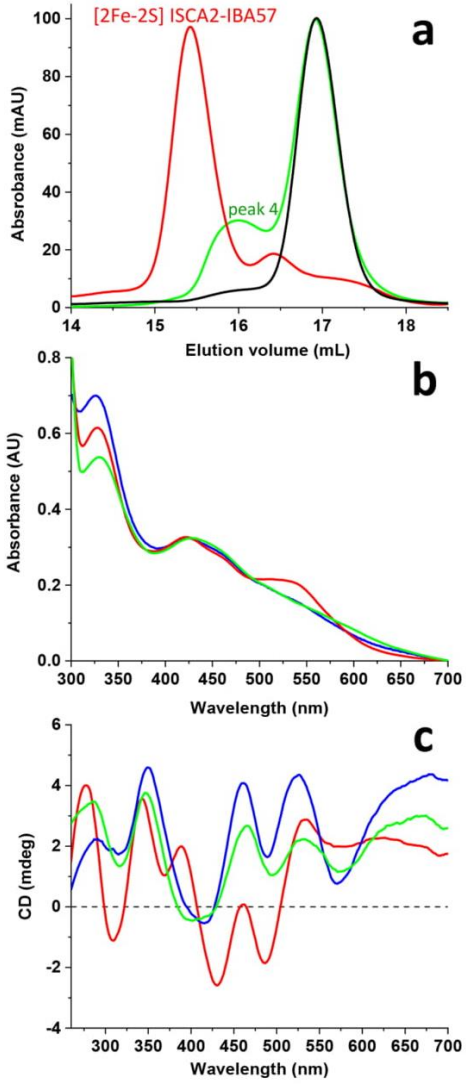

Figure 5. Cys 230 to Ala substitution affects the [2Fe-2S] ISCA2-IBA57 complex formation. (a) Elution profiles obtained for IBA57 (black), the 1:0.5 [2Fe-2S]/apo ISCA2-IBA57 mixture (red), and the 1:1 mixture of Cys230Ala IBA57 mutant and apo ISCA2 chemically reconstituted with the same conditions as those used for the wild-type complex (green) by gel filtration on analytical SuperdexTM 200 Increase 10/300 GL column. mAU: milli absorbance unit. UV−vis (b) and CD (c) spectra of chemically reconstituted ISCA2-Cys230Ala IBA57 1:1 mixture (green), of chemically reconstituted [2Fe-2S] ISCA2 (blue), and of chemically reconstituted [2Fe-2S] ISCA2-IBA57 (red). The experiments were conducted with monomeric protein concentration of ISCA2 ranging from 0.15 mM to 0.6 mM depending on the applied spectroscopic technique.

Since no further potential [2Fe-2S] cluster ligands (i.e., Cys and His) from IBA57 are within 6 Å to Cys 230, we expect that the other three cluster ligands in [2Fe-2S] ISCA2-IBA57 result from ISCA2, and they might be the three cysteine cluster ligands conserved in the ISCA protein family (i.e., Cys 79, Cys 144 and Cys 146 in ISCA2).[20,22,39] To investigate whether they are involved in cluster binding in the ISCA2-IBA57 complex, we produced three ISCA2 mutants in which either Cys 79 or Cys 144 or Cys 146 were substituted with Ser. Three 1:1 mixtures of IBA57 with each single apo ISCA2 mutant were then chemically reconstituted following the same procedure used for the wild-type protein, and UV−vis and analytical gel filtration data were collected and compared with those of [2Fe-2S] ISCA2-IBA57. Analytical gel filtration of any of the three mixtures showed that the [2Fe-2S] ISCA2-IBA57 complex is not formed in any case, while the peak of isolated IBA57 is still largely present in each mixture (Figure 6a). Specifically, in Cys144Ser ISCA2, a very broad and weak peak (peaks 4′ in Figure 6a), the same as that observed in the chemically reconstituted 1:1 mixture of Cys230Ala IBA57 and apo ISCA2 (peak 4 in Figure 5a), is present in which the Fe-S cluster is oxidatively labile and gradually degraded over a period of ∼5 h. In the mixtures with Cys79Ser and Cys146Ser ISCA2, no peak at elution volumes higher than those of IBA57 and apo ISCA2 is present (Figure 6a), similarly to what it was observed in the apo ISCA2-IBA57 mixture (Figure 1a). On the basis of these results we can propose that all the three cysteines are required for the binding of the [2Fe-2S] cluster which bridges the two proteins. The UV−vis spectra of the three chemically reconstituted mixtures of any ISCA2 mutant with IBA57s corroborate such a model. Indeed, they do not show the band at 540 nm, which is the characteristic fingerprint for the formation of the [2Fe-2S] ISCA2-IBA57 complex (Figure 6b). This indicates that the [2Fe-2S] ISCA2-IBA57 complex is

DOI: 10.1021/jacs.8b09061
J. Am. Chem. Soc. XXXX, XXX, XXX−XXX

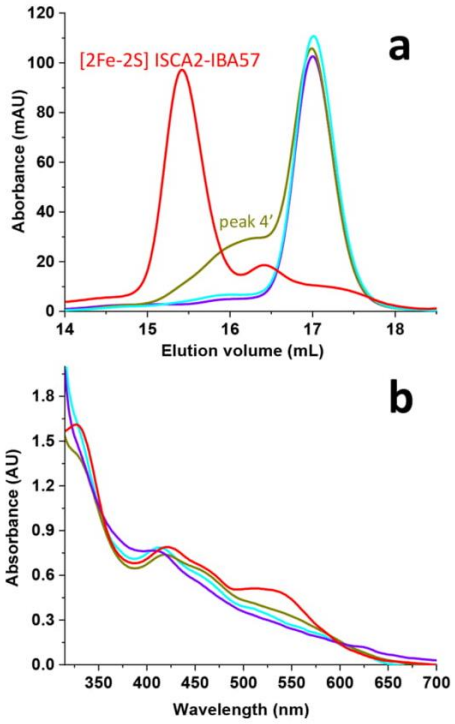

Figure 6. Cys 79, Cys 144, and Cys 146 to Ser substitutions affect the [2Fe-2S] ISCA2-IBA57 complex formation. (a) Elution profiles obtained for chemically reconstituted Cys79Ser ISCA2-IBA57 1:1 mixture (violet), Cys144Ser ISCA2-IBA57 1:1 mixture (dark yellow), Cys146Ser ISCA2-IBA57 1:1 mixture (cyano), and the 1:0.5 [2Fe-2S]/apo ISCA2-IBA57 mixture (red) by gel filtration on analytical SuperdexTM 200 Increase 10/300 GL column. mAU: milli absorbance unit. (b) UV−vis spectra of chemically reconstituted 1:1 mixtures of Cys79Ser with IBA57 (violet), Cys144Ser ISCA2 with IBA57 (dark yellow), Cys146Ser ISCA2 with IBA57 (cyano), and [2Fe-2S]/apo ISCA2 with IBA57 (red). Monomeric protein concentration of ISCA2 mutants was 0.2 mM.

not formed upon mutation of any of the ISCA2 cysteine, pointing at the importance of all three cysteines for ligating the cluster in the heterocomplex. The UV−vis spectrum of each of the three mixtures (Figure 6b) showed the presence of a cluster-bound species, which is due to the formation, upon chemical reconstitution, of the holo species of each ISCA2 mutant. Indeed, these UV−vis spectra of the mixture with any of the three mutants match those of the three chemically reconstituted ISCA2 mutants alone, previously reported.[22]

In conclusion, the [2Fe-2S] ISCA2-IBA57 complex formation is abolished in any of the three mutants, similarly to what it occurs once Cys 230 of IBA57 is substituted by Ala. From these data we can propose that the [2Fe-2S] cluster in the ISCA2-IBA57 complex is asymmetrically coordinated by Cys 79, Cys 144, and Cys 146 from ISCA2 and Cys 230 from IBA57. Such coordination in the heterodimeric ISCA2-IBA57 complex could be achieved, along the interaction between IBA57 and dimeric [2Fe-2S] ISCA2, through the displacement of Cys 79 and Cys 146 from one subunit of [2Fe-2S] ISCA2, which is thus released in solution, by Cys 230 of IBA57 and by Cys 146 of the other ISCA2 subunit.

IBA57 Does Not Bind Tetrahydrofolate Derivatives. It has been proposed that tetrahydrofolates play a role in the metabolism of iron-sulfur clusters in all domains of life by participating in the assembly or repair of Fe-S clusters and that IBA57 protein family acts as the direct link between tetrahydrofolates and Fe-S cluster enzymes by showing a folate binding site.[16,40,41] This proposal stems from experimental data on *E. coli* IBA57 homologue, that is, YgfZ protein.[16,42] IBA57 structure is similar to that of YgfZ[43] as well as to an aminomethyl-transferase involved in the mitochondrial glycine cleavage system[44] and to the C-terminal domain of a mammalian dimethylglycine dehydrogenase.[45] The two latter proteins bind tetrahydrofolate in a large central cavity, with the pterin ring of tetrahydrofolate located in the center of the cavity and the glutamate tail exposed to the external solvent (Figure 4c). This cavity is preserved in the apo proteins, indicating the presence of a rigid tetrahydrofolate binding pocket (Figure 4c). The YgfZ protein has been also shown to bind tetrahydrofolate, potentially in the same cavity, but with lower affinity than that typically observed for binding of folate substrates.[16,43] This central cavity is absent in IBA57, as a consequence of a backbone conformation of a loop of domain A and of the 3_{10}-helix of the 60-residue segment different from the same regions in the structural homologues (Figure 4c). Moreover, the residues typically involved in the interaction between tetrahydrofolate and the aminomethyl-transferase/dimethylglycine dehydrogenase proteins[44,45] are not conserved in IBA57. ^{1}H 1D ePHOGSY NMR experiments and ^{1}H−^{15}N HSQC NMR titrations between IBA57 and tetrahydrofolate derivatives as well as ^{1}H 1D ePHOGSY NMR experiments between the [2Fe-2S] ISCA2-IBA57 complex and calcium folinate showed no significant peak intensity variation in the 1D NMR experiments and no chemical shift changes in ^{1}H−^{15}N HSQC maps of ^{15}N-labeled IBA57 (Figure S7), indicating no interaction between free and complexed IBA57 and the tetrahydrofolate derivatives. From both the structural and interaction data, we conclude that tetrahydrofolate derivatives are not substrates of IBA57.

[2Fe-2S] ISCA2-IBA57 Reactivates Apo Aconitase. The oxygen resistance of the cluster in [2Fe-2S] ISCA2-IBA57 suggests that the heterocomplex might operate under aerobic cellular conditions, possibly being involved in the reactivation of mitochondrial Fe-S enzymes. It was well established, indeed, that Fe-S clusters of mitochondrial enzymes, such as that of aconitase, can fully disassemble upon exposure to oxidants.[46,47] Therefore, we have tested *in vitro* whether [2Fe-2S] ISCA2-IBA57 can recycle apo aconitase into [4Fe-4S] aconitase. To do that, aerobically purified cytosolic aconitase, which contains residual amounts of [4Fe-4S] bound cluster according to UV−vis and activity measurement (Figure S8), was anaerobically incubated with the [2Fe-2S] ISCA2-IBA57 complex for 45 min at 25 °C, and then aconitase activity was measured following a previously reported protocol.[25] The mixture showed increased activity with respect to that of untreated aconitase and is ∼70% of that obtained by the chemically reconstituted aconitase (Figure S8). We also verified that [2Fe-2S] ISCA2-IBA57 alone does not experience citrate/isocitrate activity. These data indicate that the [2Fe-2S] ISCA2-IBA57 is able to reactivate apo aconitase.

■ DISCUSSION

Human IBA57 is required for the maturation of mitochondrial [4Fe-4S] proteins (i.e., aconitase, respiratory complex I, succinate dehydrogenase, and lipoic acid synthase) in HeLa cells, while the function of the mitochondrial [2Fe-2S]

DOI: 10.1021/jacs.8b09061
J. Am. Chem. Soc. XXXX, XXX, XXX−XXX

ferrochelatase was unaffected by IBA57.[11] On this basis, it was proposed that IBA57 is specifically required for the generation of [4Fe-4S] clusters and their dedicated insertion into mitochondrial apo recipient proteins. This function has been found to be strictly related to two other proteins of the mitochondrial ISC assembly machinery, that is, ISCA1 and ISCA2, which showed the same phenotype as that of IBA57 in HeLa cells.[11] From those studies, it was concluded that the three proteins work together in a complex to assemble a [4Fe-4S] cluster.[18] This model was indirectly corroborated by the fact that very similar phenotypes for the three proteins were also found in yeast and by the finding that yeast Iba57 physically interacts with yeast Isa1 and Isa2.[12,15] This stringent functional association has been, however, revisited in a recent study, which showed that ISCA2 and IBA57 are not required under standard physiological conditions for the maturation of mitochondrial [4Fe-4S] proteins in mouse skeletal muscle and in primary cultures of neurons and that ISCA2, but not ISCA1, interacts with IBA57.[19]

Our work shows that IBA57 forms a heterodimeric complex with ISCA2, and not with ISCA1, by bridging a [2Fe-2S] cluster that is resistant to highly oxidative environments. Specifically, this complex is the final product when IBA57 is either exposed to [2Fe-2S] ISCA2 or in the presence of [2Fe-2S] GLRX5 and apo ISCA2. The latter results suggest that a cluster transfer pathway involving three partner proteins of the mitochondrial ISC machinery (GLRX5, ISCA2, and IBA57) is operative. This pathway starts with [2Fe-2S] cluster transfer from [2Fe-2S] GLRX5 to ISCA2 and ends up with the formation of a [2Fe-2S] cluster-mediated ISCA2-IBA57 complex. Cluster binding is, indeed, absolutely required to promote complex formation between ISCA2 and IBA57 proteins. No formation of a [4Fe-4S] cluster bound to the ISCA2-IBA57 complex was observed along this pathway, at variance with what it was observed in the interaction of [2Fe-2S] GLRX5 with the apo ISCA1-ISCA2 complex that is able to form a [4Fe-4S] cluster.[20,22] We also identified Cys 230 of IBA57 and Cys 79, Cys 144, and Cys 146 of ISCA2 as the ligands bridging the [2Fe-2S] cluster between the two proteins and showed that all cysteines are required to stabilize the complex formation and the [2Fe-2S] cluster against oxidative degradation.

The stability of the [2Fe-2S] cluster against oxidative degradation, observed upon its binding to the ISCA2-IBA57 complex with respect to when it is bound to ISCA2 alone, supports a model where the heterocomplex can work under aerobic cellular conditions. This model fits well with the experimental and genomic data that connect COG0354 proteins with aerobic organisms and oxidative stress.[16,48] Moreover, this model agrees with what has been recently suggested on the basis of a cell-dependent phenotype observed for both ISCA2 and IBA57,[11,19] namely that ISCA2 and IBA57 might be activated together for Fe-S biogenesis upon specific cellular conditions, such as cell proliferation (a process requiring adequate oxygen concentrations to be effective) and oxidative stress.[19] We also found that the [2Fe-2S] ISCA2-IBA57 complex is able to substantially reactivate *in vitro* human aconitase. This indicates that the [2Fe-2S] heterocomplex is able to mature aconitase by providing a [4Fe-4S] cluster. It is possible that the ability of the heterocomplex to stabilize both reduced and oxidized states of the [2Fe-2S] cluster drives a reductive coupling of two reduced $[2Fe\text{-}2S]^{+}$ clusters into an oxidized $[4Fe\text{-}4S]^{2+}$ cluster[49,50] on aconitase. The binding preference, in the ISCA2-IBA57 complex, of a [2Fe-2S] cluster over a [4Fe-4S] cluster might be explained by the fact that aerobic organisms have favored the use of the more chemically stable [2Fe-2S] clusters than the more damageable [4Fe-4S] clusters.[51] In conclusion, the [2Fe-2S] ISCA2-IBA57 complex may be required as a specific system maturing Fe-S enzymes under aerobic cellular conditions, similarly to what observed in the cytosol of human cells, where the [2Fe-2S] form of mitoNEET is resistant to oxidants and is capable of reactivating cytosolic aconitase.[52−54]

■ ASSOCIATED CONTENT

Supporting Information

The Supporting Information is available free of charge on the ACS Publications website at DOI: 10.1021/jacs.8b09061.

Figures S1−S8 (PDF)

■ AUTHOR INFORMATION

Corresponding Authors

*banci@cerm.unifi.it

*ciofi@cerm.unifi.it

ORCID

Vito Calderone: 0000-0002-7963-6241

Simone Ciofi-Baffoni: 0000-0002-2376-3321

Lucia Banci: 0000-0003-0562-5774

Author Contributions

§These authors contributed equally

Notes

The authors declare no competing financial interest.

■ ACKNOWLEDGMENTS

The authors acknowledge the support and the use of resources of Instruct-ERIC, a Landmark ESFRI project, and specifically the CERM/CIRMMP Italy Centre. This work has also been supported by iNEXT, grant number 653706, funded by the Horizon 2020 programme of the European Commission. This article is based upon work from COST Action CA15133, supported by the European Cooperation in Science and Technology (COST).

■ REFERENCES

(1) Rouault, T. A. Mammalian iron-sulphur proteins: novel insights into biogenesis and function. *Nat. Rev. Mol. Cell Biol.* **2015**, *16* (1), 45−55.

(2) Sheftel, A.; Stehling, O.; Lill, R. Iron-sulfur proteins in health and disease. *Trends Endocrinol. Metab.* **2010**, *21* (5), 302−314.

(3) Beilschmidt, L. K.; Puccio, H. M. Mammalian Fe-S cluster biogenesis and its implication in disease. *Biochimie* **2014**, *100*, 48−60.

(4) Ciofi-Baffoni, S.; Nasta, V.; Banci, L. Protein networks in the maturation of human iron-sulfur proteins. *Metallomics* **2018**, *10*, 49−72.

(5) Stehling, O.; Wilbrecht, C.; Lill, R. Mitochondrial iron-sulfur protein biogenesis and human disease. *Biochimie* **2014**, *100*, 61−77.

(6) Kaut, A.; Lange, H.; Diekert, K.; Kispal, G.; Lill, R. Isa1p is a component of the mitochondrial machinery for maturation of cellular iron-sulfur proteins and requires conserved cysteine residues for function. *J. Biol. Chem.* **2000**, *275* (21), 15955−15961.

(7) Pelzer, W.; Muhlenhoff, U.; Diekert, K.; Siegmund, K.; Kispal, G.; Lill, R. Mitochondrial Isa2p plays a crucial role in the maturation of cellular iron-sulfur proteins. *FEBS Lett.* **2000**, *476* (3), 134−139.

(8) Cozar-Castellano, I.; del Valle, M. M.; Trujillo, E.; Arteaga, M. F.; Gonzalez, T.; Martin-Vasallo, P.; Avila, J. hIscA: a protein

DOI: 10.1021/jacs.8b09061
J. Am. Chem. Soc. XXXX, XXX, XXX−XXX

implicated in the biogenesis of iron-sulfur clusters. *Biochim. Biophys. Acta, Proteins Proteomics* **2004**, *1700*, 179−188.
(9) Rodriguez-Manzaneque, M. T.; Tamarit, J.; Belli, G.; Ros, J.; Herrero, E. Grx5 is a mitochondrial glutaredoxin required for the activity of iron/sulfur enzymes. *Mol. Biol. Cell* **2002**, *13* (4), 1109−1121.
(10) Vilella, F.; Alves, R.; Rodriguez-Manzaneque, M. T.; Belli, G.; Swaminathan, S.; Sunnerhagen, P.; Herrero, E. Evolution and cellular function of monothiol glutaredoxins: involvement in iron-sulphur cluster assembly. *Comp. Funct. Genomics* **2004**, *5* (4), 328−341.
(11) Sheftel, A. D.; Wilbrecht, C.; Stehling, O.; Niggemeyer, B.; Elsasser, H. P.; Muhlenhoff, U.; Lill, R. The human mitochondrial ISCA1, ISCA2, and IBA57 proteins are required for [4Fe-4S] protein maturation. *Mol. Biol. Cell* **2012**, *23* (7), 1157−1166.
(12) Muhlenhoff, U.; Richter, N.; Pines, O.; Pierik, A. J.; Lill, R. Specialized function of yeast Isa1 and Isa2 proteins in the maturation of mitochondrial [4Fe-4S] proteins. *J. Biol. Chem.* **2011**, *286* (48), 41205−41216.
(13) Muhlenhoff, U.; Gerl, M. J.; Flauger, B.; Pirner, H. M.; Balser, S.; Richhardt, N.; Lill, R.; Stolz, J. The ISC proteins Isa1 and Isa2 are required for the function but not for the de novo synthesis of the Fe/S clusters of biotin synthase in Saccharomyces cerevisiae. *Eukaryotic Cell* **2007**, *6*, 495−504.
(14) Kim, K. D.; Chung, W. H.; Kim, H. J.; Lee, K. C.; Roe, J. H. Monothiol glutaredoxin Grx5 interacts with Fe-S scaffold proteins Isa1 and Isa2 and supports Fe-S assembly and DNA integrity in mitochondria of fission yeast. *Biochem. Biophys. Res. Commun.* **2010**, *392* (3), 467−472.
(15) Gelling, C.; Dawes, I. W.; Richhardt, N.; Lill, R.; Muhlenhoff, U. Mitochondrial Iba57p is required for Fe/S cluster formation on aconitase and activation of radical SAM enzymes. *Mol. Cell. Biol.* **2008**, *28* (5), 1851−1861.
(16) Waller, J. C.; Alvarez, S.; Naponelli, V.; Lara-Nunez, A.; Blaby, I. K.; Da Silva, V.; Ziemak, M. J.; Vickers, T. J.; Beverley, S. M.; Edison, A. S.; Rocca, J. R.; Gregory, J. F., III; Crecy-Lagard, V.; Hanson, A. D. A role for tetrahydrofolates in the metabolism of iron-sulfur clusters in all domains of life. *Proc. Natl. Acad. Sci. U. S. A.* **2010**, *107* (23), 10412−10417.
(17) Andreini, C.; Banci, L.; Rosato, A. Exploiting bacterial operons to illuminate human iron-sulfur proteins. *J. Proteome Res.* **2016**, *15*, 1308−1322.
(18) Braymer, J. J.; Lill, R. Iron-sulfur cluster biogenesis and trafficking in mitochondria. *J. Biol. Chem.* **2017**, *292* (31), 12754−12763.
(19) Beilschmidt, L. K.; Ollagnier de Choudens, S.; Fournier, M.; Sanakis, I.; Hograindleur, M. A.; Clemancey, M.; Blondin, G.; Schmucker, S.; Eisenmann, A.; Weiss, A.; Koebel, P.; Messaddeq, N.; Puccio, H.; Martelli, A. ISCA1 is essential for mitochondrial Fe4S4 biogenesis in vivo. *Nat. Commun.* **2017**, *8*, 15124.
(20) Brancaccio, D.; Gallo, A.; Mikolajczyk, M.; Zovo, K.; Palumaa, P.; Novellino, E.; Piccioli, M.; Ciofi-Baffoni, S.; Banci, L. Formation of [4Fe-4S] clusters in the mitochondrial iron-sulfur cluster assembly machinery. *J. Am. Chem. Soc.* **2014**, *136* (46), 16240−16250.
(21) Torraco, A.; Ardissone, A.; Invernizzi, F.; Rizza, T.; Fiermonte, G.; Niceta, M.; Zanetti, N.; Martinelli, D.; Vozza, A.; Verrigni, D.; Di Nottia, M.; Lamantea, E.; Diodato, D.; Tartaglia, M.; Dionisi-Vici, C.; Moroni, I.; Farina, L.; Bertini, E.; Ghezzi, D.; Carrozzo, R. Novel mutations in IBA57 are associated with leukodystrophy and variable clinical phenotypes. *J. Neurol.* **2017**, *264* (1), 102−111.
(22) Brancaccio, D.; Gallo, A.; Piccioli, M.; Novellino, E.; Ciofi-Baffoni, S.; Banci, L. [4Fe-4S] Cluster Assembly in Mitochondria and Its Impairment by Copper. *J. Am. Chem. Soc.* **2017**, *139*, 719−730.
(23) Banci, L.; Brancaccio, D.; Ciofi-Baffoni, S.; Del Conte, R.; Gadepalli, R.; Mikolajczyk, M.; Neri, S.; Piccioli, M.; Winkelmann, J. [2Fe-2S] cluster transfer in iron-sulfur protein biogenesis. *Proc. Natl. Acad. Sci. U. S. A.* **2014**, *111* (17), 6203−6208.
(24) Chen, J.; Acton, T. B.; Basu, S. K.; Montelione, G. T.; Inouye, M. Enhancement of the solubility of proteins overexpressed in Escherichia coli by heat shock. *J. Mol. Microbiol. Biotechnol.* **2002**, *4* (6), 519−524.
(25) Maione, V.; Cantini, F.; Severi, M.; Banci, L. Investigating the role of the human CIA2A-CIAO1 complex in the maturation of aconitase. *Biochim. Biophys. Acta, Gen. Subj.* **2018**, *1862* (9), 1980−1987.
(26) Banci, L.; Bertini, I.; Cefaro, C.; Ciofi-Baffoni, S.; Gallo, A.; Martinelli, M.; Sideris, D. P.; Katrakili, N.; Tokatlidis, K. MIA40 is an oxidoreductase that catalyzes oxidative protein folding in mitochondria. *Nat. Struct. Mol. Biol.* **2009**, *16* (2), 198−206.
(27) Dalvit, C.; Hommel, U. New pulsed field gradient NMR experiments for the detection of bound water in proteins. *J. Biomol. NMR* **1995**, *5*, 306−310.
(28) Uzarska, M. A.; Dutkiewicz, R.; Freibert, S. A.; Lill, R.; Muhlenhoff, U. The mitochondrial Hsp70 chaperone Ssq1 facilitates Fe/S cluster transfer from Isu1 to Grx5 by complex formation. *Mol. Biol. Cell* **2013**, *24* (12), 1830−1841.
(29) Bandyopadhyay, S.; Gama, F.; Molina-Navarro, M. M.; Gualberto, J. M.; Claxton, R.; Naik, S. G.; Huynh, B. H.; Herrero, E.; Jacquot, J. P.; Johnson, M. K.; Rouhier, N. Chloroplast monothiol glutaredoxins as scaffold proteins for the assembly and delivery of [2Fe-2S] clusters. *EMBO J.* **2008**, *27* (7), 1122−1133.
(30) Noodleman, L.; Baerends, E. J. Electronic structure, magnetic properties, ESR and optical spectra for 2-Fe ferredoxin models by LCAO-Xa valence bond theory. *J. Am. Chem. Soc.* **1984**, *106*, 2316−2327.
(31) Banci, L.; Camponeschi, F.; Ciofi-Baffoni, S.; Piccioli, M. The NMR contribution to protein-protein networking in Fe-S protein maturation. *JBIC, J. Biol. Inorg. Chem.* **2018**, *23* (4), 665−685.
(32) Banci, L.; Bertini, I.; Luchinat, C. The ^{1}H NMR parameters of magnetically coupled dimers - The Fe_2S_2 proteins as an example. *Struct. Bonding (Berlin)* **1990**, *72*, 113−135.
(33) Meyer, J.; Bruschi, M. H.; Bonicel, J. J.; Bovier-Lapierre, G. E. Amino acid sequence of [2Fe-2S] ferredoxin from Clostridium pasteurianum. *Biochemistry* **1986**, *25* (20), 6054−61.
(34) Han, S.; Czernuszewicz, R. S.; Kimura, T.; Adams, M. W. W.; Spiro, T. G. Fe2S2 protein resonance Raman spectra revisited: structural variations among adrenodoxin, ferredoxin, and red paramagnetic protein. *J. Am. Chem. Soc.* **1989**, *111* (10), 3505−3511.
(35) Chatelet, C.; Meyer, J. The [2Fe-2S] protein I (Shetna protein I) from Azotobacter vinelandii is homologous to the [2Fe-2S] ferredoxin from Clostridium pasteurianum. *JBIC, J. Biol. Inorg. Chem.* **1999**, *4* (3), 311−7.
(36) Bertrand, P.; Guigliarelli, B.; More, C. The mixed-valence [Fe(III), Fe(II)] binuclear centers of biological molecules viewed through EPR spectroscopy. *New J. Chem.* **1991**, *15*, 445−454.
(37) Banci, L.; Ciofi-Baffoni, S.; Mikolajczyk, M.; Winkelmann, J.; Bill, E.; Pandelia, M. E. Human anamorsin binds [2Fe-2S] clusters with unique electronic properties. *JBIC, J. Biol. Inorg. Chem.* **2013**, *18*, 883−893.
(38) Johansson, C.; Roos, A. K.; Montano, S. J.; Sengupta, R.; Filippakopoulos, P.; Guo, K.; von Delft, F.; Holmgren, A.; Oppermann, U.; Kavanagh, K. L. The crystal structure of human GLRX5: iron-sulfur cluster co-ordination, tetrameric assembly and monomer activity. *Biochem. J.* **2011**, *433* (2), 303−311.
(39) Zheng, L.; Cash, V. L.; Flint, D. H.; Dean, D. R. Assembly of iron-sulfur clusters. Identification of an iscSUA-hscBA-fdx gene cluster from Azotobacter vinelandii. *J. Biol. Chem.* **1998**, *273* (21), 13264−13272.
(40) Waller, J. C.; Ellens, K. W.; Alvarez, S.; Loizeau, K.; Ravanel, S.; Hanson, A. D. Mitochondrial and plastidial COG0354 proteins have folate-dependent functions in iron-sulphur cluster metabolism. *J. Exp. Bot.* **2012**, *63* (1), 403−11.
(41) Waller, J. C.; Ellens, K. W.; Hasnain, G.; Alvarez, S.; Rocca, J. R.; Hanson, A. D. Evidence that the folate-dependent proteins YgfZ and MnmEG have opposing effects on growth and on activity of the iron-sulfur enzyme MiaB. *J. Bacteriol.* **2012**, *194* (2), 362−7.
(42) Hasnain, G.; Waller, J. C.; Alvarez, S.; Ravilious, G. E.; Jez, J. M.; Hanson, A. D. Mutational analysis of YgfZ, a folate-dependent

DOI: 10.1021/jacs.8b09061
J. Am. Chem. Soc. XXXX, XXX, XXX−XXX

protein implicated in iron/sulphur cluster metabolism. *FEMS Microbiol. Lett.* **2012**, *326* (2), 168−72.
(43) Teplyakov, A.; Obmolova, G.; Sarikaya, E.; Pullalarevu, S.; Krajewski, W.; Galkin, A.; Howard, A. J.; Herzberg, O.; Gilliland, G. L. Crystal structure of the YgfZ protein from Escherichia coli suggests a folate-dependent regulatory role in one-carbon metabolism. *J. Bacteriol.* **2004**, *186* (21), 7134−40.
(44) Lee, H. H.; Kim, D. J.; Ahn, H. J.; Ha, J. Y.; Suh, S. W. Crystal structure of T-protein of the glycine cleavage system. Cofactor binding, insights into H-protein recognition, and molecular basis for understanding nonketotic hyperglycinemia. *J. Biol. Chem.* **2004**, *279* (48), 50514−23.
(45) Luka, Z.; Pakhomova, S.; Loukachevitch, L. V.; Newcomer, M. E.; Wagner, C. Folate in demethylation: the crystal structure of the rat dimethylglycine dehydrogenase complexed with tetrahydrofolate. *Biochem. Biophys. Res. Commun.* **2014**, *449* (4), 392−8.
(46) Gardner, P. R. Superoxide-driven aconitase FE-S center cycling. *Biosci. Rep.* **1997**, *17* (1), 33−42.
(47) Tong, W. H.; Rouault, T. A. Metabolic regulation of citrate and iron by aconitases: role of iron-sulfur cluster biogenesis. *BioMetals* **2007**, *20* (3−4), 549−564.
(48) Chen, J. W.; Sun, C. M.; Sheng, W. L.; Wang, Y. C.; Syu, W. J. Expression Analysis of Up-Regulated Genes Responding to Plumbagin in Escherichia coli. *J. Bacteriol.* **2006**, *188* (2), 456−63.
(49) Chandramouli, K.; Unciuleac, M. C.; Naik, S.; Dean, D. R.; Huynh, B. H.; Johnson, M. K. Formation and properties of [4Fe-4S] clusters on the IscU scaffold protein. *Biochemistry* **2007**, *46* (23), 6804−6811.
(50) Mapolelo, D. T.; Zhang, B.; Naik, S. G.; Huynh, B. H.; Johnson, M. K. Spectroscopic and functional characterization of iron-sulfur cluster-bound forms of Azotobacter vinelandii (Nif)IscA. *Biochemistry* **2012**, *51* (41), 8071−8084.
(51) Andreini, C.; Rosato, A.; Banci, L. The relationship between environmental dioxygen and iron-sulfur proteins explored at the genome level. *PLoS One* **2017**, *12*, e0171279.
(52) Camponeschi, F.; Ciofi-Baffoni, S.; Banci, L. Anamorsin/Ndor1 Complex Reduces [2Fe-2S]-MitoNEET via a Transient Protein-Protein Interaction. *J. Am. Chem. Soc.* **2017**, *139*, 9479−9482.
(53) Golinelli-Cohen, M. P.; Lescop, E.; Mons, C.; Goncalves, S.; Clemancey, M.; Santolini, J.; Guittet, E.; Blondin, G.; Latour, J. M.; Bouton, C. Redox Control of the Human Iron-Sulfur Repair Protein MitoNEET Activity via Its Iron-Sulfur Cluster. *J. Biol. Chem.* **2016**, *291* (14), 7583−7593.
(54) Ferecatu, I.; Goncalves, S.; Golinelli-Cohen, M. P.; Clemancey, M.; Martelli, A.; Riquier, S.; Guittet, E.; Latour, J. M.; Puccio, H.; Drapier, J. C.; Lescop, E.; Bouton, C. The diabetes drug target MitoNEET governs a novel trafficking pathway to rebuild an Fe-S cluster into cytosolic aconitase/iron regulatory protein 1. *J. Biol. Chem.* **2014**, *289* (41), 28070−28086.

DOI: 10.1021/jacs.8b09061
J. Am. Chem. Soc. XXXX, XXX, XXX−XXX

Supporting Information

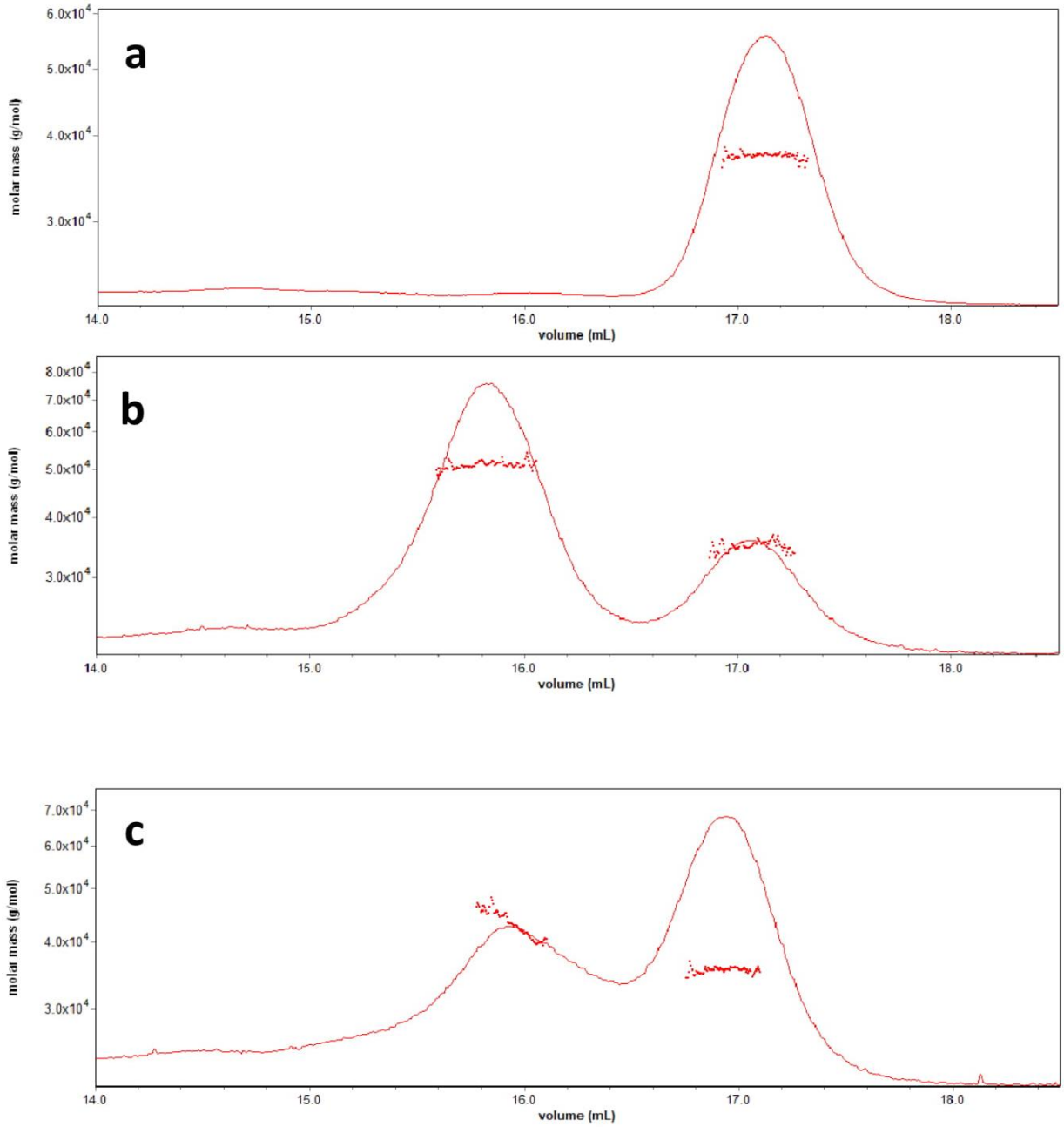

Figure S1. Complex formation between [2Fe-2S] ISCA2 and IBA57 by SEC-MALS. Molar mass versus elution volume of (a) IBA57, (b) a 1:1 (ratio based on dimeric [2Fe-2S] ISCA2 concentration vs monomeric IBA57 concentration) mixture of IBA57 and [2Fe-2S]/apo ISCA2, (c) a chemically reconstituted 1:1 apo ISCA2-Cys230Ala IBA57 mixture, obtained by gel filtration on analytical SuperdexTM 200 Increase 10/300 GL column combined with MALS detection. The red dots indicate the MALS calculated molar mass (in g/mol, or Da) of each point of the peak of the eluted protein, and the red traces refer to the light scattering.

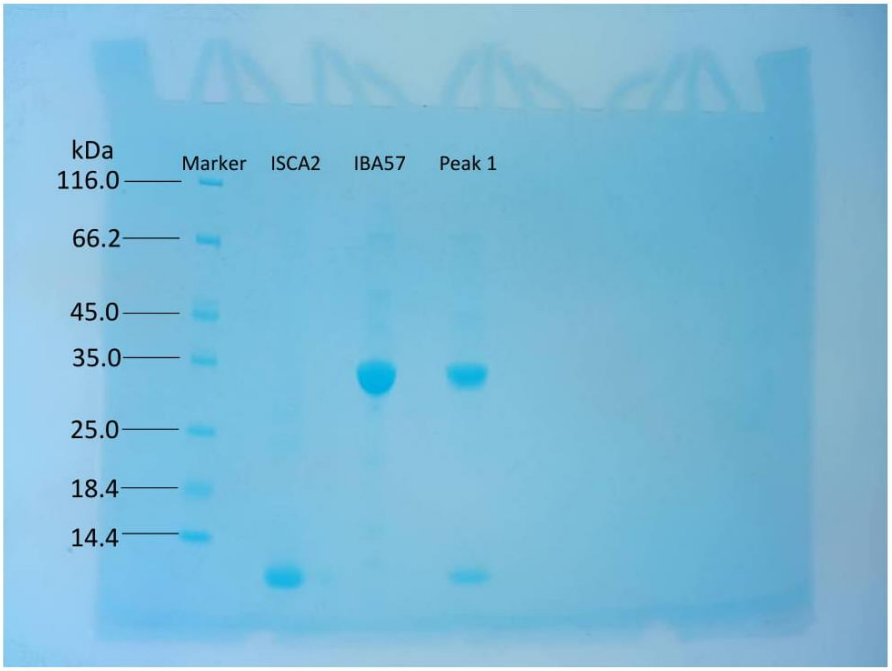

Figure S2. Complex formation between [2Fe-2S] ISCA2 and IBA57 by SDS-PAGE. SDS-PAGE was performed on the fractions eluted from the analytical gel filtration column at peak 1. ISCA2 and IBA57 used to form the heterocomplex and protein molecular weight markers are present in the gel for reference. Kilodaltons of the molecular weight markers are indicated on the left

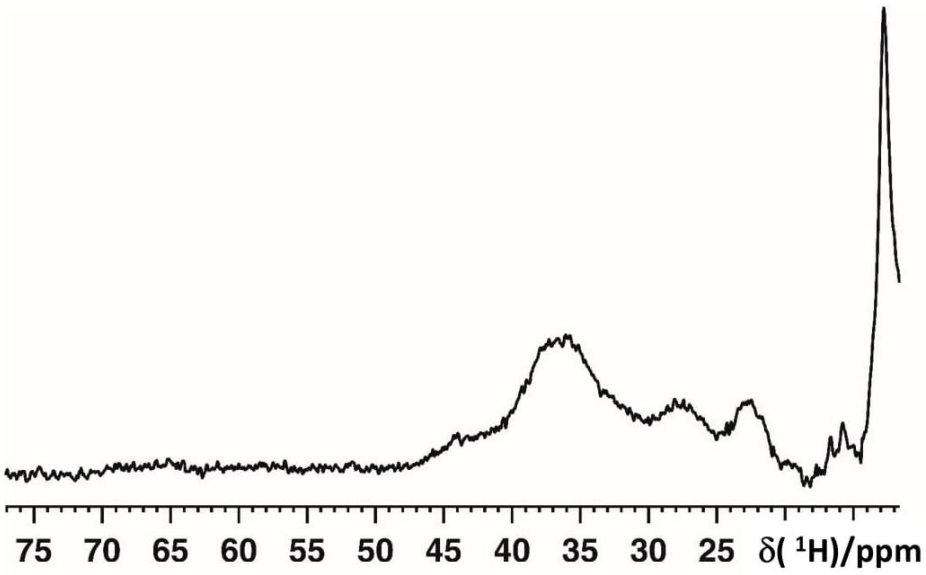

Figure S3. The ISCA2-IBA57 complex binds a [2Fe-2S]2+ cluster as observed by paramagnetic NMR spectroscopy. 1D ^{1}H NMR spectra of [2Fe-2S] ISCA2-IBA57 in 50 mM phosphate buffer, 5 mM DTT and 150 mM NaCl, pH 7.0 and 10% (v/v) D2O at 400 MHz and 298 K.

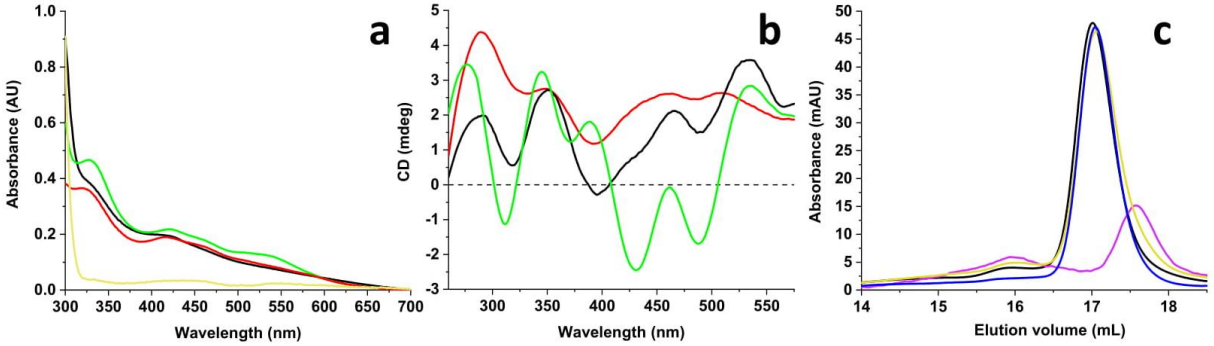

Figure S4. ISCA1 does not form a cluster-mediated complex with IBA57. (a) UV-vis, (b) CD and (c) analytical gel filtration of IBA57 (blue), apo His-tag ISCA1 (violet), chemically reconstituted [2Fe-2S] His-tag ISCA1 (red), a 1:1 mixture of His-tag apo ISCA1-IBA57 before (beige) and after (black) chemical reconstitution, and chemically reconstituted [2Fe-2S] ISCA2-IBA57 complex (green). The experiments were conducted with protein concentration of monomeric ISCA1 ranging from 0.15 mM to 0.3 mM depending on the applied spectroscopic technique.

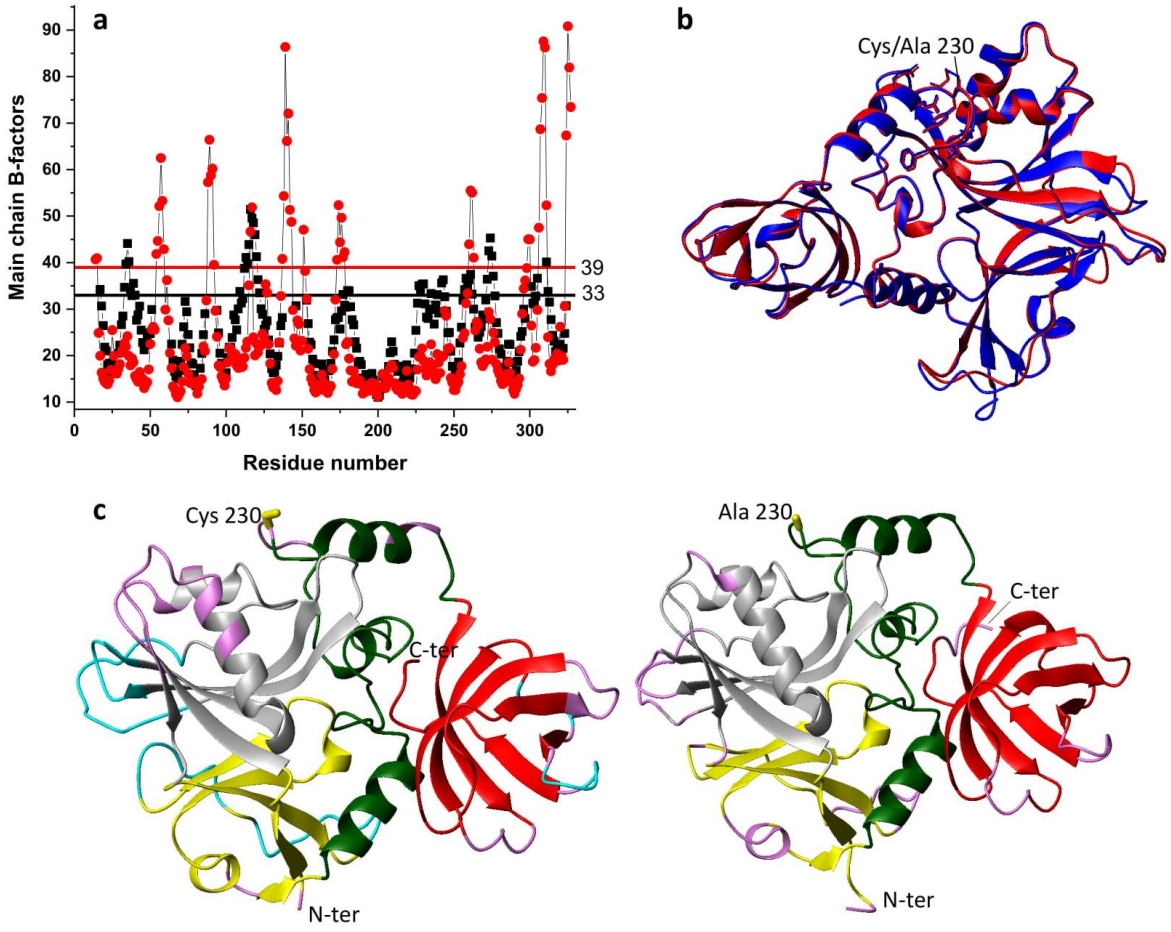

Figure S5. Comparison of the crystal structures and the B-factors of IBA57 and Cys230Ala IBA57 mutant. (a) Main chain B-factors of wild-type IBA57 (■) and Cys230Ala IBA57 mutant (●) are plotted versus residue number. The black and red horizontal lines indicate the averaged B-factor values plus one standard deviation (1σ), respectively. (b) Superimposition of the backbone of wild-type IBA57 (blue) and of Cys230Ala IBA57 mutant (red). The sidechains of the residues surrounding the conserved Cys 230 are shown in both structures. (c) The residues having a main chain B-factor value higher than the average value plus 1σ are colored in violet and the residues with very poor electron density are colored in cyano in the ribbon diagram of wild-type IBA57 (on the left) and Cys230Ala IBA57 mutant (on the right

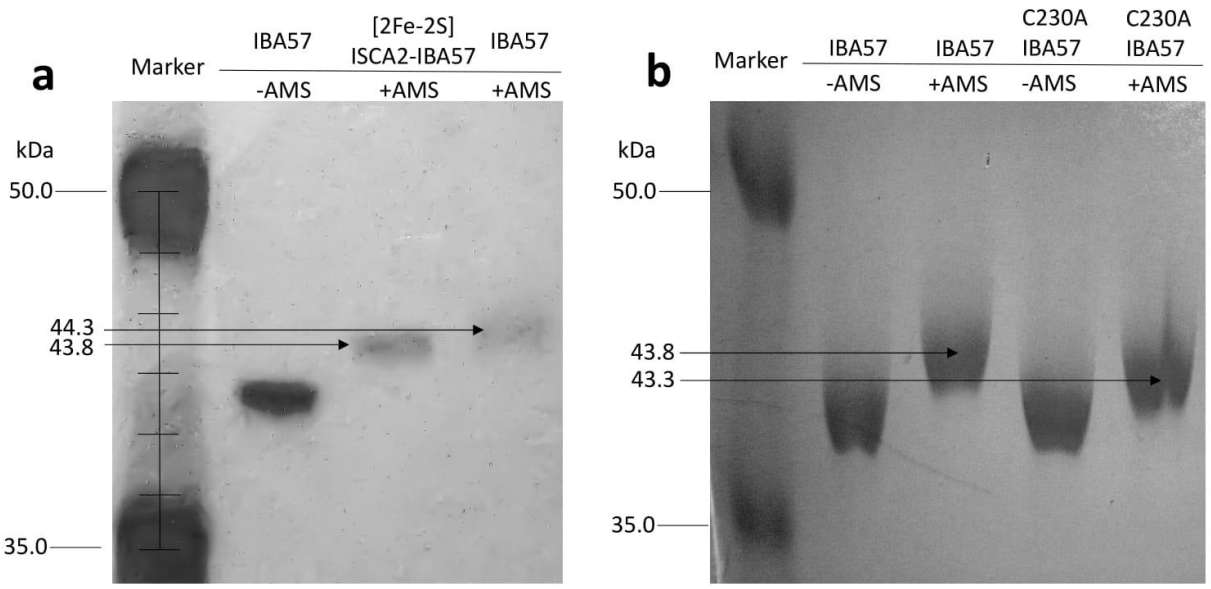

Figure S6. AMS-based alkylation gel shift assay on IBA57 and [2Fe-2S] ISCA2-IBA57. (a) Non-reducing SDS-PAGE (12%) of IBA57 (lane 2), AMS-reacted [2Fe-2S] ISCA2-IBA57 (lane 3), AMS-reacted IBA57. Kilodaltons of the molecular weight markers are indicated on the left. (b) Non-reducing SDS-PAGE (17%) of IBA57 (lane 2), AMS-reacted IBA57 (lane 3), Cys230Ala IBA57 (lane 4) and AMS-reacted Cys230Ala IBA57 (lane 5). Kilodaltons of the molecular weight markers are indicated on the left.

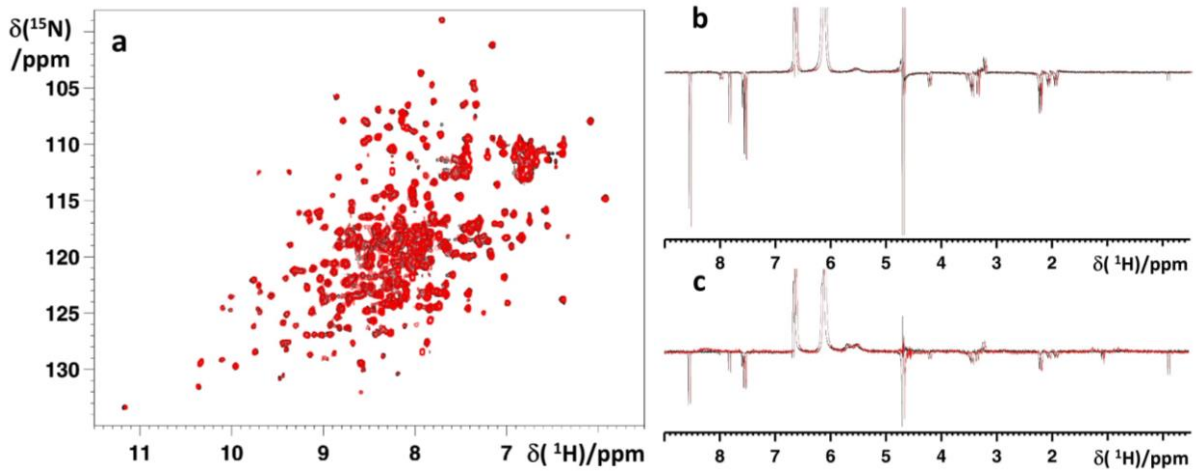

Figure S7. IBA57 does not interact with tetrahydrofolate derivatives. (a) Overlay of ^{1}H-^{15}N HSQC spectra of 15N-labelled IBA57 (0.35 mM) in the absence (red) and in the presence (black) of two equivalents of tetrahydrofolic acid. (b) Overlay of 1D 1H ePHOGSY spectra of calcium folinate (5 mM) (red) and in the presence of IBA57 protein (10 μM) (black). The two spectra were drifted of 0.05 ppm to compare signal intensities. (c) Overlay of 1D 1H ePHOGSY spectra of calcium folinate (1 mM) (red) and in the presence of [2Fe-2S] ISCA2-IBA57 complex (10 μM) (black). The two spectra were drifted of 0.05 ppm to compare signal intensities.

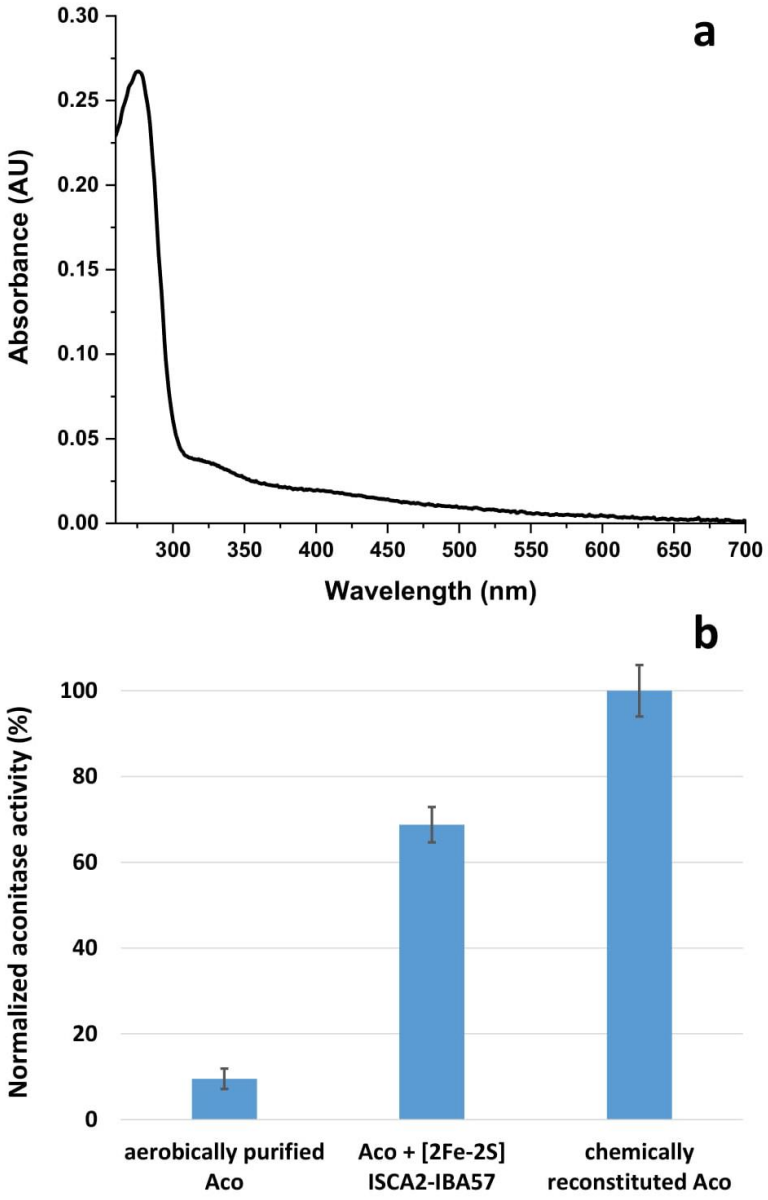

Figure S8. [2Fe-2S] ISCA2-IBA57 recycles apo aconitase into [4Fe-4S] aconitase. (a) UV-visible spectrum of aerobically purified aconitase in 50 mM phosphate buffer, 150 mM NaCl, 5 mM DTT, pH 7.0. (b) Aconitase activity assay: 5 µM aerobically purified aconitase was incubated at 25°C for 45 minutes with 25 µM of [2Fe-2S] ISCA2-IBA57 complex (Aco + [2Fe-2S] ISCA2-IBA57). Aconitase activity was then measured and it was expressed as a percentage of the activity obtained after the chemical reconstitution of the aerobically purified aconitase (chemically reconstituted Aco) performed under the same experimental conditions. Aconitase activity of aerobically purified aconitase (aerobically purified Aco) was also estimated and expressed with respect to chemically reconstituted Aco. Error bars indicate the standard deviation of results from two experiments.

.....

2.1.2 Overcoming the phasing problem using the magic triangle

I crystalized IBA57 and we determined its structure, in-house, by X-ray crystal diffraction using 5-amino-2,4,6-triiodoisophthalic acid (I3C) high energy remote SAD-phasing. We acquired sufficient data for phasing only from one single protein crystal of triclinic 3D structure.

The whole methodology is being extensively analyzed in the already submitted manuscript below.

.....

In-house high energy remote SAD-phasing using the magic triangle: how to tackle the P1 low symmetry using multiple orientations on the same human IBA57 crystal to increase multiplicity

Gourdoupis S. [#], Nasta V. [#], Ciofi-Baffoni S. [#§], Banci L. [#§] and Calderone V. [#§*]

[#] CERM - Center for Magnetic resonance, University of Florence, via Luigi Sacconi 6, 50019 Sesto Fiorentino (FI), Italy

[§] Department of Chemistry, University of Florence, via della Lastruccia 3, 50019 Sesto Fiorentino (FI), Italy

* Corresponding author

email address: calderone@cerm.unifi.it (Calderone V.)

Keywords: SAD phasing, I3C, magic triangle, P1, IBA57

Abstract

This paper describes the approach used to solve the protein structure in-house through 5-amino-2,4,6-triiodoisophthalic acid (I3C) high energy remote SAD-phasing. Multiple orientations of the same triclinic crystal have been exploited to acquire sufficient data redundancy for phasing. It is illustrated the multiplicity value that appears to be somehow a borderline between success and failure in phasing and how adding further data does not affect significantly substructure solution and model building. Furthermore, it is described how the collection of a native dataset and its joint use with the I3C derivative through a SIRAS approach decreases the data

redundancy needed by almost 50%. The protein on which this approach was carried out is human IBA57.

To our knowledge, this is the only structure present in the PDB which has been solved in-house, through remote SAD, in space group P1 and using one crystal only. All raw data used, deriving from the different orientations, will be deposited to Zenodo (https://zenodo.org) in order to enable software developers to improve methods for data processing and structure solution and for educational purposes.

Introduction

About two-thirds of recently deposited structures in the PDB have been solved using molecular replacement which requires the availability of an already solved structure of a protein homologous to the unknown one; on the contrary, experimental phasing has the advantage of being free from model bias and is required for samples that do not have any structurally related entries. Single anomalous dispersion (SAD) has become the most used method for de novo determination of protein crystal structures (Hendrickson, 2014) and it accounts for over 70% of the structures, determined by experimental phasing, deposited in the PDB (Berman, 2000, Bunkoczi *et al.*, 2015). Methods for experimental phasing based on the anomalous scattering of certain atoms (SAD and MAD), have replaced traditional methods like MIR. With the latest advances in synchrotron hardware, phasing with the weak anomalous signal from intrinsic scatterers has become a possible option, although high-quality data are normally required. These are more easily obtained when high symmetry enables a high data redundancy to be achieved, but lower symmetry examples have also proved successful (Lakomek *et al.*, 2009).

Heavy-atom soaks normally show a low success rate, but systematic heavy-atom screening with conventional heavy-metal ions has been performed using gel electrophoresis

(Boggon & Shapiro, 2000), mass spectrometry (Agniswamy *et al.*, 2008) or a database approach (Sugahara *et al.*, 2005).

The combination of phase information from a partial molecular-replacement solution and weak experimental phases has also proved to be successful in a number of cases (Tereshko *et al.*, 2008, Schuermann & Tanner, 2003, Roversi *et al.*, 2010).

Since soaking with heavy-atoms often suffers from non-specific binding, a new class of compounds has been developed that combines heavy atoms with functional groups for binding to proteins. The molecule 5-amino-2,4,6-triiodoisophthalic acid (I3C) contains three functional groups (two carboxylate groups and one amino group) that interact with proteins through hydrogen bonds. Three iodine atoms suitable for anomalous dispersion phasing are arranged in an equilateral triangle and are thus easily identifiable in the substructure. Anomalous scatterers such as halide ions or halogenated fragments have been more and more exploited for experimental phasing (Dauter & Dauter, 2007, Kim *et al.*, 2013, Liu *et al.*, 2011, Ramagopal *et al.*, 2003, Salgado *et al.*, 2005, Bauman *et al.*, 2016).

Halides such as bromine or iodine show a very large anomalous signal at the common wavelengths adopted at synchrotrons (corresponding at some absorption edge) but they still show a sufficient anomalous difference also at the lower energies typical of a diffractometer although these are further away from the proper edges. The success of such phasing depends on the occupancy, on the orderliness of the surface bound halide atoms and of course of the absence of radiation damage. In order to solve the structure of human IBA57, which crystallizes in space group P1, we have adopted a methodological approach based on an in-house remote SAD-phasing using the magic triangle I3C.

IBA57 is a 325-residue human protein which localizes to the mitochondrion and is part of the iron-sulfur cluster assembly pathway (Rouault, 2015). The maturation of mitochondrial iron-sulfur proteins requires a complex protein machinery. In the late phase of this machinery, a

[2Fe-2S] cluster is converted into a [4Fe-4S] cluster. Human IBA57 protein acts in this phase as an iron-sulfur cluster assembly component along with ISCA1 and ISCA2 (Sheftel *et al.*, 2010).

The structure of this protein was still unknown and the closest homologue whose structure was known showed 24% only sequence homology (which made molecular replacement very unlikely to be successful); for this reason, experimental phasing was the more likely way to try and solve it. We have thus adopted an approach based on an in-house I3C SAD data collection on a single P1 crystal in multiple orientations in order to gain sufficient multiplicity.

Materials and Methods

Cloning, expression and purification

Human IBA57 has been cloned, overexpressed and purified at homogeneity for crystallization experiments as described elsewhere (paper submitted).

Crystallization, data collection and structure determination

The purified IBA57 protein sample had a concentration of 0.4 mM and was dissolved in a solution containing 50 mM phosphate buffer, 150 mM NaCl and 2.5 mM TCEP. Crystallization trials on IBA57 were performed by the sitting drop vapor diffusion method at 20 °C by mixing an equal volume of the sample and of a solution containing 0.1 M MES pH 6.0 and 20 % PEG3350. Bunches of large, thin and superposed crystals started to grow overnight and grew to final size in a few days. The protruding edges of these bunches of superposed crystals were cut so as to obtain single crystals useful for diffraction. The chosen crystal was then soaked in the mother liquor containing 25 % ethylene glycol and 0.5 M 5-amino-2,4,6-triiodoisophthalic acid (I3C) (previously activated with LiOH) for 2-3 minutes since a longer time caused the crystal to crack.

The crystal diffracted to 2.0 Å resolution with data intensity being acceptably intense up to 2.3 Å; it belonged to the triclinic space group P1 (a = 38.08 Å, b = 43.03 Å, c = 59.24 Å, α = 77.90°, β = 75.63°, γ = 71.66°) with one molecule in the asymmetric unit and a solvent content of about 50%. Since the crystal belonged to the lowest possible symmetry space group and since SAD experiments need quite high data multiplicity in order to be successful, nine diffraction experiments at 100 K have been performed under several orientations (Table 1) using in-house K_α radiation on one crystal only, which proved to be the best crystal among quite poorly diffracting ones.

The data were collected by the rotation method using 1.0° oscillation for a total of 1136 degrees fully exploiting the 4-circle goniometer.

The nine datasets were processed using XDS (Kabsch, 2010) and scaled using XSCALE (Kabsch, 2010). The relevant statistics are shown in Table 2.

The analysis of the SAD Patterson maps and the first solvent flattening and chain tracing were performed with the program SHELXC/D/E (Sheldrick, 2010) as implemented in the HKL2MAP (Pape & Schneider, 2004) interface, using the first six datasets and it provided the positions of twelve iodine atoms in the asymmetric unit with good occupancies. The preliminary phases obtained were then improved by further phase refinement and density modification techniques using a solvent content of 50% with the program autoSHARP (Vonrhein *et al.*, 2007). Likewise the model tracing was performed by looping between BUCCANEER (Cowtan, 2006) and ARP/wARP (Langer *et al.*, 2008), which, in the end, allowed for a complete chain tracing. Structure determination will be explained in more details in the Results and Discussion section.

The refinement was then carried out using BUSTER (Bricogne G. *et al.*, 2016) making use of TLS restraints and water molecules were added during refinement. In between refinement cycles the model was subjected to manual adjustments using COOT (Emsley & Cowtan, 2004).

The stereochemical quality of the refined model was assessed using the program MOLPROBITY (Chen *et al.*, 2010). The Ramachandran plot was of good quality with no residues in the disallowed regions (except those residues in the loops which have been modeled anyway despite a very poor electron density). Figure 1 shows the ribbon representation of the solved structure of human IBA57 with the residue for which electron density is very poor if not absent at all highlighted in red. The relevant refinement statistics are shown in Table 2.

It also has to be pointed out that two more datasets have been collected after the above-mentioned SAD structure determination: a native dataset has been collected in-house in order to test to what extent SIRAS would have made structure determination easier, and lately, another native dataset has been collected at the synchrotron using beamline ID30B at ESRF (Grenoble, France) in order to achieve a higher resolution; in the latter case the structure was solved using the experimentally SAD-solved structure as the molecular replacement template and the structure has been refined at 1.75 Å resolution. The refinement statistics for the synchrotron collected dataset are shown in Table 2.

The coordinates and structure factors were deposited in the Protein Data Bank under the accession codes 5OLI (for the in-house I3C derivative) and 6ESR (for the higher resolution synchrotron structure).

Results and Discussion

SAD vs. SIRAS

Due to the immediate in-house availability of I3C the first attempt was that of a SAD experiment: it was in fact clear from the very beginning that experimental phasing of IBA57 would be the most likely way for solving its structure due to the absence of available models with sequence identity higher than 25%.

SAD was performed on iodine at the Cu_{α} wavelength which, although well above the L-I absorption edge of the element (2.389 Å), still grants about six electrons difference between f' and f''. The crystal was thus soaked for less than two minutes in a solution containing I3C and then put under the nitrogen flux in order to be diffracted.

While the data collection was going on, it appeared clear that the crystal belonged to space group P1 and so the collection of 360° of rotation around phi would certainly not ensure a great data redundancy due to the triclinic lowest possible symmetry. Multiplicity is in fact essential in anomalous dispersion phasing (especially in a SAD experiment) and allows for more accurate data measurements: the little anomalous differences must be greater than the error on the intensity estimate in order to be meaningful and to eventually led to structure solution.

Being the full phi rotation not enough to achieve a reasonable redundancy on a triclinic crystal, other experiments were setup; using one crystal showing a good diffraction nine datasets were collected on the same crystal exploiting the potential of the 4-circle goniometer (Table 1) leading to a total of 1136 degrees rotation.

The substructure was solved using all the nine datasets which were merged and scaled together keeping Friedel pairs separated: collectively these runs allowed to reach an anomalous multiplicity of about 5.6. The relevant intensities were then fed into the standard routine of SHELXC/D/E through the HKL2MAP interface. SHELXD found a solution with 12 iodine sites (Figure 2) with good figures of merit and correlation (CC All/Weak 24.8/11.2, CFOM= 36.0); this allowed SHELXE to trace over a hundred residues as poly Ala in one of the two hands. The chain was not continuous, but the electron density map of this solution did not appear random and it was possible to find patches of sensible density. So, this partial model output by SHELXE was then fed into the standard autoSHARP routine which refines phases, carries out density modification, traces with BUCCANEER first while performing density modification with PARROT, then carries out another solvent flattening on the model output by

BUCCANEER and in the end performs a last cycle of model building through ARP/wARP. This approach lead to a partial model traced by BUCCANEER showing 184 residues out of the 307 expected with the longest chain of 31 residues. A visual inspection of the electron density map computed with this model showed several well-defined regions and was very promising despite a not really outstanding R_{free} value (0.51). This partial model was then input again into the autoSHARP routine leading to a great improvement which yielded a model of 250 residues with the longest chain of 54 and an R_{free} of 0.40. Then again this model was used as input for a last autoSHARP routine and this eventually lead to a complete tracing of the structure with an R_{free} of 0.38. The model was then refined, and water added to the final R_{free}/R_{cryst} of 26.0/21.5. From a browsing of the PDB this is the first case, to our knowledge, of a protein structure which has been experimentally solved in-house, through SAD, using one crystal only in multiple orientations and in space group P1 which is the one with the lowest possible symmetry.

At this point it is relevant to define the smallest possible number of datasets needed to solve the structure and to identify what would be a reasonable threshold i.e. the minimum redundancy and phasing power needed to solve the phase problem. Thus we tested the SAD phasing efficiency of run 1 alone and run 1 plus the other runs which have been collected using the very same procedure applied for runs 1 to 9. What appeared evident was that it was not possible to trace the structure with a number of datasets lower than 7 although the SHELXC/D/E statistics look more or less the same in all cases. Only starting from runs 1-7 (multiplicity of about 4.8) it was possible to solve and trace the full structure possibly because of the increase of the phasing power along with the increasing number of datasets included. The dataset including runs 1 to 6 seems to be the borderline for successful structure solutions (Table 3). The same situation was also found if using a random combination of datasets. It is also to point out that, even in the unsuccessful dataset ensembles, the typical phasing statistics and the R_{free}/R_{cryst}

values appear very similar to those of the successful ensembles; nevertheless, chain tracing is not successful indicating a poor phase quality given by a not sufficient data redundancy.

We then obtained another crystal from the very same sample preparation of comparable quality to the one used for structure solution. We then collected a native dataset of it and analyzed to what extent SIRAS would be more efficient than SAD alone to solve the structure i.e. to what extent multiplicity could be lowered exploiting the isomorphous effect of iodine for structure solution.

The same procedure used for the first crystal (SHELXC/D/E and autoSHARP routine and subsequent loops with sequential partial models) was applied on the native dataset plus the various I3C datasets added one by one to the native one. In this case, three I3C datasets only were enough to succeed reducing the necessary multiplicity to a value below 3 thus decreasing it by half with respect to the SAD alone (Table 4).

Also in this case a random combination of datasets was tried out and the final result did not change.

Conclusions

The present paper deals with the experimental phasing of human IBA57. It is the only structure to our knowledge that has been solved in-house through remote SAD on an I3C derivative using one crystal only, despite the crystal is triclinic. In order to achieve sufficient multiplicity several orientations of the same crystal were collected. The redundancy threshold for successful phasing appeared to be around five, independent of the combination of datasets used. This value can be reduced to about half through SIRAS by exploiting the isomorphous differences with a second native dataset reaching a successful multiplicity value of less than three. All the raw data of the I3C derivative and the in-house native will be deposited to ZENODO (https://zenodo.org) both for educational purposes and to enable other crystallographers to

improve methods for data processing and structure solution and thus to benefit from these findings.

Acknowledgements

We thank the staff members of ID-30B beamline at ESRF (Grenoble, France) for assistance during data collection. We also thank Professor Kay Diederichs for suggestions and fruitful interactions.

The authors acknowledge the support and the use of resources of Instruct-ERIC, a Landmark ESFRI project, and specifically the CERM/CIRMMP Italy Centre.

This research is framed within the activities of the COST Action CA15133, supported by COST (European Cooperation in Science and Technology).

Tables and Figures

	Run 1	Run 2	Run 3	Run 4	Run 5	Run 6	Run 7	Run 8	Run 9
Theta (°)	0	0	0	0	0	0	0	0	0
Phi (°)	0 to 360	0	90	45	135	0	90	45	135
Kappa (°)	0	30	30	30	30	-30	-30	-30	-30
Omega (°)	0	-24 to 73	-24 to 73	-24 to 73	-24 to 73	-73 to 24	-73 to 24	-73 to 24	-73 to 24

Table 1 Description of the four angle ranges for each of the nine IBA57-I3C datasets collected

	IN-HOUSE IBA57-I3C	IBA57 SYNCHROTRON NATIVE
Diffraction source	Sealed tube	ID30B ESRF
Wavelength (Å)	1.54	0.97
Temperature (K)	100	100
Detector	Onyx CCD	Pilatus 6M
Crystal-to-detector distance (mm)	60	319.25
Oscillation range (°)	1	0.1
Total rotation range (°)	1136	360
Exposure time/image (s)	120	0.08
Space group	P1	P1
a, b, c (Å)	38.08 43.03 59.24	37.28 43.25 55.30
α, β, γ (°)	77.90 75.63 71.66	94.88 93.25 108.18
Mosaicity (°)	0.3	0.2
Resolution range (Å)	50.0 - 2.3	50.0 – 1.7
Total reflections	181082 (17654)	106801 (15660)
Unique reflections	15237 (1521)	31482 (4876)
Completeness (%)	99.9 (99.9)	95.0 (89.0)
Anomalous reflections	14701	-
Anomalous multiplicity	5.7	-
Anomalous completeness	97.5	-
$I/\sigma(I)$	10.7 (1.6)	11.9 (1.8)
$R_{p.i.m.}$	0.08	-
$R_{p.i.m.}$Ov	0.06	-
R_{merge} †	0.19	0.06
Wilson plot B factor (Å^2)	40.0	36.2
N° of sites	12	-
f'/f'' (refined)	-0.5 / 6.7	-
FOM (SHARP)	0.25	-
FOM (PARROT)	0.65	-
R_{cryst} / R_{free}‡ (%)	21.5/26.0	20.9/24.4

Protein atoms	2346	2346
Water molecules	88	107
Ligand atoms	63	-
RMSD bond lengths (Å)	0.010	0.007
RMSD bond angles (º)	1.090	0.965

Table 2 Data collection and refinement statistics of the in-house collected I3C derivative and of the synchrotron collected high resolution native dataset

†$R_{merge} = \sum_{hkl} \sum_i |I_i(hkl) - \langle I(hkl) \rangle| / \sum_{hkl} \sum_i I_i(hkl)$, where $I_i(hkl)$ is the mean intensity of the *i*th observation of symmetry-related reflections *hkl*.

‡$R_{cryst} = \sum_{hkl} \left| |F_{obs}| - |F_{calc}| \right| / \sum_{hkl} |F_{obs}|$, where F_{calc} is the calculated protein structure factor from the atomic model (R_{free} was calculated with a randomly selected 7% of the reflections).

SAD (IN-HOUSE IBA57-I3C)									
IBA57-I3C run(s)	1	1-2	1-3	1-4	1-5	1-6	1-7	1-8	1-9
Anomalous multiplicity (AIMLESS)	2.0	2.5	2.9	3.4	3.8	4.4	4.8	5.2	5.6
SHELXD CC All/Weak CFOM	24.6/11.2 35.8	25.4/10.6 36.0	25.4/10.5 35.9	25.6/12.2 37.8	25.9/11.6 37.5	24.8/11.2 36.0	25.2/10.0 35.2	26.2/10.2 36.4	25.3/11.7 37.0
SHELXE n° of residues n° of chains CC (%)	65 8 5.9	87 10 6.3	89 12 5.8	72 9 4.4	98 13 7.0	75 10 5.8	89 11 6.1	54 7 4.2	78 10 5.4
AutoSHARP FOM PP anom	FAILED FAILED	FAILED FAILED	0.20 0.49	0.21 0.51	0.19 0.55	0.24 0.53	0.24 0.54	0.19 0.58	0.24 0.64
Buccaneer Longest chain Sequenced R_{free}/R_{cryst}	FAILED FAILED FAILED FAILED	FAILED FAILED FAILED FAILED	156 17 0 0.52/0.52	142 25 0 0.52/0.50	190 29 0 0.52/0.50	154 17 0 0.50/0.50	184 31 31 0.51/0.49	136 38 0 0.50/0.50	165 30 0 0.51/0.51
ARP/wARP Longest chain Sequenced R_{free}/R_{cryst}	FAILED FAILED FAILED FAILED	FAILED FAILED FAILED FAILED	114 9 0 0.43/0.30	113 13 0 0.45/0.33	123 15 0 0.48/0.33	111 19 0 0.46/0.30	132 20 0 0.46/0.34	103 10 9 0.44/0.29	111 18 0 0.44/0.34

Table 3 Statistics for each ensemble of datasets of the substructure solution, phase refinement and chain tracing for SAD. The red characters show the failure in chain tracing with the relevant redundancy value; the green show the successful values.

SIRAS (IBA57 IN-HOUSE IBA57-I3C + IN-HOUSE NATIVE IBA57)									
IBA57-I3C run(s)	1	1-2	1-3	1-4	1-5	1-6	1-7	1-8	1-9
Anomalous multiplicity (AIMLESS)	2.0	2.5	2.9	3.4	3.8	4.4	4.8	5.2	5.6
SHELXD CC All/Weak CFOM	22.1/12.6 34.7	20.9/11.4 32.2	21.4/11.9 33.3	21.2/11.4 32.6	22.2/12.3 34.5	22.2/18.8 35.0	23.0/13.4 36.4	23.6/14.2 37.7	22.7/13.2 35.9
SHELXE n° of residues n° of chains CC (%)	 110 15 8.8	 96 14 7.9	 103 13 9.3	 86 10 10.2	 94 12 7.7	 101 12 7.50	 92 9 8.9	 95 13 9.0	 85 11 7.4
AutoSHARP FOM PP anom PP iso	 0.20 0.62 1.05	 0.24 0.65 1.15	 0.21 0.60 1.0	 0.21 0.61 1.01	 0.20 0.61 1.00	 0.18 0.60 0.92	 0.19 0.58 0.86	 0.22 0.65 1.00	 0.22 0.66 0.99
Buccaneer Longest chain Sequenced R_{free}/R_{cryst}	61 14 0 0.53/0.52	127 24 14 0.52/0.53	277 81 200 0.47/0.47	241 22 0 0.51/0.51	153 26 17 0.54/0.53	190 33 30 0.51/0.50	172 18 2 0.49/0.48	285 64 255 0.45/0.45	180 24 0 0.52/0.52
ARP/wARP Longest chain Sequenced R_{free}/R_{cryst}	64 11 0 0.49/0.33	80 9 0 0.50/0.33	179 27 44 0.44/0.30	134 13 0 0.46/0.31	110 10 0 0.49/0.35	145 27 0 0.47/0.33	111 11 0 0.51/0.35	213 48 118 0.38/0.30	94 9 7 0.49/0.35

Table 4 Statistics for each ensemble of datasets of the substructure solution, phase refinement and chain tracing for SIRAS. The red characters show the failure in chain tracing with the relevant redundancy value; the green show the successful values.

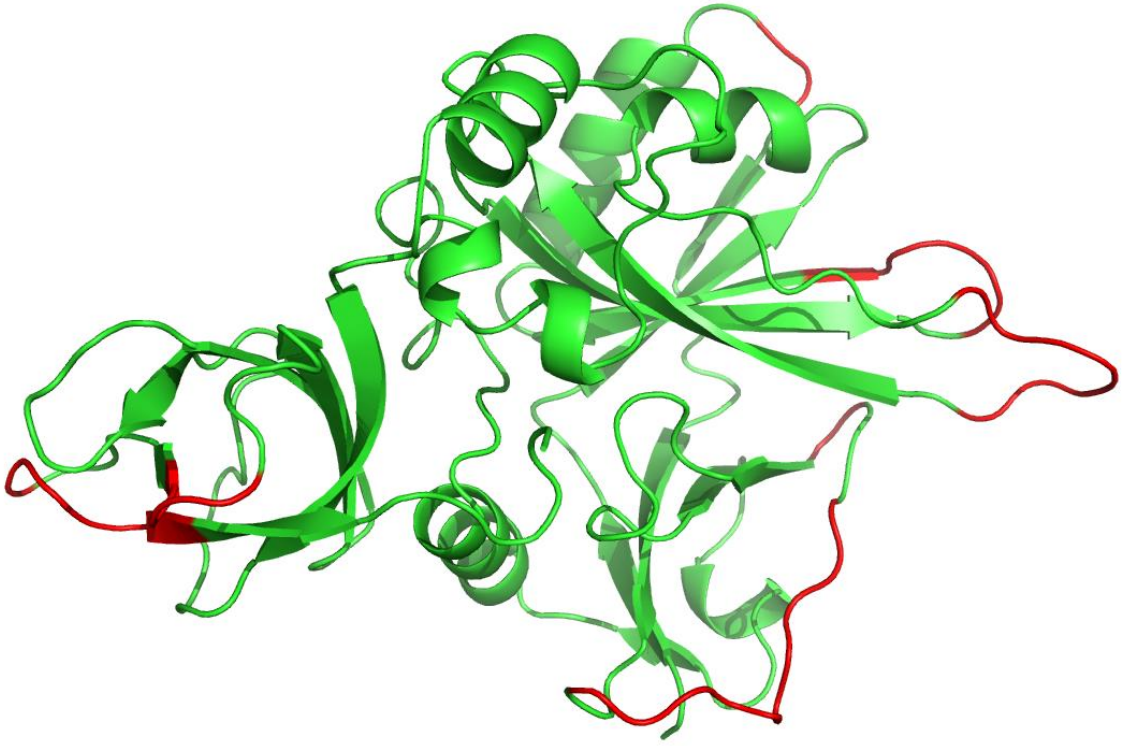

Fig. 1 Secondary structure ribbon representation of the structure of human IBA57. Highlighted in red the residues for which very poor or no electron density at all is observed.

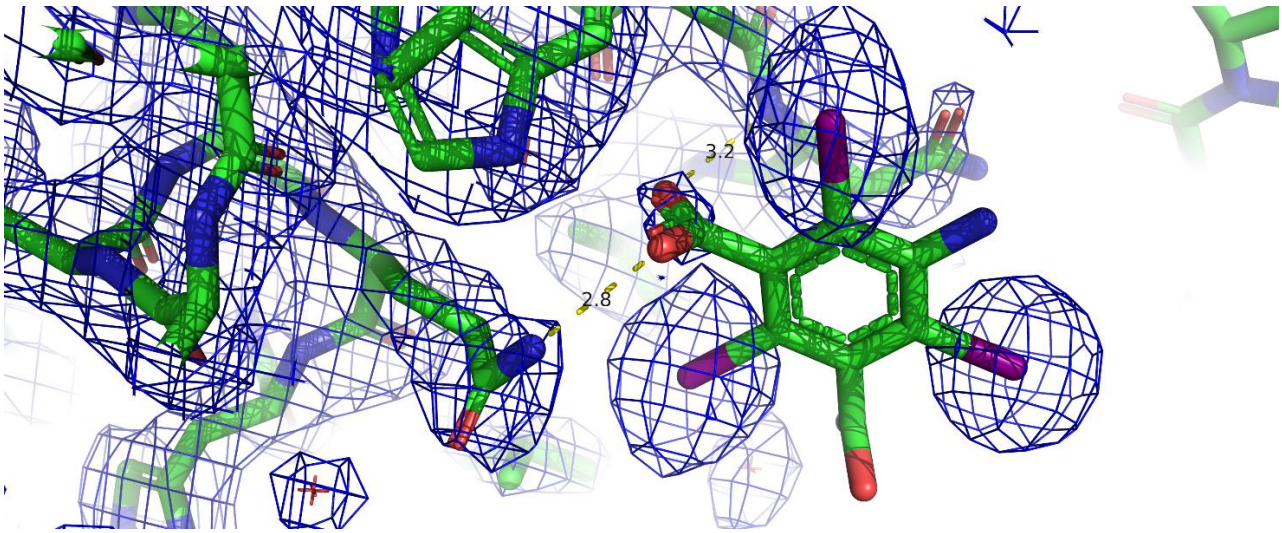

Fig. 2 Detail of the electron density of one of the four molecules of I3C bound through hydrogen bonds to two residues on the surface of IBA57

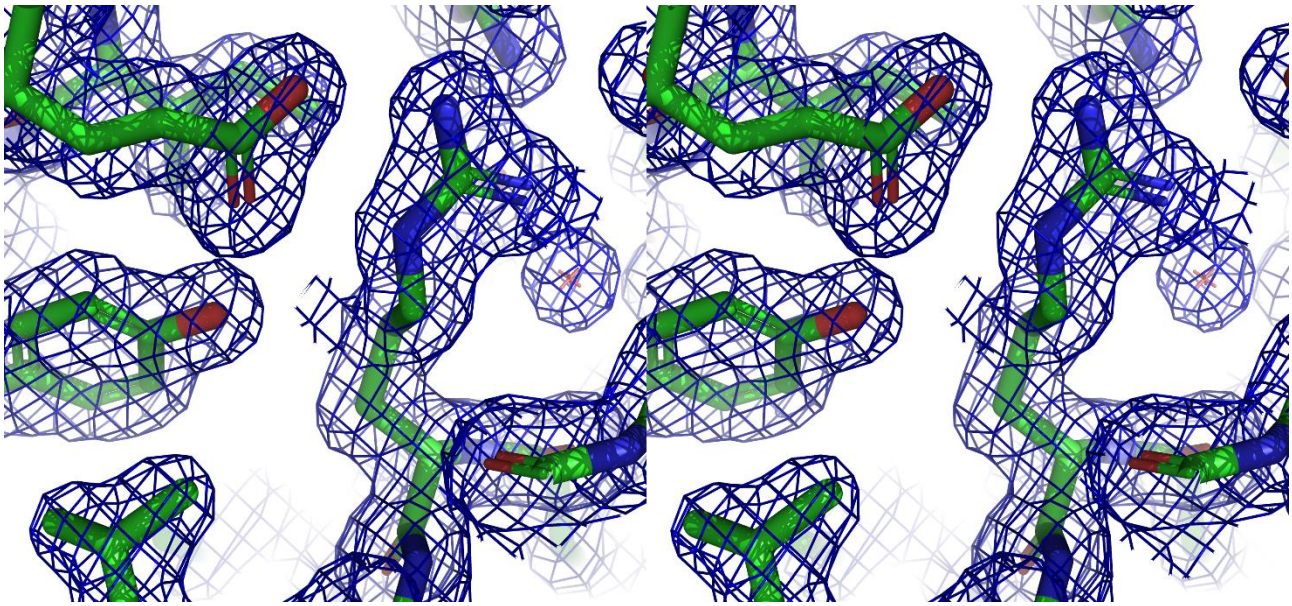

Fig. 3 Stereo representation of the quality of the electron density of 6ESR

References

Agniswamy, J., Joyce, M. G., Hammer, C. H. & Sun, P. D. (2008). *Acta Crystallogr D Biol Crystallogr* **64**, 354-367.

Bauman, J. D., Harrison, J. J. & Arnold, E. (2016). *IUCrJ* **3**, 51-60.

Berman, H. M. (2000). *Nucleic Acids Research* **28**, 235-242.

Boggon, T. J. & Shapiro, L. (2000). *Structure* **8**, R143-R149.

Bricogne G., Blanc E., Brandl M., Flensburg C., Keller P., Paciorek W., Roversi P., Sharff A., Smart O.S., Vonrhein C. & T.O., W. (2016). *Cambridge, United Kingdom: Global Phasing Ltd.*

Bunkoczi, G., McCoy, A. J., Echols, N., Grosse-Kunstleve, R. W., Adams, P. D., Holton, J. M., Read, R. J. & Terwilliger, T. C. (2015). *Nat Methods* **12**, 127-130.

Chen, V. B., Arendall, W. B., III, Headd, J. J., Keedy, D. A., Immormino, R. M., Kapral, G. J., Murray, L. W., Richardson, J. S. & Richardson, D. C. (2010). *Acta Crystallogr. D Biol. Crystallogr* **66**, 12-21.

Cowtan, K. (2006). *Acta Cryst. D* **62**, 1002-1011.

Dauter, M. & Dauter, Z. (2007). *Methods Mol Biol* **364**, 149-158.

Emsley, P. & Cowtan, K. (2004). *Acta Crystallogr. D. Biol. Crystallogr* **60**, 2126-2132.

Hendrickson, W. A. (2014). *Q Rev Biophys* **47**, 49-93.

Kabsch, W. (2010). *Acta Crystallogr. D. Biol. Crystallogr* **66**, 125-132.

Kim, M. K., Lee, S., An, Y. J., Jeong, C. S., Ji, C. J., Lee, J. W. & Cha, S. S. (2013). *Mol Cells* **36**, 74-81.

Lakomek, K., Dickmanns, A., Mueller, U., Kollmann, K., Deuschl, F., Berndt, A., Lubke, T. & Ficner, R. (2009). *Acta Crystallogr D Biol Crystallogr* **65**, 220-228.

Langer, G., Cohen, S. X., Lamzin, V. S. & Perrakis, A. (2008). *Nat. Protoc* **3**.

Liu, X., Zhang, H., Wang, X. J., Li, L. F. & Su, X. D. (2011). *PLoS One* **6**, e24227.

Pape, T. & Schneider, T. R. (2004). *Journal of Applied Crystallography* **37**, 843-844.

Ramagopal, U. A., Dauter, M. & Dauter, Z. (2003). *Acta Crystallographica Section D Biological Crystallography* **59**, 868-875.

Rouault, T. A. (2015). *Nat Rev Mol Cell Biol* **16**, 45-55.

Roversi, P., Johnson, S. & Lea, S. M. (2010). *Acta Crystallogr D Biol Crystallogr* **66**, 420-425.

Salgado, P. S., Walsh, M. A., Laurila, M. R., Stuart, D. I. & Grimes, J. M. (2005). *Acta Crystallogr D Biol Crystallogr* **61**, 108-111.

Schuermann, J. P. & Tanner, J. J. (2003). *Acta Crystallographica Section D Biological Crystallography* **59**, 1731-1736.

Sheftel, A., Stehling, O. & Lill, R. (2010). *Trends Endocrinol Metab* **21**, 302-314.

Sheldrick, G. M. (2010). *Acta Crystallogr. D. Biol. Crystallogr* **66**, 479-485.

Sugahara, M., Asada, Y., Ayama, H., Ukawa, H., Taka, H. & Kunishima, N. (2005). *Acta Crystallogr D Biol Crystallogr* **61**, 1302-1305.

Tereshko, V., Uysal, S., Koide, A., Margalef, K., Koide, S. & Kossiakoff, A. A. (2008). *Protein Sci* **17**, 1175-1187.

Vonrhein, C., Blanc, E., Roversi, P. & Bricogne, G. (2007). *Methods Mol. Biol* **364**, 215-230.

.....

2.2 NFU1 characterization and potential role of BOLA3

Both the genes of BOLA3 and NFU1 are located on the same chromosome (2p13) while the expression level of the one is directly affected by the expression level of the other. [39] BOLA3 is indispensable for the stability of NFU1 [65] and together are implicated in functioning late in the mitochondrial Fe-S cluster assembly machinery. [66] These observations point out a correlation between the two proteins, a correlation that I tried to identify, interpret and explain.

I developed a protocol for the expression and purification of NFU1 from *E. coli* cells. I also produced BOLA3 and GLRX5 by following protocols already developed here at the Magnetic Resonance Center (CERM). [25][27] By a combination of NMR, EPR, UV/Vis, UV/Vis CD, DLS and SEC techniques I managed to demonstrate that (i) apo NFU1 is a mixture of monomer and dimer in solution and that the ratio between the two forms is ionic strength dependent, (ii) NFU1 binds a [4Fe-4S] cluster in an homo-dimeric state either by incubating the protein with an excess of $FeCl_3$ and Na_2S or with [2Fe-2S] GLRX5-BOLA3 and GSH, at the presence of dithiothreitol (DTT), under anaerobic conditions and (iii) no cluster uptake was observed neither upon incubation of NFU1 with [2Fe-2S] GLRX5 nor [4Fe-4S] NFU1 with GLRX5.

This behavior suggests a direct functional connection between NFU1 and BOLA3 and an obvious demonstration of the role of BOLA3 as a potential «switch» partner which turns ON and OFF the cluster transfer on the pathway of NFU1.

This work is extensively analyzed in the manuscript below while further data analysis and experiments are ongoing to complete it.

.....

Mitochondrial human NFU1 assembles a [4Fe-4S] cluster upon interaction with [2Fe-2S] BOLA3-GLRX5

Authors...

[1]Magnetic Resonance Center CERM, University of Florence, Via Luigi Sacconi 6, 50019, Sesto Fiorentino, Florence, Italy.

[2]Department of Chemistry, University of Florence, Via della Lastruccia 3, 50019 Sesto Fiorentino, Florence, Italy.

Introduction

Mitochondria play a key role in the maturation of all iron-sulfur (Fe-S) proteins throughout the cell. [1][2][3]A pool of mitochondrial proteins, which form the mitochondrial iron-sulfur cluster (ISC) assembly machinery, are required for the assembly of both mitochondrial and cytosolic/nuclear iron-sulfur. [4] In mitochondrial ISC assembly machinery, [4Fe-4S] clusters are synthesized by scaffold proteins, such as ISCU and ISCAs proteins in humans, and then specifically transferred to apo client proteins by the so-called iron-sulfur cluster targeting factors. One of these factors is the universally present mitochondrial NFU1, which in humans is required for the proper assembly of a subset of mitochondrial [4Fe-4S] proteins, which include components of respiratory complexes I and II, and lipoic acid synthase. [5][6][7] It has been proposed that mitochondrial NFU1, assisted by BOLA3, another protein of the mitochondrial ISC machinery, [5] functions to facilitate [4Fe-4S] transfer to apo client proteins preventing oxidative damage to the cluster. [8] BOLA3 has been also found to form a stable dimeric heterocomplex with monothiol glutaredoxin 5 (GLRX5), [8][9][10] a component of the mitochondrial ISC assembly machinery that operates upstream in the machinery by receiving a [2Fe-2S] cluster *de novo* assembled on the ISCU scaffold protein. [4][11] The dimeric GLRX5-BOLA3 complex is formed both as apo and with a bridged

[2Fe-2S] cluster, and the holo form of the heterocomplex is preferentially formed with respect to homodimeric [2Fe-2S] GLRX5. [8][9] The proposed functional role of the [2Fe-2S] heterocomplex is that of transferring the cluster to apo acceptor(s), although the target(s) need(s) to be identified. [9][10]

What makes mitochondrial NFU1 and BOLA3 particularly compelling to study is their involvement in human diseases. Point mutations in, or deficiencies of, NFU1 or BOLA3 protein cause two fatal mitochondrial diseases called multiple mitochondrial dysfunction syndromes, related to functional NFU1 and BOLA3 deficiency (MMDS1 and MMDS2, respectively), and characterized by symptoms such as lactic acidosis, hyperglycinemia and reduced activity of respiratory chain complexes I and II. [5][6][12][13][14][15][16][17] Somewhat surprisingly, given the severity of the human phenotype, is that depletion or deletion of NFU1 from HeLa cells [6] and yeast *Saccharomyces cerevisiae*, [18] causes only a very mild growth phenotype in culture. However, a specific impact on several enzymatic activities of [4Fe-4S] mitochondrial proteins has been detected. The similarities of phenotypes in patients with MMDS mutations in mitochondrial NFU1 or in BOLA3 are in agreement with the proposal that the two proteins act as protein partners in a common step of the mitochondrial ISC assembly machinery. [6][8]The physical interactions of mitochondrial NFU1 with BOLA3, and with ISCA1 and ISCA2, [8] the two members of the mitochondrial ISC assembly machinery receiving two [2Fe-2S] clusters from GLRX5 and coupling them to form a [4Fe-4S] cluster, [19] supported a mechanism where NFU1 receives a [4Fe-4S] cluster assembled on a ISCA1-ISCA2 hetero-complex [19] and then transfers the [4Fe-4S] cluster to apo client proteins with the assistance of BOLA3. [8] However, this mechanism does not take into account the possible interaction with the GLRX5-BOLA3 complex, whose function remains undefined, as well as it does not explain how BOLA3 functions with NFU1 in cluster transfer to apo client proteins.

Analyses of genomic DNA, transcripts, and translation products indicate that alternative splicing of a common pre-mRNA results in synthesis of two NFU human isoforms with distinct subcellular localizations. Isoform I is localized in the mitochondria, whereas isoform II is present in the cytosol and the nucleus. [7] A recent structural characterization of human apo NFU1 isoform II showed that the protein is monomeric in solution and adopts a dumbbell-shaped structure with well-structured N- and

C- terminal domains connected by a flexible linker. [23] It has been also shown that chemically reconstituted NFU1 isoform II binds a [4Fe-4S] cluster by forming a trimer of dimers, each containing a [4Fe-4S] cluster. [23] Specifically, combined NMR and SAXS data identified three N-terminal domains involved in the formation of a tripartite interface, while two conserved cysteines in the C-terminal domain ligate a [4Fe-4S] cluster to form a dimer by bridging two C-terminal domains.

In order to assess define the role of BOLA3 in this mechanism, we have here first characterized the mitochondrial holo isoform I of human NFU1 (mNFU1 hereafter) by NMR, and then investigated, by NMR and UV-visible absorption/CD spectroscopies, cluster transfer/assembly on human apo mNFU1 upon the interaction with human [2Fe-2S] BOLA3-GLRX5 or [2Fe-2S] GLRX5.

Results and Discussion

Mitochondrial human NFU1 isoform I in its apo and [4Fe-4S] cluster bound states

Human mNFU1 purified from *E. coli* cells was always isolated in the apo form in all our tested conditions. The protein was thus chemically reconstituted following a standard protocol (see Materials and Methods for details). UV-visible absorption of chemically reconstituted mNFU1 (**Figure S1**) showed the presence of a broad band centered at 420 nm, as previously reported, [7] which typically dominates the absorption spectra of all biological $[4Fe\text{-}4S]^{2+}$ centers. [25] The CD spectrum of chemically reconstituted mNFU1 (**Figure S1**) in the UV-visible region is very weak and featureless, which is also characteristic of many biological $[4Fe\text{-}4S]^{2+}$ clusters. [25][26] Moreover, the extinction coefficient at 420 nm of 8.3 $mM^{-1}\,cm^{-1}$, based on the mNFU1 monomeric concentration, is indicative of approximately one $[4Fe\text{-}4S]^{2+}$ cluster per mNFU1 dimer. [22][24]

To further corroborate the formation of a dimeric, [4Fe-4S] cluster-loaded species, ^{15}N heteronuclear NMR measurements (i.e. $^{1}H\text{-}^{15}N$ heteronuclear single-quantum correlation (HSQC) and R_2, R_1 and $^{15}N\{^{1}H\}$ NOE relaxation experiments) were performed on both apo and $[4Fe\text{-}4S]^{2+}$ ^{15}N-labeled mNFU1. The comparison of the $^{1}H\text{-}^{15}N$ HSQC spectra of apo mNFU1 (**Figure 1A**, red) and those of the

chemically reconstituted $[4Fe\text{-}4S]^{2+}$ mNFU1 (**Figure 1A**, blue), acquired in the presence of 5 mM DTT, revealed that Fe-S cluster binding led to large chemical shift perturbations and significant line broadening. Moreover, only one set of peaks was observed in both $^{1}H\text{-}^{15}N$ spectra, indicating the presence of a single species for both the apo and the holo forms. Two sets of signals with variable peak volume, one corresponding to the apo form and the other to the $[4Fe\text{-}4S]^{2+}$ form, were observed only when the chemical reconstitution process was not efficient (**Figure S1**). This behavior differs from what previously reported [23], where, in the NMR spectrum of [4Fe-4S] NFU1 cytosolic isoform II, a few residues of the N-terminal domain exhibited two sets of peaks with equal peak volume, which were, respectively, assigned to the free N-terminal domains and to the N-terminal domains that form the tripartite interface in the trimer of dimers of [4Fe-4S] NFU1. These divergent NMR features suggested different protein aggregation properties in our [4Fe-4S] mNFU1 sample with respect to what previously obtained for the cytosolic isoform II of NFU1.

From the average R_2/R_1 ratios an estimate of the reorientational correlation time was obtained for the various forms. Apo mNFU1 in the absence of NaCl has a reorientational correlation time of 13.5 ns, the value expected for a monomeric globular protein of 22 kDa (data not shown). However, analytical gel-filtration and SEC-MALS, performed on the same sample, showed, in addition to a major species corresponding to the monomer, the presence of a minor species, eluting with a molar mass of 47 kDa (**Figure S2C**), which is close to the molecular weight of a homodimeric molecule of mNFU1 (44 kDa). The monomeric and dimeric forms are in equilibrium, which is almost fully shifted toward the monomeric state upon increase of the ionic strength up to 150 mM NaCl (**Figure S2D**). In agreement with this, the reorientational correlation time decreased from 13.5 to 11.75 ns by addition of 150 mM NaCl, consistent with a monomeric protein of 19 kDa (data not shown). This value is lower than that expected for a molecule of 22 kDa molecular weight, suggesting that some flexibility between the two domains of mNFU1 is present, as previously observed in the cytosolic isoform II of NFU1. [23] The reorientational correlation time obtained for the chemically reconstituted $[4Fe\text{-}4S]^{2+}$ mNFU1 in the presence of 150 mM NaCl is 15.1 ns, indicating the occurrence of protein dimerization upon cluster

binding (data not shown), in agreement with the UV-vis and ^{1}H-^{15}N HSQC data that also suggested the presence of a dimeric holo species. Again, this value is lower than the value expected for a globular dimeric protein of 44 kDa, possibly suggesting some flexibility between the two domains of mNFU1. To better address this point, we are now producing the C-terminal domain form of mNFU1 and compare the reorientational correlation times of apo and holo forms. In any case, the calculated value of 15.1 ns fully excluded the presence of the trimer of dimers previously observed. [23] The different aggregation properties can be rationalized considering that different NFU1 isoforms have been used in the two studies. Indeed, the cytosolic isoform II of NFU1 previously studied by NMR and SAXS [23] consisted of residues 16-254, while in our studies the mitochondrial isoform of NFU1 consists of 59-254 residues. [7] It seems that the N-terminal tail drives the formation of the bundling of three [4Fe-4S] clusters in a single aggregate of cytosolic isoform II of [4Fe-4S] NFU1, thus possibly discriminating the function or the target specificity of [4Fe-4S] NFU1 between the two cellular compartments. This interpretation is consistent with the structural model of the cytosolic isoform II of [4Fe-4S] NFU1, in which, indeed, the N-terminal domain forms the tripartite interface of the trimer.

1D ^{1}H paramagnetic NMR spectroscopy was applied to investigate the cluster binding properties of $[4Fe\text{-}4S]^{2+}$ mNFU1. The paramagnetic 1D ^{1}H NMR spectrum of $[4Fe\text{-}4S]^{2+}$ mNFU1 showed the presence of three intense hyperfine shifted signals in the 20-11 ppm spectral region (19.9, 19.4, 12.6 ppm, **Figure 1B**). The temperature dependence of these signals indicates that they have an anti-Curie behavior. The values and the anti-Curie temperature dependence of the chemical shift of these signals, as well as their linewidths, are typical of βCH_2 signals of Cys residues bound to a $[4Fe\text{-}4S]^{2+}$ cluster with an S=0 electronic ground state, with the paramagnetism arising from excited states of the electron spin ladder, that are partially populated at room temperature. [23] The three intense hyperfine shifted signals can be tentatively assigned to one β-CH_2 proton of three out of four Cys ligands, according to the sequence-specific assignment of Cys β-CH_2 protons in analogous protein-bound $[4Fe\text{-}4S]^{2+}$ cluster. [20] The β-CH_2 proton of the fourth Cys ligand is possibly enveloped in the diamagnetic region or too broad to be detected.

The data suggest the presence of a dimeric $[4Fe\text{-}4S]^{2+}$ mNFU1 coordinating the cluster with the two cysteines of the conserved CXXC motif of the C-terminal domain. Two weaker hyperfine shifted signals at 14.4 and 13.3 ppm are also present in the same region showing an anti-Curie temperature dependence (**Figure 1B**). These data indicate the presence of a minor species still with a $[4Fe\text{-}4S]^{2+}$ cluster. By adding 10 mM glutathione (GSH) to this sample, the 1D ^{1}H paramagnetic NMR spectrum changes showing the presence of two further hyperfine shifted signals at 15.2 and 11.2 ppm (**Figure 1B**), indicating that GSH modifies the coordination environment, likely acting as a ligand with its Cys residue. However, GSH does not fully replace the Cys ligand(s) since the three signals at 19.9, 19.4, 12.6 ppm are still detected (**Figure 1B**). A mixture of at least two $[4Fe\text{-}4S]^{2+}$ species is present, one with all protein-derived Cys ligands and the other with one GSH ligand and three protein-derived Cys ligands. Upon addition of 5 mM dithiothreitol (DTT) on the latter sample, the 1D ^{1}H paramagnetic NMR spectrum shows further changes. Specifically, the three original signals at 19.9, 19.4, 12.6 ppm as well as the two GSH-derived signals disappear and three strong signals at 20.1, 14.4 and 13.3 ppm and a low intense signal at 17.8 ppm appear, all having an anti-Curie temperature dependence (**Figure 1B**). The size and the anti-Curie temperature dependence of the chemical shift of these signals indicate that a $[4Fe\text{-}4S]^{2+}$ cluster with an S=0 electronic ground state is bound to mNFU1 also in the presence of DTT.

These data support the conclusion that the coordination environment is again modified by addition of DTT, which acts as a cluster ligand and displaces GSH from coordination. In agreement with this interpretation of the NMR data, the paramagnetic 1D ^{1}H NMR spectrum of $[4Fe\text{-}4S]^{2+}$ mNFU1 acquired in the presence of 5 mM DTT only is perfectly superimposable with that acquired in the presence of 10 mM GSH and 5 mM DTT (**Figure 1B**), confirming that DTT fully displaced GSH in the coordination sphere of the cluster, which thus does not participate anymore in cluster binding in this experimental condition. Specifically, since three intense hyperfine shifted signals are still detected in the paramagnetic 1D ^{1}H NMR spectrum in the presence of DTT, we can assume that only a Cys ligand is replaced by a DTT molecule (DTT-bound $[4Fe\text{-}4S]^{2+}$ mNFU1, hereafter), and most probably the same occurs in the presence of GSH only. Finally, the chemical shifts of the signals of $[4Fe\text{-}4S]^{2+}$ mNFU1 acquired in the presence of 5 mM DTT match those of the minor species detected with no DTT and GSH, indicating

that DTT-bound $[4Fe\text{-}4S]^{2+}$ mNFU1 is present as minor form in the original sample. The latter form is originated by the presence of DTT in the reaction mixture of the chemical reconstitution, which is not completely removed from the solution by PD-10 desalting column as involved in cluster binding (see Materials and Methods for details).

The effect of DTT and GSH on the protein aggregation state of $[4Fe\text{-}4S]^{2+}$ mNFU1 was then investigated to verify whether cluster binding by GSH/DTT molecules monomerizes [4Fe-4S] mNFU1. $^{1}H\text{-}^{15}N$ HSQC experiments and ^{15}N relaxation experiments were thus acquired upon the presence/lack of GSH and/or DTT. In the $^{1}H\text{-}^{15}N$ HSQC spectrum acquired on GSH- and DTT-free $[4Fe\text{-}4S]^{2+}$ mNFU1 two sets of signals with different intensities (70% vs. 30%) for some NHs have been detected (data now shown). This result matches with the paramagnetic NMR data which also showed the presence of a major species assigned to $[4Fe\text{-}4S]^{2+}$ mNFU1 with all protein-derived Cys ligands and a minor species assigned to DTT-bound $[4Fe\text{-}4S]^{2+}$ mNFU1. Upon addition of 5 mM GSH, the intensity of the two sets of signals changes by detecting the increase of intensity of the weak signals and a corresponding decrease of intensity of the strong signals (data not shown). Upon addition of 5 mM DTT, only one set of signals is observed corresponding to the chemical shifts of the weak signals (data not shown). The chemical shifts of all these signals do not correspond to the chemical shifts of apo mNFU1 (data not shown). These data corroborate the previous conclusions that i) GSH and DTT can replace a Cys ligand competing for the same coordination site, ii) DTT fully substitutes a Cys ligand in the coordination sphere of the cluster, while GSH partially does; and showed that both GSH and DTT do not promote the formation of a monomeric $[4Fe\text{-}4S]^{2+}$ mNFU1 form with two GSH or one/two DTT molecules bound to the cluster, since no apo mNFU1 is formed in solution. Following the interaction between apo mNFU1 and GSH by $^{1}H\text{-}^{15}N$ HSQC experiments, we observe that the chemical shifts of few signals (Cys 213, Ser 215, Ser 216, Ile 217, Ile 218, Leu 220) change upon addition of 5 mM GSH (data not shown). These residues include Cys 213 of the conserved CXXC motif and are clustered in the first two turns of the α-helix that follows to the CXXC motif. Cys 213 is the expected cluster ligand and is more solvent exposed

than Cys 210, the other expected ligand of the conserved CXXC motif (**Figure 2C**). These data show an interaction between GSH and the region close to the solvent-exposed Cys 213, suggesting that this

cysteine can be the preferential site to be displaced by GSH in the $[4Fe\text{-}4S]^{2+}$ mNFU1. RELAXATION data in progress

In conclusion, the NMR data indicate that mNFU1 binds a $[4Fe\text{-}4S]^{2+}$ cluster coordinating it via the two cysteines of the CXXC motif of the C-terminal domain in a cluster-bridged dimeric state. This species is in equilibrium with a dimeric $[4Fe\text{-}4S]^{2+}$ cluster-bound species where a Cys ligand is replaced by a S-donor small molecule ligand, such as GSH or DTT (**Scheme 1**). This equilibrium can have a functional significance. Indeed, the proteins involved metal transfer, i.e. metallochaperones, typically have an accessible coordination site that is invaded by the donor atom of the metal-receiving partner to promote a rapid metal-exchange reaction. The equilibrium in **Scheme 1** can thus mimic this mechanism, i.e. cluster transfer from $[4Fe\text{-}4S]^{2+}$ mNFU1 to apo client proteins is promoted by a S-based ligand-exchange reaction. This mechanism is in agreement with the proposed functional role of mNFU1, which acts as iron-sulfur cluster targeting factor.

BOLA3 drives the [4Fe-4S] cluster assembly from the [2Fe-2S] BOLA3-GLRX5 hetero-complex to mitochondrial NFU1

We investigated by NMR and UV-visible/CD spectroscopy the interaction between the [2Fe-2S] BOLA3-GLRX5 hetero-complex, [9][27] and apo mNFU1, to test whether Fe-S cluster transfer/assembly occurs. The experiments were performed by adding apo mNFU1 to the [2Fe-2S] BOLA3-GLRX5 hetero-complex or vice versa, ^{15}N-labeling one protein at a time for each experiment. By comparing the UV-visible spectra of the [2Fe-2S] ^{15}N GLRX5-BOLA3 hetero complex before and after the addition of apo mNFU1, it resulted a change from the characteristic absorption bands of the [2Fe-2S] cluster to that of [4Fe-4S] bands, demonstrating that cluster transfer and assembly of a [4Fe-4S] cluster from [2Fe-2S] ^{15}N GLRX5-BOLA3 to mNFU1. The same reaction, followed by visible CD, showed the loss of intensity of the CD

signals of the [2Fe-2S] ^{15}N GLRX5-BOLA3 hetero-complex, in agreement with the formation of a [4Fe-4S] cluster, whose CD signals are typically of very low intensities.

Further interaction data have been collected between BOLA3 and [4Fe-4S]/apo mNFU1 and between GLRX5 and mNFU1 in different experimental conditions, in order to better characterize the role of BOLA3 and mNFU1 in the mitochondrial ISC assembly machinery. The analysis of these data is now under investigation.

References

[1] Ciofi-Baffoni S. et al.; Metallomics. 2018 Jan 24;10(1):49-72. doi: 10.1039/c7mt00269f.
[2] Melber A. et al.; Methods Enzymol. 2018;599:265-292. doi: 10.1016/bs.mie.2017.09.004.
[3] Lill R. et al.; Eur J Cell Biol. 2015 Jul-Sep;94(7-9):280-91. doi: 10.1016/j.ejcb.2015.05.002.
[4] Stehling O. et al.; Biochimie. 2014 May;100:61-77. doi: 10.1016/j.biochi.2014.01.010.
[5] Cameron JM et al.; Am J Hum Genet. 2011 Oct 7;89(4):486-95. doi: 10.1016/j.ajhg.2011.08.011.
[6] Navarro-Sastre et al.; Am J Hum Genet. 2011 Nov 11;89(5):656-67. doi: 10.1016/j.ajhg.2011.10.005.
[7] Tong WH et al.; Proc Natl Acad Sci U S A. 2003 Aug 19;100(17):9762-7.
[8] Melber A.; Elife. 2016 Aug 17;5. pii: e15991. doi: 10.7554/eLife.15991.
[9] Nasta V. et al.; Biochim Biophys Acta. 2017 Aug;1861(8):2119-2131. doi: 10.1016/j.bbagen.2017.05.005.
[10] Sen S. et al.; Metallomics. 2018 Aug 23. doi: 10.1039/c8mt00128f.
[11] Uzarska MA et al.; Mol Biol Cell. 2013 Jun;24(12):1830-41. doi: 10.1091/mbc.E12-09-0644. Epub 2013 Apr 24.
[12] Ahting U. et al.; Front Genet. 2015 Apr 13;6:123. doi: 10.3389/fgene.2015.00123.
[13] Invernizzi F. et al.; Front Genet. 2014 Nov 20;5:412. doi: 10.3389/fgene.2014.00412.
[14] Nizon M. et al.; Mitochondrion. 2014 Mar;15:59-64. doi: 10.1016/j.mito.2014.01.003.
[15] Tonduti D. et al.; Orphanet J Rare Dis. 2015 Feb 8;10:13. doi: 10.1186/s13023-015-0237-6.
[16] Baker PR 2nd et al.; Brain. 2014 Feb;137(Pt 2):366-79. doi: 10.1093/brain/awt328.
[17] Haack TB et al.; J Inherit Metab Dis. 2013 Jan;36(1):55-62. doi: 10.1007/s10545-012-9489-7.
[18] Schilke B. et al.; Proc Natl Acad Sci U S A. 1999 Aug 31;96(18):10206-11.
[19] Brancaccio D. et al.; J Am Chem Soc. 2017 Jan 18;139(2):719-730. doi: 10.1021/jacs.6b09567.
[20] Ivano Bertini et al., J. Am. Chem. Soc., 1992, 114 (9), pp 3332–3340; doi: 10.1021/ja00035a026
[21] Banci et al., J Biol Inorg Chem. 2018 Jun;23(4):665-685. doi: 10.1007/s00775-018-1552-x. Epub 2018 Mar 22.
[22] Agar JN et al.; Biochemistry. 2000 Jul 11; 39(27):7856-62.
[23] Cai K. et al.; Structure. 2016 Dec 6;24(12):2080-2091. doi: 10.1016/j.str.2016.08.020.
[24] Bandyopadhyay S. et al.; J Biol Chem. 2008 May 16;283(20):14092-9. doi: 10.1074/jbc.M709161200.
[25] Freibert SA. et al.; Methods Enzymol. 2018;599:197-226. doi: 10.1016/bs.mie.2017.11.034.
[26] Mapolelo DT et al.; Biochemistry. 2012 Oct 16;51(41):8071-84. doi: 10.1021/bi3006658.
[27] Uzarska MA et al.; eLife. 2016; 5: e16673. doi: 10.7554/eLife.16673

Figures

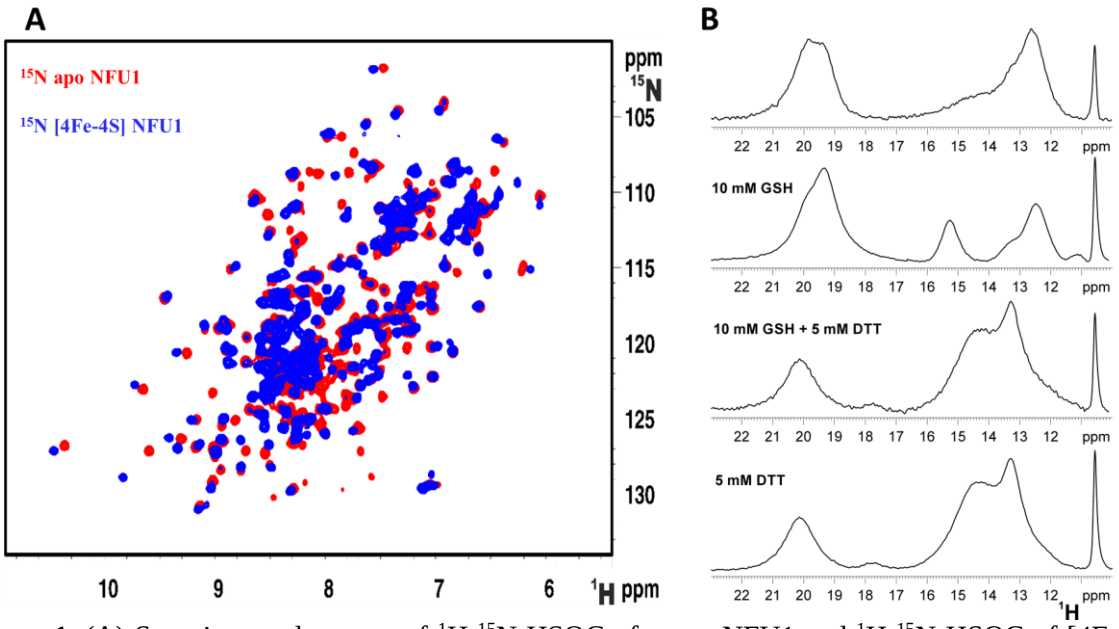

Figure 1. (A) Superimposed spectra of ^{1}H-^{15}N HSQC of apo mNFU1 and ^{1}H-^{15}N HSQC of [4Fe-4S] mNFU1 at 298K and (B) EPR spectra of [4Fe-4S] mNFU1 with/without GSH and/or DTT

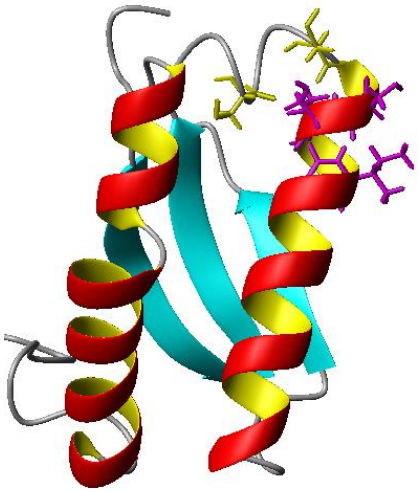

Figure 2C. Residues of the apo mNFU1 structure which interact with GSH. Cys residues indicated with a yellow color.

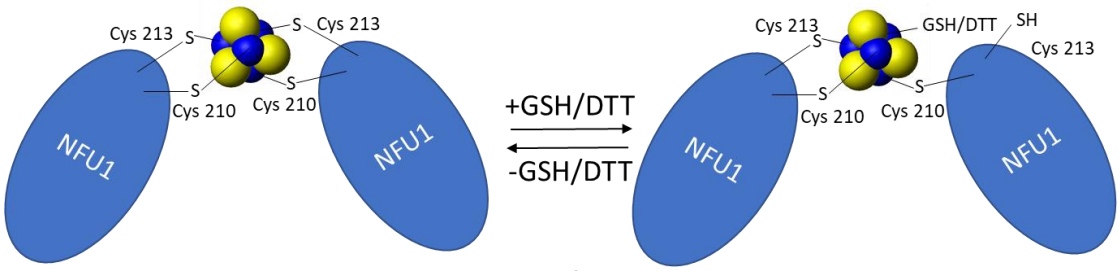

Scheme 1. Equilibrium with a dimeric $[4Fe\text{-}4S]^{2+}$ cluster-bound species where a Cys ligand is replaced by a S-donor small molecule ligand, such as GSH or DTT

Supplementary figures

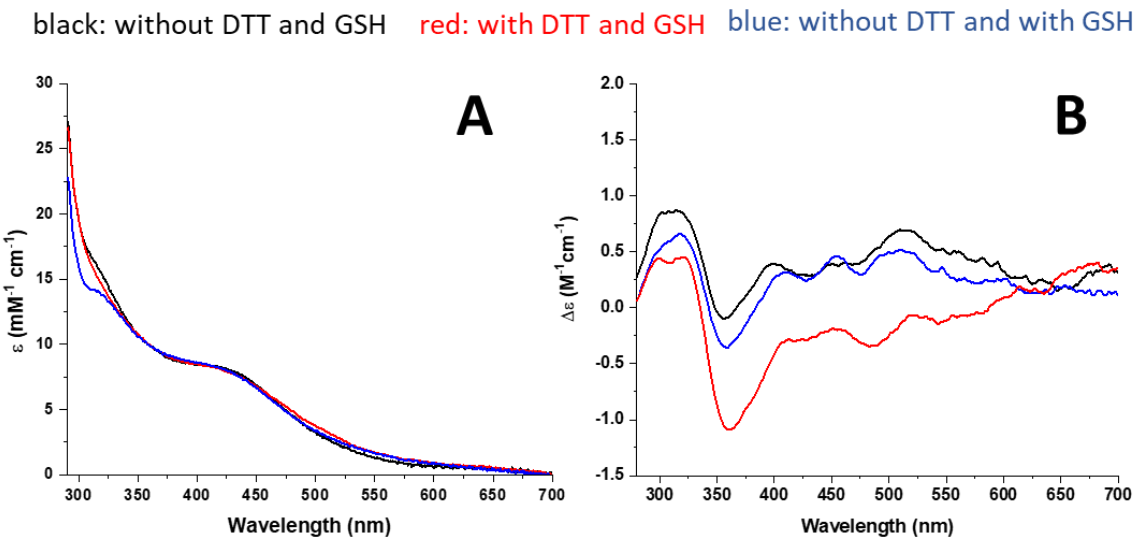

Figure S1. (A) UV-vis spectra and (B) UV-vis CD spectra of chemically reconstituted [4Fe-4S] mNFU1.

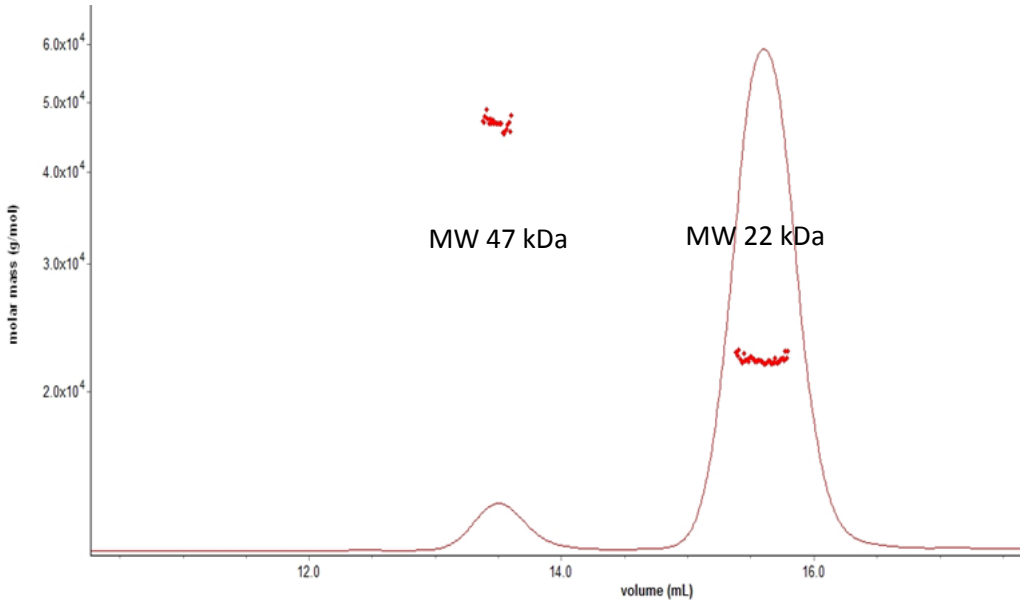

Figure 2SC. SEC-MALS of apo mNFU1.

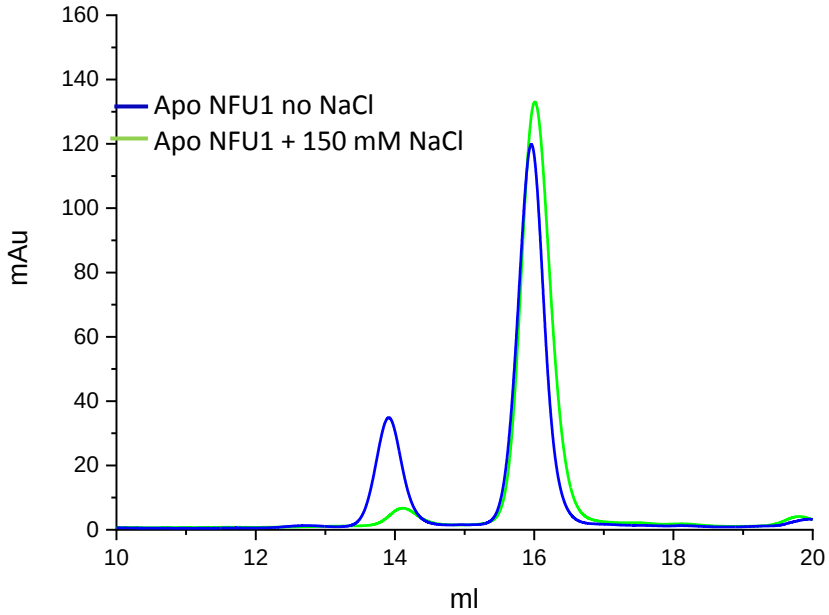

Figure 2SD. SEC of apo mNFU1 with and without salt.

CHAPTER 3

METHODOLOGY

3.1 Protein Production

Protein production is a biotechnological process resulting in the expression and isolation of a recombinant protein. This comprises the insertion of the recombinant DNA in an appropriate host/expression system, the transcription of the DNA to mRNA and translation into the polypeptide chain and finally the isolation of the protein from the rest of the proteasome.

There are several expression systems to choose, depending on the needs, difficulties and final yield of the protein expression. These include bacteria, insect, yeast, mammalian cells or even cell free expression systems.

During my doctoral studies I used bacteria as the expression system for all the proteins that I produced and specifically BL21(DE3) Competent Escherichia coli and BL21-Gold(DE3) Competent Escherichia coli cell strains. Bacteria were chosen since the recombinant protein expression is high, quick, low cost, the scale up is easy and the genetics are simple.

All the plasmids of the proteins that I studied have the protein gene inserted in a T7 expression vector including ampicillin resistance and a Tobacco Etch Virus nuclear-inclusion-a endopeptidase (TEV protease) recognition site before the gene and after the polyhistidine tag (His6 tag).

There are many factors that can be altered to facilitate a higher protein yield (vector, tag, host strain, growth medium, temperature, IPTG concentration, duration of induction step and more). It is self-evident that no protocol can be a panacea for the production of any given protein, hence, the design of the protocol is a product of empirical experimentation.

The protocols that I developed for the production of NFU1 and IBA57 are extensively reported below.

.....

Expression and purification of apo NFU1

Step 1:

Transform DNA plasmid into BL21-Gold(DE3) Competent Escherichia coli cell strain.

a) Take competent cell stock out of -80 °C freezer and place on ice to thaw for 5 minutes.

b) Take 50 µL, put them into an Eppendorf and put on ice.

c) Take 1 µL of plasmid DNA and add to the thawed competent cells. Mix briefly (gently by tapping NOT with pipet up and down) *and let incubate on ice for 30 minutes. Longer incubation will not affect negatively.*

d) Heat-shock the competent cells at 42°C for 45 seconds.

e) Place on ice and let incubate for 3 minutes.

f) Add heat-shocked cells to 0.25 mL of Lysogeny Broth (LB) *in a sterile culture tube, but DO NOT ADD antibiotic. Shake at 37°C for 1 hour.*

g) Place the cell culture onto LB agar Petri plates with ampicillin (100 µg/mL). Incubate the plate at 37°C for 16 hours.

Step 2:

Inoculate your culture and express protein

a) In one 2 L Fernbach culture flask put 1 L of LB, along with ampicillin. Ampicillin is added into the LB at 100 µg/mL final concentration.

b) Pick a couple of colony scoops from your Petri plate using a sterile inoculation loop and add to the LB/ampicillin 2 L Fernbach culture flask. Shake the culture at 37°C until OD_{600} = 3-5.

c) Spin down the cells (3,000 RPM for 20 min.) and re-suspend your cell pellet in 1 L volume of sterile LB (or Minimal medium for ^{15}N labelling) + Ampicillin 100 µg/mL into a 2 L Fernbach culture flask.

d) Shake at 30°C until OD_{600} increases by 1-2 units. (About 1,5 hours)

e) Add 250 µM $FeCl_3$ and induce the culture to express protein by adding 1 mM of isopropyl ß-D-1-thiogalactopyranoside (IPTG).

f) Keep the culture shaking at 30°C, over the night, so that OD_{600} = 10-14

Step 3:

Cell pellet with protein.

a) Centrifuge at 6,000 RPM for 20 minutes at 4° C. Weigh and count how much of cell pellet you have. You can freeze the cell pellet at -20°C (for use within 2 weeks) *or -80°C* (long-term).

Step 4:

Lysis of the bacteria.

a) Re-suspend the (frozen) cell paste as best as you can in the Lysis Buffer. Let this suspension incubate for 15-20 minutes at room temperature with occasional mixing.

b) Centrifuge using a preparative ultra-centrifuge at 40,000 RPM for 45 minutes at 4°C. (NFU1 should be in the supernatant.)

Purification of the protein.

Use a His-trap FF 5 mL column loaded with Nickel at a Chromatography unit. All the purification steps are carried out at room temperature, 5 mL/min system flow (under press flow control to avoid over pressure).

c) Equilibrate the His-trap column with the binding buffer.

d) Apply the supernatant (from the previous centrifuge step) *to the column. Then, by using ONLY the binding buffer, wash the column while collecting all the flow through in a beaker until UV absorption is stabilized close to zero.* (NFU1 should be bound to the His-trap at this time)

e) Elute the captive protein of the His-trap column using a gradient 0-60% of elution buffer in 20 Column Volumes (CV) *and collect the eluate in fractions of 5 mL.*

f) Wash with 3 CV of 100% Elution Buffer. (Keep collecting in fractions of 5 mL)

g) From the graph chose which fractions should contain NFU1 and evaluate about the protein amount by UV-vis or other techniques.

h) Concentrate the volume of the solution containing NFU1 at 6 mL.

i) Add Tris: 2 M, pH 8 until 20 mM

j) Add EDTA: 0.5 M, pH 8 until 2 mM

k) Add TCEP-HCL: 250 mM until 2 mM. (Check that the pH is greater than 7 and close to 8 with pH paper)

l) Add TEV protease 100 µL for every 10 mg of fusion protein.

m) Incubate at room temperature over the night. (This mixture can be stored at 4°C for a couple of days with no loss of protein)

Step 5:

a) Add 500 µL of NaCl 4M. (That is for being able to check the difference in conductivity at the graph during the chromatography)

b) Exchange the protein buffer with binding buffer + 0.2 mM TCEP-HCL using a Chromatography unit equipped with Hiprep 26/10 desalting column. (Set system flow at 10-15 mL/min)

c) Equilibrate the His-trap 5 mL column with 3 CV binding buffer using a peristaltic pump. (Set system flow at 5 mL/min)

d) Adjust the "IN" valve into the beaker that contains your protein mixture. Set the His-trap column over the beaker so that the "OUT" flow is poured into the latter. Let it like that for 2

hours. (This process is called overloading. In that step you separate the NFU1 from the His-tail. His-tail binds to the column while NFU1 elutes. It is good to overload so that you increase the amount of the His-tail that binds to the His-trap column)

e) Collect the flow through containing NFU1 in an appropriate beaker. Collect 2 CV with Binding Buffer to collect any residual NFU1 in the column.

f) Wash the column with 4 CV of elution buffer collecting in a beaker. (The eluate must contain NFU1-His-tail protein, TEV protease and His-tail)

g) Wash the column with water 5 CV and then with 3 CV 20% Ethanol (bacteriostatic) *and store the column at 4°C.*

After the purification.

Evaluate the purity of the protein by SDS-page denaturing and reducing. The protein can now be reduced with 5 mM DTT and concentrated by ultrafiltration 10 kDa MWCO and changed in NMR buffer.

If the purity is not satisfactory, a size exclusion Chromatography can be performed using Superdex-75 column of appropriate capacity.

Buffers used:

Lysis Buffer

1.26 gr CelLytic Express (C1990) powder dissolved in 25 mL mQ-H_2O. 1 gr of CelLytic Express (C1990) powder per 1 gr of wet cell paste is the best though if you have a lot of cell paste you can dissolve 0.1 gr of cell paste per milliliter and add 1.26 gr of CelLytic Express (C1990) powder per 25 mL mQ-H_2O. In the latter case you have to incubate more time in room temperature.

Binding Buffer

20 mM NaPi, 500 mM NaCl, 30 mM Imidazole, pH 7.8

Elution Buffer

Binding + 500 mM Imidazole, pH 7.8

NMR Buffer

50 mM NaPi, 5 mM DTT, 150 mM NaCl, pH 7

.....

Expression and purification of IBA57

Step 1:

Transform DNA plasmid into BL21-Gold(DE3) Competent Escherichia coli cell strain.

a) Take competent cell stock out of -80°C freezer and place on ice to thaw for 5 minutes.

b) Take 50 µL, put them into an Eppendorf and put on ice.

c) Take 1 µL of plasmid DNA and add to the thawed competent cells. Mix briefly (gently by tapping NOT with pipet up and down) *and let incubate on ice for 30 minutes. Longer incubation will not affect negatively.*

d) Heat-shock the competent cells at 42°C for 45seconds.

e) Place on ice and let incubate for 3 minutes.

f) Add heat-shocked cells to 0.3 mL of Lysogeny Broth (LB) *in a sterile culture tube, but DO NOT ADD antibiotic. Shake at 37°C for 1 hour.*

g) Place the cell culture onto LB agar Petri plates. Make sure the plates have ampicillin. Incubate the plate at 37°C for 16 hours.

Step 2:

Inoculate your culture and express protein

a) In one 2 L Fernbach culture flask put 1 L LB, along with ampicillin. Ampicillin is added into the LB at 100 µg/mL final concentration.

b) Add 15 mL (3% v/v) of Ethanol. [67]

c) Pick a couple of colony scoops from your Petri plate using a sterile inoculation loop and add to the LB/ampicillin 2 L Fernbach culture flask. Shake the culture at 37°C O/N.

d) Next day, spin down the cells (3,000 RPM for 20 min.) and re-suspend your cell pellet in 1 L volume of sterile LB (or Minimal medium for ^{15}N labeling) + Ampicillin 100 µg/mL + 3% v/v Ethanol into a 2 L Fernbach culture flask.

e) Shake at 37°C and so that the OD_{600} increases. (About 1 hour)

f) Shake at 42°C for ten minutes. (by heat shocking, the cells produce heat-shock chaperone and co-chaperon proteins that promote the folding of the expressed protein)

g) Shake at 37°C for 20 minutes.

h) Put the culture on ice for 30 minutes.

i) Shake at 37°C for 20 minutes.

j) Induce the culture to express protein by adding 0.1 mM IPTG.

k) Keep the culture shaking at 18-20°C O/N.

Step 3:

Cell pellet with protein.

a) Centrifuge at 6,000 RPM for 20 minutes at 4°C. You can freeze the cell pellet at -20°C (for use within 2 weeks) *or -80°C* (long-term).

Step 4:

Lysis of the bacteria.

a) Re-suspend the (frozen) cell paste as best as you can in the Binding Buffer.

b) Sonicate your mixture at maximum power, 30 seconds ON and 3 minutes OFF, ten times.

c) Add TCEP-HCL 1-2 mM.

d) Centrifuge using a preparative ultra-centrifuge at 40,000 RPM for 45 minutes at 4°C. (IBA57 should be in the supernatant.)

Purification of the protein.

Use a His-trap FF 5 mL column loaded with Nickel at a Chromatography unit. All the purification steps are carried out at room temperature, 5 mL/min system flow (under press flow control to avoid over pressure).

a) Equilibrate the His-trap column with the binding buffer.

b) Apply the supernatant (from the previous centrifuge step) *to the column. Then, by using ONLY the binding buffer, wash the column while collecting all the flow through in a beaker until UV absorption is stabilized close to zero.* (IBA57 should be bound to the His-trap at this time)

c) Elute the captive protein of the His-trap column using the elution buffer in 20 CV and collect the eluate in fractions of 5mL.

d) Wash with 3 CV of 100% Elution Buffer. (Keep collecting in fractions of 5mL)

e) From the graph chose which fractions should contain IBA57 and evaluate about the protein amount by UV or other techniques.

f) Concentrate the volume of the solution containing IBA57 at 6mL.

g) Add TCEP-HCL: 250 mM until 2 mM. (Check that the pH is greater than 7 and close to 8 with pH paper)

h) Add TEV protease 100 µL for every 10 mg of fusion protein.

i) Incubate at room temperature over the night. (This mixture can be stored at 4°C for a couple of days with no loss of protein)

Step 5:

a) Add 500 µL of NaCl 4 M. (That is for being able to check the difference in conductivity at the graph during the chromatography)

b) Exchange the protein buffer with binding buffer + 0.2 mM TCEP-HCL using a Chromatography unit equipped with Hiprep 26/10 desalting column. (Set system flow at 10-15 mL/min)

c) Equilibrate the His-trap 5 mL column with 3 CV binding buffer using a peristaltic pump. (Set system flow at 5 mL/min)

d) Adjust the "IN" valve into the beaker that contains your protein mixture. Set the His-trap column over the beaker so that the "OUT" flow is poured into the latter. Let it like that for 2 hours. (That process is called overloading. In that step you separate the IBA57 from the His-tail. His-tail binds to the column while IBA57 elutes. It is good to overload so that you increase the amount of the His-tail that binds to the His-trap column)

e) Collect the flow through containing IBA57 protein in an appropriate beaker.

f) Wash the column with 4 CV of elution buffer collecting in a beaker. (The eluate must contain IBA57-His-tail protein, TEV protease and His-tail)

g) Wash the column with water 5 CV and then with 3 CV 20% Ethanol (bacteriostatic) *and store the column at 4°C*

After the purification.

Evaluate the purity of the protein by SDS-page denaturing and reducing. The protein can now be reduced with 5mM DTT and concentrated by ultrafiltration 10 kDa MWCO and changed in NMR buffer.

If the purity is not satisfactory, a size exclusion Chromatography can be performed using Superdex-75 column of appropriate capacity.

Buffers used:

Binding Buffer

50 mM NaPi, 500 mM NaCl, 20 mM Imidazole, pH 7.6

Elution Buffer

Binding + 500 mM Imidazole, pH 7.6

NMR Buffer

50 mM NaPi, 5 mM DTT, pH 7

.....

3.2 Protein characterization

Ultraviolet–visible (UV-vis) spectroscopy

The principle of the UV-vis spectroscopy resides on the property of electrons to absorb energy upon ultraviolet or visible light exposure and get excited to energetically higher molecular orbitals. UV-vis spectroscopy measures this transition, from the ground to the excited state.

This technique was exploited to estimate protein concentration and observe the ''fingerprint'' spectra given by the iron transition of the Fe-S clusters.

UV-vis Circular Dichroism (CD) spectroscopy

UV-vis CD spectroscopy is a variation of the aforementioned technique in which the sample is exposed to circularly polarized light so that the absorption of the left-hand circular and the right-hand circular polarized light is differentiated. This technique gives rise to distinct spectra for chiral molecules, which would have been silent by the classic approach.

UV CD spectroscopy was exploited to investigate the secondary structure of proteins, while UV-vis CD spectroscopy was used to observe the transition of electrons in the Fe-S cluster which gives characteristic spectra for the various types and coordination of the cluster.

Size Exclusion Chromatography – Multi Angle Light Scattering (SEC-MALS)

Size Exclusion Chromatography (SEC) is a technique in which you apply a solution mixture to a polymer and you separate its contents by size. The larger the radius of the molecule the quickest its movement inside the polymer, hence, larger radius molecules elute faster than smaller ones. The final result is the separation of the molecules considering their size.

Multi-Angle Light Scattering (MALS) is a technique in which you expose a solution mixture to a light source and depending by how the molecules scatter the light you can determine the molar mass and the size of the molecules in solution. The light scatters when it hits the molecules, and the scattering intensity fluctuates over time due the Brownian motion of the molecules. This intensity fluctuation contains information about the time scale of the movement of the particles which is mathematically translated to the absolute molar mass and the average size of the molecules.

SEC-MALS is the combination of the aforementioned techniques and it was used to determine the molar mass of ISCA2, IBA57, NFU1 and [2Fe-2S]ISCA2-IBA57.

Small-angle X-ray scattering (SAXS)

SAXS is one of the X-ray scattering techniques and is used to quantify the density differences in a sample at the nanoscale level. It delivers structural information after exposing the sample to X-ray radiation and analyzing the recorded scattering behavior at small angles.

SAXS was exploited for acquiring structural information for the [2Fe-2S]ISCA2-IBA57.

X-ray crystallography

X-ray crystallography is one of the X-ray scattering techniques and is used to determine the atomic molecular structure of a crystal. An X-ray beam is sent upon the crystal and the electron density of the crystal can be determined by measuring the angles and intensities of the beam diffraction. This electron density contains all the information of the chemical bonds and their orientations.

The structure of IBA57 was determined by X-ray crystallography.

Nuclear Magnetic Resonance (NMR) spectroscopy

NMR spectroscopy is based on the physical phenomenon of the resonance transition between magnetic energy levels of nuclei which are initially aligned to an external magnetic field, thereafter perturbed with an electromagnetic radio frequency radiation and finally left to relax. Each nucleus emits a frequency upon this relaxation which contains information about the chemical environment around it and can be translated to structural information.

NMR spectroscopy was used extensively throughout my doctorate studies, especially to investigate protein-protein interactions.

CHAPTER 4

CONCLUSIONS AND PERSPECTIVES

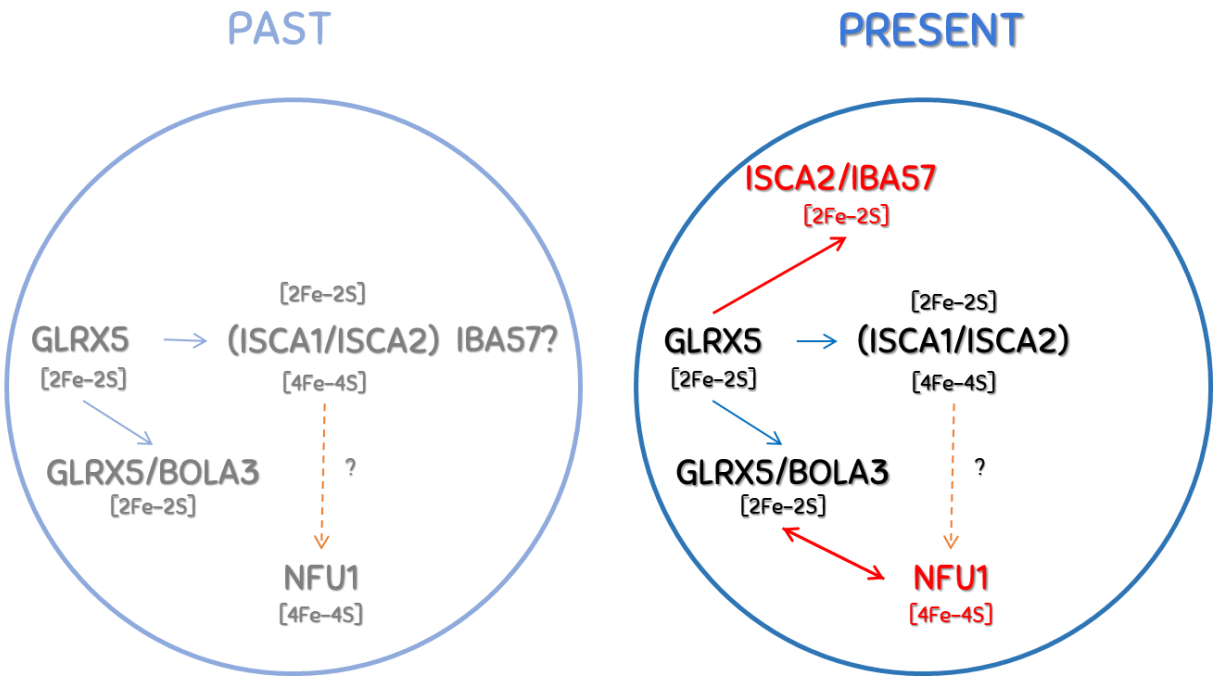

Figure 5. Schematic illustration of the scientific contribution of these studies. Blue arrows indicate well resolved steps of the pathway; **red-bold arrows** indicate the novel aspects from my studies

My studies shed light on the late steps of the mitochondrial Fe-S cluster assembly machinery and specifically on where GLRX5, BOLA3, NFU1, ISCA1, ISCA2 and IBA57 proteins function.

It is now demonstrated that [2Fe-2S] GLRX5 passes a cluster to ISCA2 and IBA57 to form a [2Fe-2S] ISCA2-IBA57 hetero-dimeric complex which has oxygen resistance and can increase the Aconitase activity. The latter could be an indication of the potential functional role of IBA57 as oxygen protective/restorer of the Fe-S clusters upon oxidative stress, working along with ISCA2.

The structure of IBA57 was determined and structural aspects of the [2Fe-2S] ISCA2-IBA57 construct were revealed as well. ISCA1 was also excluded as a possible functional partner of IBA57.

The function and role of BOLA3 and NFU1 was also explicated. [2Fe-2S] GLRX5 cannot give any cluster to NFU1 though the [2Fe-2S] GLRX5-BOLA3 complex transfers and assembles a [4Fe-4S] cluster on NFU1, at the presence of DTT and GSH, underlining the

importance of the role of BOLA3 as a ''switch'' protein which opens the gate to the pathway regulated by NFU1.

In conclusion, our studies identify new routes in the late steps of the mitochondrial Fe-S cluster assembly machinery (**Figure 5**), which inspire new possible molecular models on how the proteins involved in this late phase of the machinery are connected and function. The next steps after this study is to investigate whether [2Fe-2S] GLRX5-BOLA3 can transfer the cluster to apo ISCA1-ISCA2 and to ISCA2-IBA57 to fully conclude on the role of BOLA3. Other important aspects are to investigate and verify the ISCA1-NFU1 correlation that has already been hypothesized, [19] puzzle out the cluster transfer from NFU1 to LIAS, discover the actual role and function of BOLA1 and understand better the common and distinct functions of the homologues ISCA1 and ISCA2.

Reference list

References

[1] "organism". Chambers 21st Century Dictionary (online ed.). 1999.
[2] Wächtershäuser, Günter (1988-12-01). "Before enzymes and templates: theory of surface metabolism". Microbiol. Mol. Biol. Rev. 52 (4): 452–84.
[3] Wächtershäuser, G (January 1990). "Evolution of the first metabolic cycles". Proceedings of the National Academy of Sciences of the United States of America. 87 (1): 200–4.
[4] Günter Wächtershäuser, G (1992). "Groundworks for an evolutionary biochemistry: The iron-sulphur world". Progress in Biophysics and Molecular Biology. 58 (2): 85–201.
[5] Günter Wächtershäuser, G (2006). "From volcanic origins of chemoautotrophic life to Bacteria, Archaea and Eukarya". Philosophical Transactions of the Royal Society B: Biological Sciences. 361 (1474): 1787–806.
[6] Wächtershäuser, Günter (2007). "On the Chemistry and Evolution of the Pioneer Organism". Chemistry & Biodiversity. 4 (4): 584-602.
[7] Greenwood and Earnshaw, pp. 1098–1104.
[8] "Iron". Micronutrient Information Center, Linus Pauling Institute, Oregon State University, Corvallis, Oregon. April 2016.
[9] Nelson, D. L.; Cox, M. M. (2000). Lehninger, Principles of Biochemistry (3rd ed.). New York: Worth Publishing. ISBN 1-57259-153-6.
[10] Braymer, J.J. & Lill, R. Iron-sulfur cluster biogenesis and trafficking in mitochondria. J Biol Chem 292, 12754-12763 (2017).
[11] Iron-sulfur cluster proteins: electron transfer and beyond; Kamil Brzóska, Sylwia Męczyńska and Marcin Kruszewski*; Acta Biochimica Polonica Vol. 53 No. 4/2006, 685–691.
[12] Marc Fontecave; Iron-sulfur clusters: ever-expanding roles; Nature Chemical Biology, volume2, pages171–174 (2006).
[13] Richard Cammack; Iron—Sulfur Clusters in Enzymes: Themes and Variations; Advances in Inorganic Chemistry Volume 38, 1992, Pages 281-322.
[14] Rouault T.A. et al. Iron-sulphur cluster biogenesis and mitochondrial iron homeostasis. Nat Rev Mol Cell Biol 6, 345-351 (2005).
[15] Johnson D.C et al; M.K. STRUCTURE, FUNCTION, AND FORMATION OF BIOLOGICAL IRON-SULFUR CLUSTERS. Annu. Rev. Biochem. 74, 247-281 (2005).
[16] Johnson M.K. et al Iron-Sulfur Proteins. Encyclopedia of Inorganic Chemistry (2006).at http://onlinelibrary.wiley.com/doi/10.1002/0470862106.ia116/full.

[17] Lill R. et al; Iron-sulfur-protein biogenesis in eukaryotes. Trends Biochem. Sci 30, 133-141 (2005).

[18] Lill R. et al Eukaryotic iron– sulfur cluster biogenesis and its role in maintaining genome stability. In: Rouault, T. (Ed.), Iron–Sulfur Clusters in Chemistry and Biology. Walter de Gruyter GmbH, Berlin/Boston, pp. 541–598.

Reference list

[19] Alexander C Adam et al; The Nfs1 interacting protein Isd11 has an essential role in Fe/S cluster biogenesis in mitochondria; The EMBO Journal (2006) 25, 174-183.

[20] Terali K et al; The effect of the adaptor protein Isd11 on the quaternary structure of the eukaryotic cysteine desulphurase Nfs1.; Biochem Biophys Res Commun. 2013 Oct 18;440(2):235-40.

[21] Yoon T et al; Iron-sulfur cluster biosynthesis. Characterization of frataxin as an iron donor for assembly of [2Fe-2S] clusters in ISU-type proteins; J Am Chem Soc. 2003 May 21;125(20):6078-84.

[22] Robert et al; Ferredoxin, in conjunction with NADPH and ferredoxin-NADP reductase, transfers electrons to the IscS/IscU complex to promote iron–sulfur cluster assembly; Biochimica et Biophysica Acta (BBA) - Proteins and Proteomics; Volume 1854, Issue 9, September 2015, Pages 1113-1117.

[23] The Human Iron-Sulfur Assembly Complex Catalyzes the Synthesis of [2Fe-2S] Clusters on ISCU2 That Can Be Transferred to Acceptor Molecules.; Fox NG, Chakrabarti M, McCormick SP, Lindahl PA, Barondeau DP.; Biochemistry. 2015 Jun 30;

[24] Cai K et al; Human mitochondrial chaperone (mtHSP70) and cysteine desulfurase (NFS1) bind preferentially to the disordered conformation, whereas co-chaperone (HSC20) binds to the structured conformation of the iron-sulfur cluster scaffold protein (ISCU); J Biol Chem. 2013 Oct 4;288(40):28755-70.

[25] Uzarska MA et al; Mitochondrial Bol1 and Bol3 function as assembly factors for specific iron-sulfur proteins.; Elife. 2016 Aug 17;5. pii: e16673.

[26] Brancaccio D et al; Formation of [4Fe-4S] clusters in the mitochondrial iron-sulfur cluster assembly machinery.; J Am Chem Soc. 2014 Nov 19;136(46):16240-50.

[27] Banci L et al; [2Fe-2S] cluster transfer in iron-sulfur protein biogenesis.; Proc Natl Acad Sci U S A. 2014 Apr 29;111(17):6203-8.

[28] Sheftel AD et al; The human mitochondrial ISCA1, ISCA2, and IBA57 proteins are required for [4Fe-4S] protein maturation.; Mol Biol Cell. 2012 Apr;23(7):1157-66.

[29] Ferrer-Cortès Xet al; Protein expression profiles in patients carrying NFU1 mutations. Contribution to the pathophysiology of the disease.; Inherit Metab Dis. 2013 Sep;36(5):841-7.

[30] Bych K; The iron-sulphur protein Ind1 is required for effective complex I assembly.; EMBO J. 2008 Jun 18;27(12):1736-46.

[31] Wydro MM; Insights into the pathogenic character of a common NUBPL branch-site mutation associated with mitochondrial disease and complex I deficiency using a yeast model; Dis Model Mech. 2013 Sep;6(5):1279-84.

[32] Land T; Targeting of a human iron-sulfur cluster assembly enzyme, nifs, to different subcellular compartments is regulated through alternative AUG utilization; Mol Cell. 1998 Dec; 2(6):807-15.

[33] Margulis L, Sagan D (1986). Origins of Sex. Three Billion Years of Genetic Recombination. New Haven: Yale University Press. pp. 69–71, 87. ISBN 0 300 03340 0.

[34] William F. Martin and Miklós Müller "Origin of mitochondria and hydrogenosomes", Springer Verlag, Heidelberg 2007.

[35] Roland Lill et al; Mechanisms of iron–sulfur protein maturation in mitochondria, cytosol and nucleus of eukaryotes; BBA Volume 1763, Issue 7, July 2006, Pages 652-667.

[36] Metallomics and the. Cell. Edited by Lucia Banci. Springer, Dordrecht 2013, XXXVI+609 pp., hardcover, E 181.85.—ISBN 978-94-007-5560-4.

[37] Oliver Stehling et al; The Role of Mitochondria in Cellular Iron–Sulfur Protein Biogenesis: Mechanisms, Connected Processes, and Diseases; doi: 10.1101/cshperspect.a011312

[38] Puccio H et al; Friedreich ataxia: a paradigm for mitochondrial diseases. Curr. Opin. Genet. Dev. 12, 272-277 (2002).

[39] Seyda A et al; A novel syndrome affecting multiple mitochondrial functions, located by microcell-mediated transfer to chromosome 2p14-2p13. Am J Hum Genet. 2001 Feb;68(2):386-96.

[40] Navarro-Sastre A; A fatal mitochondrial disease is associated with defective NFU1 function in the maturation of a subset of mitochondrial Fe-S proteins. Am. J. Hum. Genet. 89: 656-667, 2011.

[41] Baker P. R. et al; Variant non ketotic hyperglycinemia is caused by mutations in LIAS, BOLA3 and the novel gene GLRX5. Brain 137: 366-379, 2014.

[42] Ajit Bolar, N. A. et al; Mutation of the iron-sulfur cluster assembly gene IBA57 causes severe myopathy and encephalopathy. Hum. Molec. Genet. 22: 2590-2602, 2013.

[43] Debray F.-G. et al; Mutation of the iron-sulfur cluster assembly gene IBA57 causes fatal infantile leukodystrophy. J. Inherit. Metab. Dis. 38: 1147-1153, 2015.

[44] Torraco A et al Novel mutations in IBA57 are associated with leukodystrophy and variable clinical phenotypes. J. Neurol. 264: 102-111, 2017.

[45] Liu, M. et al; Phenotypic spectrum of mutations in IBA57, a candidate gene for cavitating leukoencephalopathy. Clin. Genet. 93: 235-241, 2018.

[46] Ishiyama A et al; IBA57 mutations abrogate iron-sulfur cluster assembly leading to cavitating leukoencephalopathy. Neurol. Genet. 3: e184, 2017. Note: Electronic Article.

Reference list

[47] Al-Hassnan, Z. N. et al ISCA2 mutation causes infantile neurodegenerative mitochondrial disorder. J. Med. Genet. 52: 186-194, 2015.

[48] Alaimo, J. T. et al; Loss-of-function mutations in ISCA2 disrupt 4Fe-4S cluster machinery and cause a fatal leukodystrophy with hyperglycinemia and mtDNA depletion. Hum. Mutat. 39: 537-549, 2018.

[49] Alfadhel, M. et al; Further delineation of the phenotypic spectrum of ISCA2 defect: a report of ten new cases. Europ. J. Paediat. Neurol. 22: 46-55, 2018.

[50] Toldo, I. et al; Neonatal mitochondrial leukoencephalopathy with brain and spinal involvement and high lactate: expanding the phenotype of ISCA2 gene mutations. Metab. Brain Dis. 33: 805-812, 2018.

[51] Shukla, A. et al Homozygous p.(Glu8Lys) variant in ISCA1 is associated with a multiple mitochondrial dysfunctions syndrome. J. Hum. Genet. 62: 723-727, 2017.

[52] Vogtle, F.-N. et al; Mutations in PMPCB encoding the catalytic subunit of the mitochondrial presequence protease cause neurodegeneration in early childhood. Am. J. Hum. Genet. 102: 557-573, 2018.

[53] Johansson C et al; "The crystal structure of human GLRX5: iron-sulfur cluster co-ordination, tetrameric assembly and monomer activity". Biochem. J. 433 (2): 303–11.

[54] Camaschella C; "Recent advances in the understanding of inherited sideroblastic anaemia". British Journal of Haematology. 143 (1): 27–38.

[55] Li H et al; Monothiol CGFS glutaredoxins and BolA-like proteins: [2Fe-2S] binding partners in iron homeostasis.; Biochemistry. 2012 Jun 5;51(22):4377-89.

[56] Nasta V et al; Structural insights into the molecular function of human [2Fe-2S] BOLA1-GRX5 and [2Fe-2S] BOLA3-GRX5 complexes.; Biochim Biophys Acta. 2017 Aug;1861(8):2119-2131.

[57] Cozar-Castellano I. et al; hIscA: a protein implicated in the biogenesis of iron-sulfur clusters; Biochim. Biophys. Acta 1700:179-188(2004)

[58] Multiple Mitochondrial Dysfunctions Syndrome in https://clinicaltrials.gov/

[59] François-Guillaume Debray et al; Mutation of the iron-sulfur cluster assembly gene IBA57 causes fatal infantile leukodystrophy; J Inherit Metab Dis (2015) 38:1147–1153

[60] Peter F Lindley; Iron in biology: a structural viewpoint; Reports on Progress in Physics, Volume 59, Number 7.

[61] Beinert H. et al; Iron-sulfur clusters: nature's modular, multipurpose structures.; Science. 1997 Aug 1;277(5326):653-9.

Reference list

[62] Tracey A. Rouault & Wing-Hang Tong; Iron–sulphur cluster biogenesis and mitochondrial iron homeostasis; Nature Reviews Molecular Cell Biology volume 6, pages 345–351 (2005).

[63] Louis Noodleman, Michael E. Pique, Victoria A. Roberts; Iron–Sulfur Clusters: Properties and Functions; Wiley Encyclopedia of Chemical Biology.

[64] Ivano Bertini et al; Biological Inorganic Chemistry - Structure and Reactivity - (University Science Books, 2007); page 50.

[65] Lebigot E. et al; Impact of mutations within the [Fe-S] cluster or the lipoic acid biosynthesis pathways on mitochondrial protein expression profiles in fibroblasts from patients.; Mol Genet Metab. 2017 Nov.

[66] Melber A. et al; Role of Nfu1 and Bol3 in iron-sulfur cluster transfer to mitochondrial clients.; Elife. 2016 Aug 17.

[67] Gaurav Chhetri et al.; An efficient protocol to enhance recombinant protein expression using ethanol in Escherichia coli; MethodsX. 2015; 2: 385–391.

Acknowledgements

1. *Thanks Mom, for raising a man it ain't easy.*
2. *You put aback your needs only and just to please me.*
3. *Grandma, thank you so much for being my father.*
4. *Supporting me for good, cooking, you were my barber.*

5. *Daddy, believe it or not, I thank you, too;*
6. *An example not to follow; wrong things I shouldn't do.*
7. *Boufo, thank you for looking up to your brother,*
8. *Making me feel important, I'll never understand that.*

9. *Malone, Jojo, Tipra, Liago, Manu, Vs,*
10. *Kotra, Bates, Rob, Ryan, thanks for being my friends.*
11. *Dear CERM-ians, I thank you all, you're Power-Rangers.*
12. *Lucia and Simo, thank you for respecting a stranger.*

13. *Vicky & Etta thanks, believing that I am perfect.*
14. *Well, I wasn't. I pray you'll find somebody better.*
15. *Eventually the time came to say that "I'm done!*
16. *PhD completed! Thanks Christ, you'll always be my God."*

Here to mention my godfather, Nick Nassopoulos. There are no words to describe the gratitude for his help on this journey. Just… THANKS.